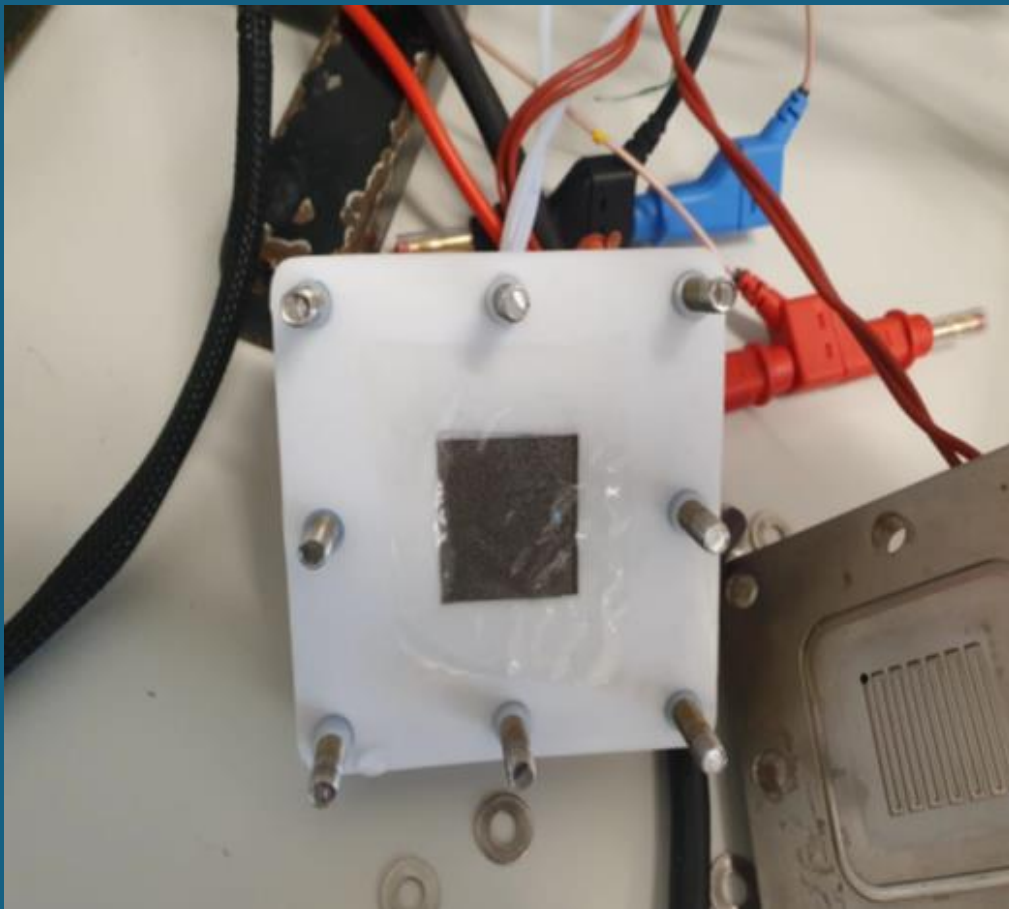


# Benefit Analysis Of Critical Raw Materials' Retrieval Strategies From Used Hydrogen Production Membranes – Apurva Venkatesh



# BENEFIT ANALYSIS OF CRITICAL RAW MATERIALS' RETRIEVAL STRATEGIES FROM USED HYDROGEN PRODUCTION MEMBRANES

## MASTER OF SCIENCE THESIS

For obtaining the degree of Master of Science in Aerospace Engineering at Delft  
University of Technology

Apurva Venkatesh

27.06.2024

Faculty of Aerospace Engineering · Delft University of Technology



Delft University of Technology  
Faculty of Aerospace Engineering  
Department of Aerospace Structures and Materials

GRADUATION COMMITTEE

Date: 27.06.2024

Chair holder:

\_\_\_\_\_  
Dr. Julie J. E. Teuwen

Committee members:

\_\_\_\_\_  
Dr. Santiago J. Garcia Espallargas

\_\_\_\_\_  
Dr. Calvin D. Rans

\_\_\_\_\_  
Dr. Baris Kumru

*Dedicated to*  
*Yamini Boyapati*

# ACKNOWLEDGEMENT

As my days went by in the Netherlands, my graduation is an event which I steadily lost hope of ever achieving. Writing this Acknowledgement section means just as much, if not more, as writing my entire thesis. It is a reminder of the wonderful people that I have met, cherished, and will continue to treasure in my life.

I would like to start by thanking my supervisor, Dr. Santiago J. Garcia Espallargas, for his unwavering support throughout my Masters. His inputs helped take my thesis to a higher level. The friendly and unbiased culture he has cultivated in Novam and his flexible teaching tailored to an individual student's needs are surely something I will inculcate and spread, wherever I end up working. I am highly grateful and indebted to the help he has personally provided in ensuring that I complete my Master studies successfully, despite all the obstacles I have encountered. I also offer my deepest gratitude to Shanta and Jill Morales for helping me navigate my university years with their actions filled with care and kindness. I would also like to thank Dr. Calvin D. Rans and all the other professors whom I have met for challenging my way of thinking and guiding me to be a better engineer. I promise to honour their teachings by upholding a high standard of integrity and quality in my work.

I owe my degree to my family – Amma, Satish anna, Kamal anna, Juliet anni, Yamini, Mahalakshmi, Balaji anna, Karthick anna, Vignesh anna, Aanchal akka, Sharmila akka, Vinodh anna, Harshit, Elif Sensei, Qiuyu Miao, Shaafi anna, Fathima akka, Logesh anna, Kris, Mike, Farah, Narasimhan, Ajeesh uncle, Uppi, Lakshmi chithhi, Meera chithi, Vignesh chithappa, Vinod maama, Adhvaith, Arya, Lakshmi mma, Vinaayaganna, Shivar appa, Muruganna, Vishnu appa, Ayyapanna, Parvathi mma, Chachupaati, Thaatha, and Kachutipaati who have helped shape not only my educational life but my personal life as well. They have been with me through my struggles and pushed me to realize my potential, even when life seemed impossible. Their affectionate words, incessant roasting, playfighting (of course instigated by me!), and advice instilled an unbreakable fighting spirit, prior non-existent dimensions of love, optimism, and a strong sense of responsibility within me. The lessons I learnt from every one of them will stay with me forever.

Next, I would like to thank my closest friends and well-wishers – Lourdes Gallestegui Pujana, Dr. Harry, Ruocho, Pascal, Jingjing, Lakshmi, Filippo, Adithya, Stefna, Kirubashini, Irem, Shalini, Tinashe, Roy Awaters, Caitlin van Den Hondel, Liliana Baron, Yamini akka, Dr. Tiju Thomas, Sathiesh anna, Ida, Arini, Manish Bhaiyya, Harish, Endino, Madhura, Inge, Rajendran appa, Girish uncle, Kavin, Matthias, Charan, Hussain uncle, Maathaji, Saswat, Natesh anna, Sanjay, Rashmi, Ravi, Ayumi, Sreejith, Edward, Marlon, Anton, Riccardo, Alejandro, Denize, Miisa, Tingyu, Laura, and Daniel for our countless hours of chats and outings. Special thanks to Roy and Caitlin for being more than lab supervisors! Your experience and joviality made lab work more enjoyable than it already was.

I conclude this section by acknowledging my own growth, determination, inner strength, and willpower. My time in Netherlands brought out a version of myself that I am highly proud of!

-Apurva Venkatesh

# ABSTRACT

With the advent of hydrogen and its derivatives being the emerging green fuel sources in aviation, the question of its sustainable production arises. Out of the various production methods, anion exchange membrane water electrolysis (AEMWE) stands out because of the less corrosive environment and the use of base metal electrocatalysts. Even so, for better performance, the expensive and exhaustible Platinum Group Metals - Platinum, Iridium, Ruthenium, etc. are the preferred electrocatalyst choices. The rarity of these metals has earned them a place in the European Union's Critical Raw Materials (CRM) list. Furthermore, the commonly chosen Nickel and Cobalt electrocatalysts are also CRMs. For the purpose of a circular economy and to ensure the uninterrupted supply of these CRMs, the current work estimates the amount of Nickel, Cobalt and Platinum exhausted in AEMWE electrocatalysts per year from 2035-2050.

To convey the issue of membrane degradation in alkaline media and the importance of catalysts for electrolysis, lab-scale electrolyser cell runs and material characterisation were carried out using the best-performing commercial anion exchange membrane, Sustainion X37-50 Grade RT. Thermogravimetric analysis, Fourier Transform InfraRed spectroscopy, and chronopotentiometry were performed. Even for a lower current density of 0.3 A/cm<sup>2</sup>, 1.890 V was required. The unstable nature of the chronopotentiometry curves and the higher potential needed to maintain a small current emphasized the need for catalysts. The shift in the degradation temperature and the FTIR spectra variation confirmed the degradation of the membrane.

Following this, the amount of CRMs exhausted from 2035-2050 was calculated by assessing the global hydrogen aviation demand evolution and AEMWE's contribution. LDS, MDS, and HDS of 10%, 30%, and 60% denoting the hydrogen demand met by AEMWE production were fixed. Using Enapter's 1 MW capacity AEM Nexus 1000 electrolyser model specifications and state-of-the art catalyst loading trends, Nickel, Cobalt, and Platinum exhaustion trends were determined.

The final step was analysing the retrieval strategies available for CRM recovery. New developments in hydrometallurgy, pyrometallurgy, and bio metallurgy were researched and weighed against current industry practices. The weighing was based on time, temperature, pH, and recovery efficiency. Microwave-assisted hydrometallurgy using aqua regia was the optimal route for Platinum. For Nickel and Cobalt, ultrasound-assisted hydrometallurgy with lemon-juice/H<sub>2</sub>O<sub>2</sub> leachant system was the viable technique. Employing these techniques, 98.3% Platinum, 100% Nickel, and 100% Cobalt can be recovered. It was also determined that for nickel and cobalt, the analysed bio metallurgical methods could be employed for retrieval, if they could be modified for time optimization.

# TABLE OF CONTENTS

ACKNOWLEDGEMENT .....	5
ABSTRACT .....	6
TABLE OF CONTENTS .....	7
LIST OF FIGURES .....	10
LIST OF TABLES .....	12
ACRONYMS AND ABBREVIATIONS .....	13
LIST OF ACRONYMS .....	13
LIST OF ABBREVIATIONS .....	13
1. INTRODUCTION .....	15
1.1. AVIATION AND THE NZE SCENARIO .....	16
1.1.1. POTENTIAL OF HYDROGEN .....	16
1.2. THESIS DOCUMENT GUIDE .....	21
2. LITERATURE ANALYSIS .....	23
2.1 ANION EXCHANGE MEMBRANE WATER ELECTROLYSER CELL .....	23
2.1.1. ENDPLATES .....	23
2.1.2. CURRENT COLLECTORS .....	24
2.1.3. BIPOLAR PLATES .....	24
2.1.4. GASKETS .....	24
2.1.5. TRANSPORT LAYERS .....	24
2.1.6. ELECTROCATALYST LAYERS .....	24
2.1.7. ANION EXCHANGE MEMBRANE .....	29
2.2. STATE-OF-THE-ART AEMWE ELECTROCATALYSTS .....	31
2.2.1. DESIGN STRATEGIES .....	31
2.3. MATERIAL RETRIEVAL STRATEGIES .....	33
2.3.1. PYRO-METALLURGY: .....	33
2.3.2. HYDROMETALLURGY: .....	33
2.3.3. BIO-METALLURGY: .....	34
3. RESEARCH QUESTION FORMULATION .....	37
3.1. KNOWLEDGE GAP AND RESEARCH OBJECTIVE .....	37
3.2. RESEARCH QUESTION .....	37
4. EXPERIMENTAL WORK .....	39
4.1. MATERIALS .....	39
4.2. METHODOLOGY .....	39
4.2.1. MEMBRANE ACTIVATION .....	39
4.2.2. DETERMINATION OF THE OPTIMAL RUNNING CONDITIONS .....	39
4.2.3. ELECTROCHEMICAL CHARACTERIZATION .....	39

4.2.4. MATERIAL CHARACTERIZATION .....	40
4.3. RESULTS AND DISCUSSION.....	42
4.3.1. CHRONOPOTENTIOMETRY CURVES .....	42
4.3.2. TGA CURVES .....	44
4.3.3. FTIR SPECTRUM.....	45
5. RETRIEVABLE CRM PREDICTION FROM 2035-2050.....	47
5.1. METHODOLOGY .....	47
5.1.1. HYDROGEN DEMAND PREDICTION.....	47
5.1.2. CATALYST LOADING SELECTION .....	51
5.1.3. AEMWE SYSTEM SPECIFICATIONS .....	52
5.1.4. MEMBRANE AREA CALCULATION .....	53
5.1.5. LDS, MDS, HDS .....	54
5.2. PLATINUM, NICKEL, AND COBALT RECOVERABLE AMOUNT CALCULATION .....	55
5.2.1. RECYCLABLE AMOUNT PROJECTION .....	55
6. BENEFIT ANALYSIS OF THE CATALYST RECOVERY STRATEGIES .....	58
6.1. INDUSTRIAL RECYCLING METHOD .....	60
6.1.1. PYRO-METALLURGICAL PROCESS.....	61
6.1.2. HYDROMETALLURGICAL PROCESS.....	61
6.2. OPTMIZATION ROUTES .....	62
6.2.1. PYROMETALLURGICAL PROCESS OPTIMIZATION .....	62
6.2.2. PYROMETALLURGY ELIMINATION/ HYDROMETALLURGY OPTIMIZATION .....	64
6.2.3. BIO METALLURGY .....	66
6.3. BENEFIT ANALYSIS .....	68
6.3.1. METHODOLOGY .....	68
6.3.2. SCORING SCHEME.....	69
6.3.3. OPTIMAL RETRIEVAL PROCESS DETERMINATION.....	69
6.3.4. CRM RECOVERY FROM 2035-2050.....	71
6.4. OTHER RECOMMENDATIONS .....	73
7. CONCLUSION .....	74
8. GUIDELINES FOR FUTURE WORK .....	75
REFERENCES .....	76
APPENDICES .....	89
APPENDIX A.....	90
DIFFERENT INDUSTRIAL RECOVERY ROUTES .....	90
Anglo Platinum process.....	90
Hartley Platinum Process.....	91
Impala Platinum process.....	92
Boliden Rönnskär route .....	93
PLATIRUS project .....	94
Panton process .....	94



# LIST OF FIGURES

Figure 1: Energy sector investment (Note: 'e' represents estimated values) (Source: [2])	15
Figure 2: Capacity additions for hydrogen electrolysis and CCUS projects (Source: [2])	15
Figure 3: Hydrogen technologies in aviation sector (Source: [14])	17
Figure 4: Hydrogen feedstocks (Source: [9])	18
Figure 5: Electrolysis development over the years (Source: [19])	19
Figure 6: Working of PEMWE, AWE, and AEMWE (Reproduced from [21])	19
Figure 7: Critical Raw Materials global share - 2023 (Source: [24])	20
Figure 8: The 10R strategies for a circular economy (Source: )	21
Figure 9: AEMWE exploded view (Source: [19])	23
Figure 10: Role of electrocatalysts (Source: [29])	25
Figure 11: LSV curves for Pt, $\alpha$ -Ni(OH) <sub>2</sub> /Pt, $\beta$ -Ni(OH) <sub>2</sub> /Pt (Adapted from [30])	27
Figure 12: Tafel plots for Pt, $\alpha$ -Ni(OH) <sub>2</sub> /Pt, $\beta$ -Ni(OH) <sub>2</sub> /Pt (Adapted from [30])	27
Figure 13: HER volcano plot (Source: [35])	28
Figure 14: OER volcano plot (Source: [32])	28
Figure 15: Common alkaline-stable AEM cations (Reproduced from [28])	29
Figure 16: Sustainion structure (Source: [39])	30
Figure 17: Alkaline degradation mechanisms in QA groups (Source: [28])	30
Figure 18: Smelting using copper collector (Adapted from: [64])	33
Figure 19: Hydrometallurgical processes (Adapted from: [67])	34
Figure 20: Organisms involved in bioleaching (Source: [68])	35
Figure 21: Bioleaching mechanisms (Source: [69])	35
Figure 22: Bioaccumulation mechanisms (Source: [69])	36
Figure 23: Laboratory-scale AEMWE	40
Figure 24: MEA cross-section	40
Figure 25: TGA4000 thermogravimetric analyser	41
Figure 26: FTIR spectrum of cellulose (Source: [75])	41
Figure 27: Spectrum 100 FT-IR spectrometer	42
Figure 28: Chronopotentiometry curves for various flow rates	42
Figure 29: Chronopotentiometry curves for different membrane activation time.	43
Figure 30: Chronopotentiometry curve for an electrolyser system employing catalysts (Source: [76])	44
Figure 31: TGA curves of pristine and 72-hrs 1M KOH-treated Sustainion	45
Figure 32: FTIR spectra of the membrane before and after the cell run	45
Figure 33: FTIR spectra of Sustainion under different media (Source: [78])	46
Figure 34: Global direct hydrogen demand prediction by various organizations till 2050 (Source: [80])	48
Figure 35: Operational fleet of hydrogen-powered aircraft (2035-2050) (Source: [83])	49
Figure 36: Global flight retirement trend (Source: [83])	50
Figure 37: Global hydrogen demand (Source: [83])	51
Figure 38: Platinum available for recycling per year from 2035-2050	56
Figure 39: Nickel available for recycling per year from 2035-2050	56
Figure 40: Cobalt available for recycling per year from 2035-2050	56
Figure 41: The Umicore recovery process (Source: [108])	60
Figure 42: Umicore Lithium battery recycling route (Source: [114])	61
Figure 43: Clean production strategies (source: [115])	62
Figure 44: PMT and HMT processes utilized in the LCA (Source: [123])	63
Figure 45: Microwave assisted smelting (Source: [124])	63
Figure 46: Kell's process (Source: Sedibelo Resources)	64
Figure 47: Platinum recovery rate at 150°C using NaCN from Chromobacterium violaceum (Source: [149])	66
Figure 48: Platinum recovered using MW-assisted HMT	72
Figure 49: Nickel recovered using US-assisted HMT	72
Figure 50: Cobalt recovered using US-assisted HMT	72
Figure 51: Anglo Platinum metal recovery process (Adapted from [169])	90
Figure 52: Rustenburg smelter (source: Adapted from [169])	90

Figure 53: Hartley Platinum Base Metal refining process (Source: [170]).....	91
Figure 54: Impala Platinum nickel and cobalt recovery circuit (source: [170]) .....	92
Figure 55: Boliden Rönnskär precious and base metal recovery route (source: [171]) .....	93
Figure 56: PLATIRUS circuit for PGM recovery (Source: [172]) .....	94
Figure 57:Panton process (Source: [83]) .....	94

# LIST OF TABLES

Table 1: List of acronyms .....	13
Table 2: List of abbreviations .....	13
Table 3: Hydrogen-based jet fuels (Adapted from [14]).....	17
Table 4: Voltage obtained from chronopotentiometry for different electrolyte flow rates.....	43
Table 5: Voltage obtained from chronopotentiometry for different membrane activation times. ....	44
Table 6: Platinum loading in literature.....	51
Table 7: Nickel loading in literature .....	52
Table 8: Cobalt loading in literature .....	52
Table 9: Equipment specifications for AEM Flex 120 and AEM Nexus 1000 (Source: [102], [103]) .....	52
Table 10: Recyclable CRM amounts in 2050 .....	57
Table 11: Patents related to metal recovery technologies. ....	58
Table 12: Platinum recovery at various temperatures (Adapted from [131]).....	64
Table 13: Novel solvents used in hydrometallurgy.....	65
Table 14: Bioleaching advances in Platinum, Nickel, and Cobalt recovery .....	66
Table 15: Biosorption of Platinum, Nickel, and Cobalt.....	68
Table 16: Benefit analysis scoring scheme .....	69
Table 17: Viable strategy determination for Platinum .....	70
Table 18: Viable strategy determination for Nickel .....	70
Table 19: Viable strategy determination for Cobalt .....	71
Table 21: Recycled CRMs for 2050 .....	72

# ACRONYMS AND ABBREVIATIONS

## LIST OF ACRONYMS

Table 1: List of acronyms

ACRONYM	EXPANSION
CAPEX	Capital Expenditure
OPEX	Operational Expenditure
IRENA	International Renewable Energy Agency
PLATIRUS	Platinum Group Metals Recovery Using Secondary Raw Materials

## LIST OF ABBREVIATIONS

Table 2: List of abbreviations

ABBREVIATION	EXPANSION
AEM	Anion Exchange Membrane
AEMWE	Anion Exchange Membrane Water Electrolyser
AI	Artificial Intelligence
AWE	Alkaline Water Electrolyser
BASF	Baden Aniline and Soda Factory
BET	Brunauer–Emmett–Teller
CBA	Cost Benefit Analysis
CCR	Continuous Catalyst Regeneration
CCUS	Carbon Capture Utilization and Storage
CP	Chronopotentiometry
CRM	Critical Raw Materials
CV	Cyclic Voltammetry
GDL	Gas Diffusion Layers
ECSA	ElectroChemical active Surface Area
EoL	End of Life
FC	Fuel cell
FTIR	Fourier Transform InfraRed
EU	European Union
HER	Hydrogen Evolution Reaction
HMT	Hydrometallurgical
IEA	International Energy Agency
KPI	Key Performance Indicators
LCA	Life Cycle Assessment
LSV	Linear Sweep Voltammetry
LREE	Light Rare-Earth Elements
MEA	Metal Electrode Assembly
MPL	Microporous layers
NV	Naamloze Vennootschap (public limited liability company)
OER	Oxygen Evolution Reaction
PEMWE	Proton Exchange Membrane Water Electrolyser
PGM	Platinum-Group Metals
PLC	Public Limited Company

PMT	Pyrometallurgical
PTFE	Polytetrafluoroethylene
PTL	Porous Transport Layers
PVC	Polyvinylchloride
RT	Room Temperature
SAF	Sustainable Aviation Fuel
TGA	Thermogravimetric analysis
UN	United Nations
WEEE	Waste from Electrical and Electronic Equipment

# 1. INTRODUCTION

Out of the ten major challenges facing humanity in the upcoming decades, energy ranks first, followed by water, food, environment, and poverty amongst the top five. With fossil fuels running out, the world is turning towards renewable energy sources to meet the ever-increasing demand. The glaring issues with solar, geothermal, tidal and wind energies is their dependence on geography and time of the year [1].

In addition, the critical materials that would be necessary to bring about the energy transition are also geopolitically constrained with countries like Chile, China, Indonesia, etc. commanding the mining arena, and China dominating the processing field and supplying 60% of the world’s refined manganese and lithium, 70% of cobalt, and 100% of dysprosium and natural graphite. According to the graph from the International Energy Agency’s (IEA) World Energy Outlook 2023 edition (Figure 1), a 10% increase is expected in coal supply investment [2].

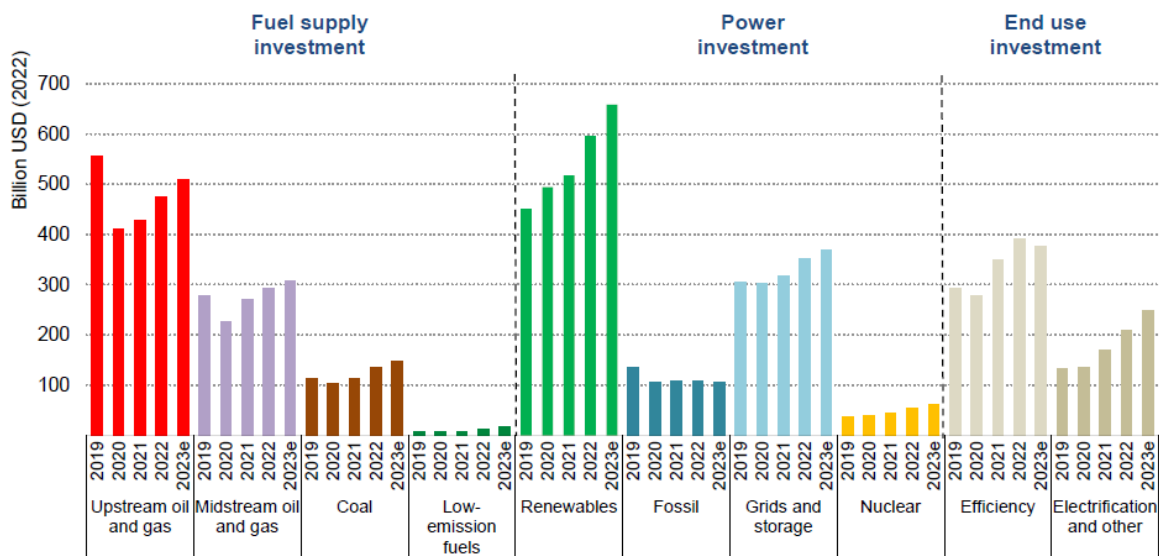


Figure 1: Energy sector investment (Note: 'e' represents estimated values) (Source: [2])

Even though the values for the fuel sector look bleak, the geopolitics and climate crisis scenarios have led to increased policies in hydrogen, CO<sub>2</sub> capture (Carbon Capture Utilization and Storage (CCUS)), and bioenergy sectors. This is illustrated in Figure 2 [2].

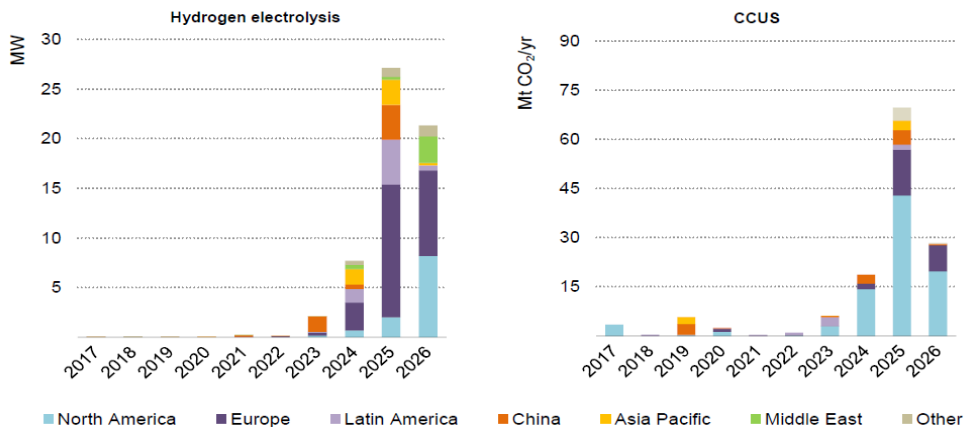


Figure 2: Capacity additions for hydrogen electrolysis and CCUS projects (Source: [2])

Furthermore, a spur in the policies will be seen because of the 1.5°C goal of the Paris Agreement treaty set in the 2015 United Nations Climate Change Conference. The treaty's overarching goal is to constrain the rise of global temperature within 1.5°C pre-industrial levels.<sup>1</sup> To attain this, a 45% emission reduction must be realized by 2030 and by 2050, there must be a 100% reduction. This is termed the Net Zero Emission (NZE) scenario.<sup>2,3</sup> To meet the energy transition infrastructure needed for this, a 60-65% representation of renewables in the electricity generation sector - around 33,000 GW of renewable power - is needed [3][4][5]. For a complete overview of the power situation, renewable energy production and consumption by all the countries, the reader is directed to IEA's Electricity Market Report 2023 [6] and IRENA's Renewable Energy Statistics 2023 [7].

## 1.1. AVIATION AND THE NZE SCENARIO

Global aviation contributed to 2.4% of the total CO<sub>2</sub> emissions in 2019 [8]. During the Covid-19 pandemic, the value dipped, but the 2022 contribution was already 800 Mt tonnes, reaching about 80% of its pre-pandemic value. According to IEA's findings, the aviation sector is deemed not to be on track for meeting the NZE scenario based on its current trajectory. International collaborations, private sector strategies, governmental policies, technological developments in the airframe, material and engine designs, and innovation in fuels are needed for a radical change. In particular, sustainable aviation fuels (SAFs) are considered important for decarbonising the aviation sector.<sup>4</sup> A noteworthy initiative is the European Union (EU)'s ReFuelEU legislation which has the objective of increasing the supply and demand of SAFs.<sup>5</sup> In lieu of this, 7 and 104 additional SAF production plants are needed by 2030 and 2050, respectively, just to meet EU's aviation demands.<sup>6</sup> While talking about SAFs, hydrogen and hydrogen-based fuels are frontrunners due to their greener combustion product - water.

### 1.1.1. POTENTIAL OF HYDROGEN

Hydrogen as a fuel source has been gaining impetus in the recent years, as evidenced by the increase in hydrogen research publications which jumped from 500 p. a. in 2010 to 1000 p. a. in 2021 [9]. Hydrogen is found aplenty on Earth in combination with many elements, with water and hydrocarbons being the chief sources due to their ready availability. In addition to being a SAF, it can also be used as feed for other SAFs, storage media and energy carrier [10][11]. Hydrogen is known for its non-toxicity, zero emissions, immense energy content, sustainability, and renewability [12][13].

For the fast-developing aviation sector, CSIRO (Commonwealth Scientific and Industrial Research Organisation) has identified several hydrogen technologies by 2050 (summarized in Figure 3). Of particular interest are the fuel cells (FC) being developed for propulsion systems [14]. For example, Universal Hydrogen conducted test flights with a 40-seat regional aircraft with one of its engines being FC-powered. Another instance is ZeroAvia's hydrogen electric engine powering a 19-seater.<sup>4</sup> These systems are designed to incorporate hydrogen and hydrogen-based jet fuels like ethanol, methanol, ammonia, dimethyl ether, methane, etc. [14] The various SAFs and their pros and cons are given in Table 3.

---

<sup>1</sup> <https://unfccc.int/process-and-meetings/the-paris-agreement>

<sup>2</sup> <https://www.un.org/en/climatechange/net-zero-coalition>

<sup>3</sup> <https://www.iea.org/reports/global-energy-and-climate-model/net-zero-emissions-by-2050-scenario-nze>

<sup>4</sup> <https://www.iea.org/energy-system/transport/aviation>

<sup>5</sup> <https://www.consilium.europa.eu/en/press/press-releases/2023/10/09/refuelev-aviation-initiative-council-adopts-new-law-to-decarbonise-the-aviation-sector/>

<sup>6</sup> <https://www.easa.europa.eu/eco/eaer/topics/sustainable-aviation-fuels/current-landscape-future-saf-industry#production-capacity-and-demand-beyond-2030-to-2050>

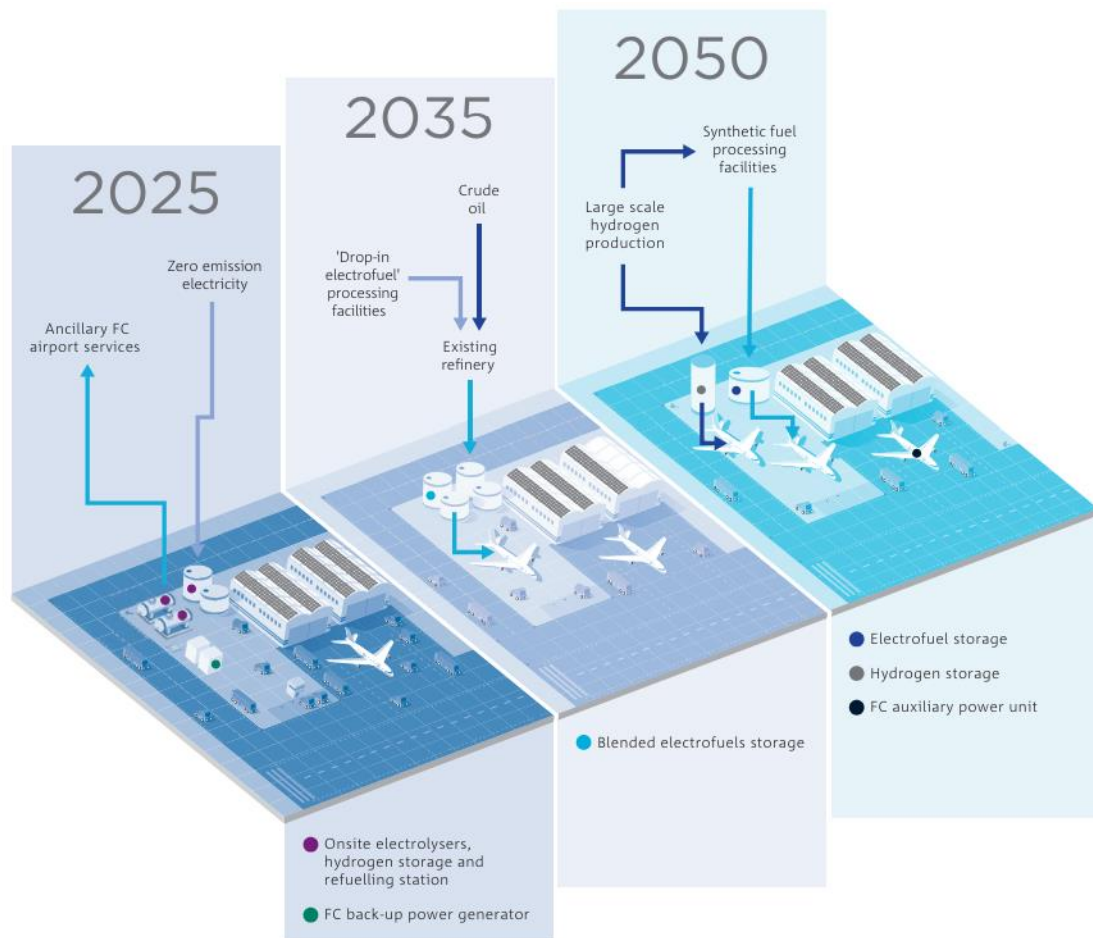


Figure 3: Hydrogen technologies in aviation sector (Source: [14])

Table 3: Hydrogen-based jet fuels (Adapted from [14])

SAF	ADVANTAGES	DISADVANTAGES
Hydrogen (H <sub>2</sub> )	<ul style="list-style-type: none"> <li>• Produces H<sub>2</sub>O as the combustion byproduct</li> <li>• Excellent specific energy density</li> </ul>	<ul style="list-style-type: none"> <li>• May lead to increased NO<sub>x</sub> at higher combustion temperatures</li> </ul>
Ammonia (NH <sub>3</sub> )	<ul style="list-style-type: none"> <li>• Well-developed product and transport infrastructure</li> </ul>	<ul style="list-style-type: none"> <li>• Toxic</li> <li>• Requires high ignition temperatures</li> <li>• NO<sub>x</sub> released upon combustion</li> </ul>
Dimethyl ether (CH <sub>3</sub> OCH <sub>3</sub> )	<ul style="list-style-type: none"> <li>• Low particulate emissions</li> </ul>	<ul style="list-style-type: none"> <li>• Displays interactions with elastomers that are different from the conventional kerosene</li> </ul>
Ethanol (C <sub>2</sub> H <sub>5</sub> OH)	<ul style="list-style-type: none"> <li>• Already a well-established fuel</li> </ul>	<ul style="list-style-type: none"> <li>• Like dimethyl ether, it displays interactions with elastomers that are different from the conventional kerosene</li> </ul>
Methane (CH <sub>4</sub> )	<ul style="list-style-type: none"> <li>• Can use existing infrastructure of natural gas</li> <li>• Already researched and used in turbines</li> </ul>	<ul style="list-style-type: none"> <li>• To reach adequate densities, cryogenic temperatures must be reached</li> </ul>
Methanol (CH <sub>3</sub> OH)	<ul style="list-style-type: none"> <li>• Cheaper than ethanol</li> <li>• Water-extinguishable flames</li> </ul>	<ul style="list-style-type: none"> <li>• Has clear flames while burning that are difficult to detect</li> </ul>

By 2050, IATA predicts 120 Million tonnes (Mt) of hydrogen would be needed, out of which 20 Mt would go into H<sub>2</sub> powered aircraft and 100 Mt into the manufacture of aviation fuel.<sup>7</sup> Extracting hydrogen can be done via conventional methods which involves using fossil fuels or via environment-friendly renewable technologies where it is obtained from water or biomass [15]. The various feedstocks for hydrogen production are shown in Figure 4.

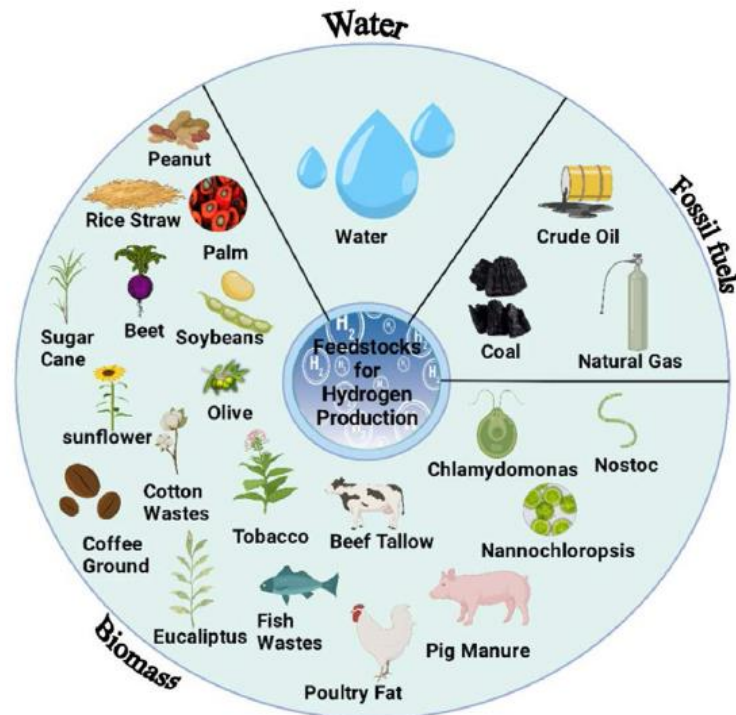


Figure 4: Hydrogen feedstocks (Source: [9])

Depending on the energy utilized, method of production, emission levels, and the cost, this colourless commodity obtained can be classified as grey, blue, pink/purple, yellow, red, white, turquoise, green, aqua, and brown or black hydrogen. A thorough review of the hydrogen types, including the production methods and the economic evaluation is covered by Santos et al. [16] Briefly, ‘brown/black hydrogen’ encompasses technologies such as coal and biomass gasification. It is considered the least environment friendly, as it emits 20 kgs of CO<sub>2</sub> per 1 kg of H<sub>2</sub>. ‘Grey hydrogen’ has techniques such as steam methane reforming, autothermal reforming, and partial oxidation. Of these, steam methane reforming is an established technology and meets 80% of the global hydrogen demand. The global focus is to shift from brown/black and grey hydrogen to green hydrogen. Green hydrogen employs water-splitting which results in minimal carbon footprint. For this aspect, it is also known as renewable, low-carbon, or clean hydrogen [16]. The splitting is achieved via,

- Electrolysis – Splitting is achieved by passing direct current through water.
- Thermolysis – Water is heated to above 2,500°C.
- Photolysis – Light energy is used for the splitting. For this purpose, photocatalysts such as titanium dioxide (TiO<sub>2</sub>) and graphitic carbon nitride (g-C<sub>3</sub>N<sub>4</sub>) are used for visible light absorption [15].

Regular electrolysis as a means of hydrogen production has been favoured because of the ease of the process, high purity end product, easy source availability, facile scalability, and upon combining with renewable power sources, a zero carbon footprint process [17][18]. It can be sub-categorised into alkaline water electrolysis (AWE), proton exchange membrane water electrolysis (PEMWE), and anion exchange membrane water electrolysis (AEMWE). A history of electrolysis development is presented in Figure 5.

<sup>7</sup> <https://www.hydrogeninsight.com/transport/global-aviation-industry-projected-to-need-120-million-tonnes-of-clean-hydrogen-a-year-by-2050-iata/2-1-1371024>

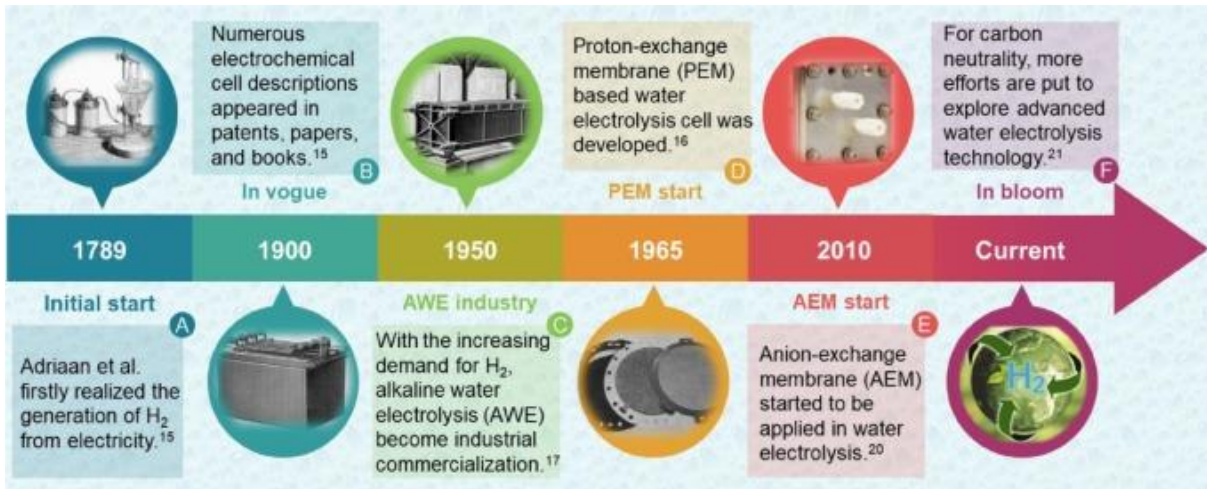


Figure 5: Electrolysis development over the years (Source: [19])

A detailed mechanism of an electrolyser cell and the reactions that occur are explained in the subsequent chapter. In brief, a water electrolyser cell consists of 2 electrodes – a cathode and an anode, present in an electrolyte solution. Upon current application via an external circuit, ion transport is facilitated by the electrolyte, and hydrogen is produced at the cathode and oxygen evolves at the anode. In an AWE, these electrodes are separated by a porous diaphragm.  $\text{OH}^-$  is the transported ion and alkaline electrolytes are employed. The diaphragm is replaced by a membrane in PEMWE and AEMWE. The membrane provides better contact between the electrodes and enhances ion transportation. Since PEMWE uses  $\text{H}^+$  ions, highly acidic electrolytes are used. Consequentially, the cell requires electrodes and catalysts made from resilient platinum group metals (PGM) – Osmium, Iridium, Platinum, Palladium, Ruthenium, and Rhodium. Hence, its counterpart, AEMWE, has been garnering attention as it combines the advantages of both AWE and PEMWE. It has the ability to provide better contact between the electrodes (which is absent in AWE) and the ability to use non-platinum group metals as catalysts (which is the drawback of PEMWE), because of its mildly alkaline environment [20][21]. A schematic overview of their working is presented in Figure 6.

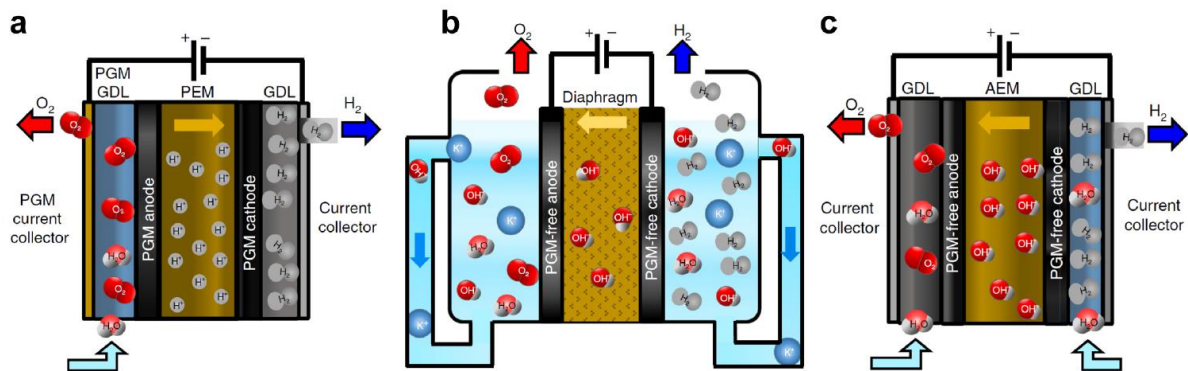


Figure 6: Working of PEMWE, AWE, and AEMWE (Reproduced from [21])

Though AEMWE has the option of using non-PGM catalysts, most of the research done still use PGM-based candidates for an optimized performance. In addition to the PGM group, manganese, cobalt, vanadium, and light rare-earth elements (LREE) such as cerium and lanthanum are also employed [22]. All the stated elements belong to the European Union’s (EU) fifth Critical Raw Materials’ list (Figure 7) published in 2023 - *Study on the critical raw materials for the EU 2023 : final report* [23]. This list is formulated based on a material’s supply risk and its economic importance. In lieu of this, nickel, despite its diversified availability, is part of the

Strategic Raw Materials category. This was to reflect the private contract agreements and ownership of production capacities and projects based on this metal [23].

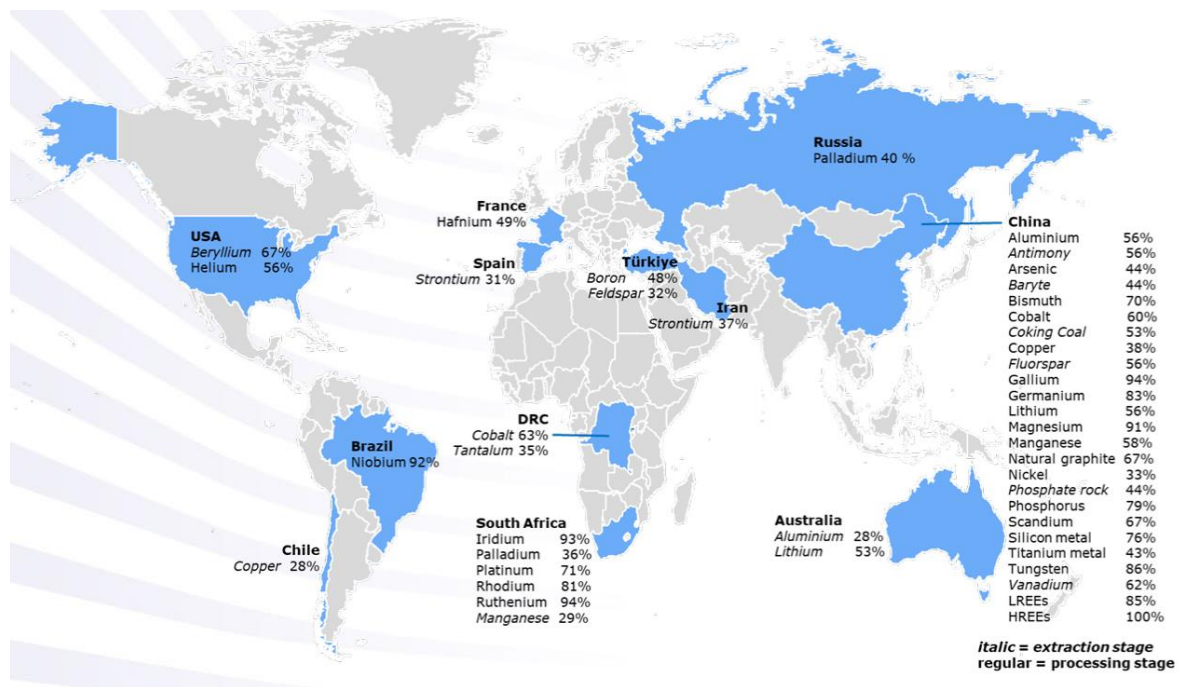


Figure 7: Critical Raw Materials global share - 2023 (Source: [24])

Amongst the 34 CRMs published by the EU, the literature study performed identified **platinum, nickel, and cobalt** as prospective electrocatalysts for future AEMWE plants. Especially for platinum, out of the estimated 70,000 metric tonnes present in Earth's reserves, 10,000 tonnes have already been mined from 1741, with around 180 metric tonnes being mined just in 2023.<sup>8,9,10</sup>

The question of their continued supply can be answered by creating a circular economy. The 10RO framework developed by Reike et al. [25] has the following designation: R0- refuse, R1- rethink, R2- reduce, R3- reuse, R4- repair, R5- refurbish, R6- remanufacture, R7- repurpose, R8- recycle, and R9- recover. R0, R1, and R2 fall under short loop and relates to better manufacturing and utilization. In cases where this is not achievable, medium loops (R3-R7) are sought after, which deals with lifetime expansion of a product and its components. Long loops – R8 and R9 come next, where material value is recaptured. The framework is visualized in Figure 8.

<sup>8</sup> <https://online.kitco.com/fundamentals/platinum-investment>

<sup>9</sup> <https://learn.apmex.com/answers/how-much-platinum-is-in-the-world/#:~:text=There%20have%20been%20about%2010%2C000,reserves%20in%20the%20Earth's%20crust.>

<sup>10</sup> <https://www.statista.com/statistics/1170691/mine-production-of-platinum-worldwide/>

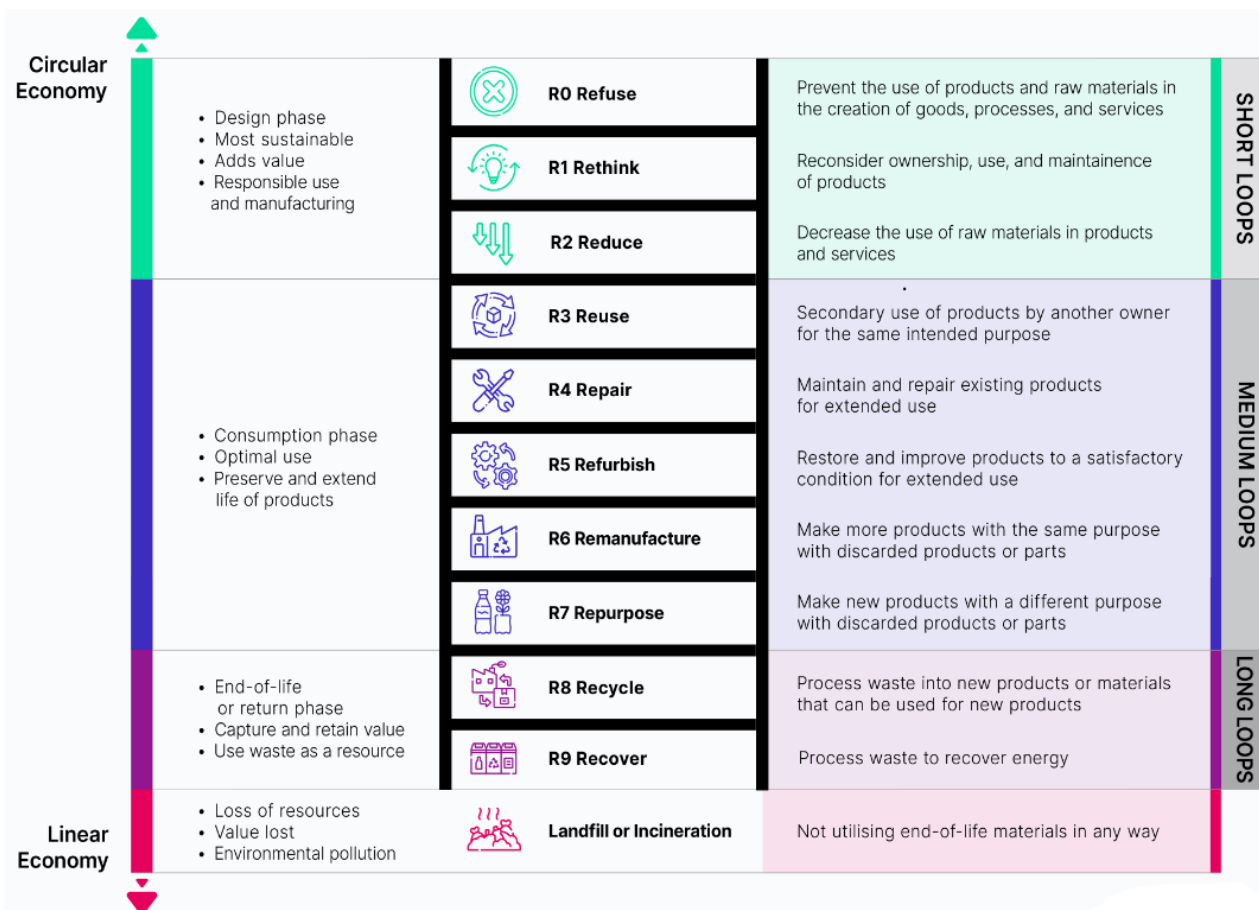


Figure 8: The 10R strategies for a circular economy (Source: <sup>11</sup>)

The lower the R number for an economy, the more circular it is. But it is to be noted that R9 is still better than the detrimental action of incineration or landfill, where no resource is recovered and pollution levels are raised. Especially for the present discussion of electrocatalysts and CRMs, applying all the R strategies wherever possible is highly desired. Dealing at the R9 level, there are many routes available for catalyst recovery and recycling, which primarily falls under the broad category of metallurgy. In brief, the metallurgical routes are sub-categorised as pyro-, hydro-, and bio-metallurgy. Many metal mining, refining, and recycling plants like Boliden AB, Anglo American Platinum Limited, Johnson Maththey PLC, Umicore N.V., etc. avail pyro- and hydrometallurgy techniques for both primary and secondary source-based production of catalysts. A detailed explanation for the recovery routes is covered in the literature analysis section and those that can be incorporated in existing plants is discussed in this thesis.

## 1.2. THESIS DOCUMENT GUIDE

The current thesis recognizes the potential of AEMWE technology in hydrogen production and takes advantage of its infancy to propose various strategies to recycle Platinum, Nickel, and Cobalt, which can then be implemented industry wide. After presenting the literature study that expands on the working principle of the electrolyser, different state-of-the-art electrocatalysts and material retrieval strategies available in Chapter 2. LITERATURE ANALYSIS, the scope is presented in Chapter 3. RESEARCH QUESTION FORMULATION. In Chapter 4.4. EXPERIMENTAL WORK, the report delves into the experimental section of the thesis that was performed to showcase basic anion exchange membrane degradation and convey the relevance of catalysts. As the title suggests, “Chapter 5. RETRIEVABLE CRM PREDICTION FROM 2035-2050” model the CRM exhaustion. Using global aviation hydrogen demand data and electrolyser model equipment specifications from

<sup>11</sup> <https://www.circularise.com/blogs/r-strategies-for-a-circular-economy#:~:text=Enter%20the%2010%20R%2DStrategies.R8%20Recycle%20and%20R9%20Recover.>

the leading AEMWE company, Enapter, the recyclable amount estimates for Platinum, Nickel, and Cobalt from 2035-2050 are provided. “Chapter 6. BENEFIT ANALYSIS OF THE CATALYST RECOVERY STRATEGIES” navigates through available recovery strategies, assessing them using benefit analysis. The thesis report comes to an end with a summarization of the chapters in Chapter 7. CONCLUSION, and a provision of recommendations in Chapter 8. GUIDELINES FOR FUTURE WORK.

## 2. LITERATURE ANALYSIS

For understanding the role that catalysts play in water electrolysis, the working principle and the components of an AEMWE cell must be known. Then the ways in which catalysts are developed for alkaline media and the role CRMs play in this must be understood. Following this, ways of recovery available in the industry must be known. To achieve this comprehension, this chapter has three distinctions - first, the components and working of an AEMWE cell are described. Next, the reader is presented with various state-of-the-art catalysts and then, descriptions of the several metal recovery techniques available are explored.

### 2.1 ANION EXCHANGE MEMBRANE WATER ELECTROLYSER CELL

Being similar in its working to PEMWE, AEMWE comprises similar components with the obvious difference in the membrane material. An exploded view of a lab-scale AEMWE cell is presented in Figure 9.

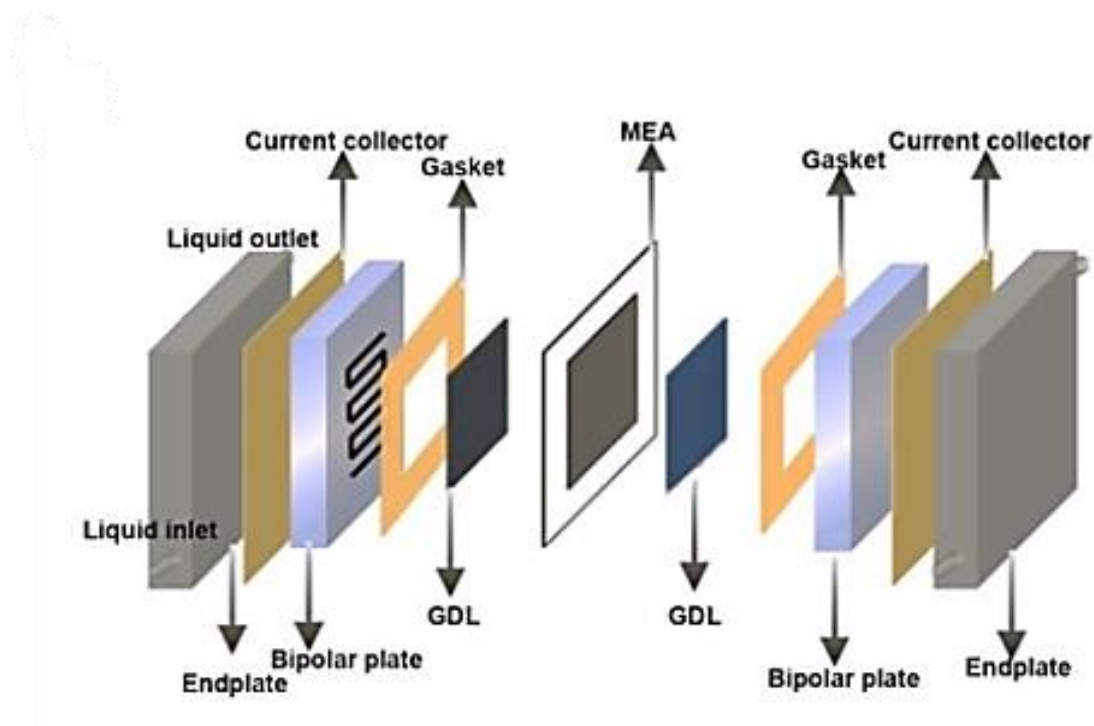


Figure 9: AEMWE exploded view (Source: [19])

Beginning at the outer ends, the electrolyser has the end plates, the current collectors, the bipolar plates in which flow channels for the electrolyte are present, gaskets, transport layers, catalyst layers and the anion exchange membrane. The gas diffusion layers, catalyst layers and the membrane together are considered the core of the electrolyser cell and are collectively called the Metal Electrode Assembly (MEA). A brief description of the components is presented below.

#### 2.1.1. ENDPLATES

The function of the endplates is to hold the entire set-up together with the help of bolts and provide necessary compression. They are usually made of stainless steel or aluminium. The material choice is defined by the working temperature of the electrolyser (60-80°C) and good alkaline stability in case of leakage. Stainless steel has better stability compared to Aluminium [22].

## 2.1.2. CURRENT COLLECTORS

Power to the electrolytic cell is supplied via the current collectors by means of leads connected to a potentiostat. Gold-plated copper is used as it provides high electrical conductivity, thus reducing the resistance input to the overall cell [22].

## 2.1.3. BIPOLAR PLATES

Made from alkaline-compatible metals like nickel or stainless steel, the flow fields channelize the electrolyte to and from the cell. Owing to the passivation of nickel from oxidation and the iron impurities from stainless steel leading to an increase in the OER kinetics in systems using Ni and Co catalysts, switching to the conventional Pt or Au coatings can cause a fairly stable contact resistance value [22].

## 2.1.4. GASKETS

Next to the bipolar plates are the gaskets that frame the MEA components. Polytetrafluoroethylene (PTFE) is chosen due to its thermal and chemical inertness, low coefficient of friction, availability, excellent insulation, good compressibility, manufacturing ease, and resistance to corrosion. The gaskets provide necessary compression to the cell [26][27]. Depending on the pressure needed, the gasket thickness on the cathode and the anode side can be varied. It is key to remember that gaskets are used when ambient pressure is maintained. Industrially, sophisticated machinery is required to supply the needed pressure [22].

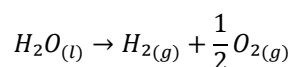
## 2.1.5. TRANSPORT LAYERS

Transport layers, also known as gas diffusion layers (GDL) or porous transport layers (PTL), give structural support, allow for the circulation of the fluid reactants and products – electrolyte, cathodic hydrogen, and anodic oxygen, and prevent electron and gas crossover [22][28]. Being in contact with the electrolyte, they must be alkaline-compatible. They must also facilitate electron movement between the current collectors and catalyst particles. This requires them to be electrically conductive, and they should also not block the active sites of the catalyst. At the anode half, GDL/PTL must endure large potentials often exceeding 2V. Given these requirements, the materials used are meshes made from nickel or its alloy and stainless steel. Carbon paper is used on the cathode side alone. In the anodic half, the high potentials combined with the high pH oxidises and degrades the carbon GDL.

Adding a microporous layer (MPL) at the interface of the PTL and catalyst leads to enhanced electronic and ionic contacts and better site accessibility. The difference between MPL and GDL lie in their size. The MPL thickness is in the micrometre range and it possesses smaller mesh dimensions [22].

## 2.1.6. ELECTROCATALYST LAYERS

The role of the electrocatalyst is to lower the activation barrier associated with the water-splitting reaction [29].



For the above water electrolysis reaction to take place at standard pressure and temperature, a thermodynamic lower energy limit given by  $\Delta G=237.2$  kJ/mol is required. Practically, it translates to 33 kWh to produce 1 kg of hydrogen at 1.23 V. In reality, due to the losses incurred during the electrolyser's operation, operating voltages ranging from 1.60 to 2.00 V are observed [30]. The role catalysts play in reducing the activation energy, and hence, the overall cell potential is depicted in Figure 10. In general, different catalysts are employed for the cathodic and anodic half-cells to facilitate the different kinetics pertaining to each half.

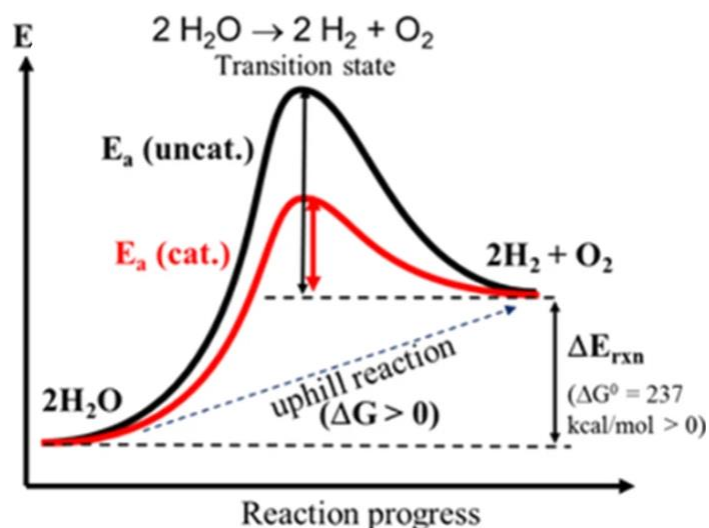
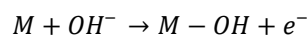


Figure 10: Role of electrocatalysts (Source: [29])

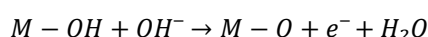
### 2.1.6.1. OER and HER kinetics

#### 2.1.6.1.1. Oxygen Evolution Reaction kinetics

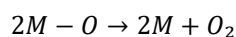
The oxygen evolution occurs at the anode and is a 4-electron process. A lot of intermediates are involved in this process. The first step involves M-OH formation from OH<sup>-</sup> adsorption on the electrocatalyst.



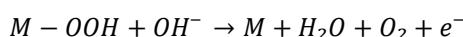
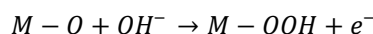
This intermediate couples with another OH<sup>-</sup> to generate M-O.



Oxygen then evolves by the diffusion of two M-O, given by,



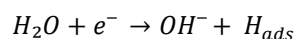
In an indirect route, the M-O intermediate couples with an OH<sup>-</sup> to give M-OOH, which in turn couples with another OH<sup>-</sup> in a proton-coupled electron transfer to produce oxygen.



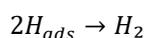
Because of the amount of complex steps involved, oxygen evolution kinetics is relatively slow, and a lot of research revolves around developing stable and efficient OER electrocatalysts [31].

#### 2.1.6.1.2. Hydrogen Evolution Reaction kinetics

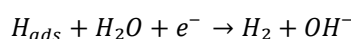
In an electrolyser, hydrogen evolves at the cathode in a 2-electron process. In alkaline medium, this occurs via the Volmer step, followed by the chemical Tafel step or the electrochemical Heyrovsky step. In the Volmer step, a water molecule reacts with an electron to generate an adsorbed hydrogen atom (H<sub>ads</sub>) on the electrocatalysts.



This H<sub>ads</sub> can then combine with another H<sub>ads</sub> to produce hydrogen, termed the Tafel step.



The H<sub>ads</sub> may also react with an electron and a water molecule to produce hydrogen. This route of hydrogen production is called the Heyrovsky step.



Prior to hydrogen adsorption, the tightly bound H-O-H bond must be broken. Hence, hydrogen binding energy, water dissociation ability, water adsorption on active sites, and aqueous OH<sup>-</sup> adsorption are the main factors that determine HER kinetics [31].

### 2.1.6.1.3 Catalyst performance metrics

A catalyst's performance is measured in terms of its overpotential, mass/specific activity, turnover frequency, stability, and Faradaic efficiency.

The overpotential,  $\eta$ , is defined as the difference between the applied potential,  $E_{\text{applied}}$ , and the thermodynamically defined potential,  $E_0$ , for a particular current density under equilibrium.

$$\eta = E_{\text{applied}} - E_0$$

For the comparison between electrocatalysts (both OER and HER), a current density of 10 mA/cm<sup>2</sup> is considered the benchmark. This value takes into account the photoelectrochemical water-splitting efficiency of 12.3% [31].

It is also crucial to include the resistance contributed by conducting the ions and electrons, named the ohmic resistance,  $iR$ . The ohmic corrected overpotential is then given by,

$$\eta = E_{\text{applied}} - E_0 - iR$$

### Mass activity

At a given overpotential, the mass activity is the normalization of current based on the electrocatalyst's mass loading. This value has more importance when evaluating critical metals as more activity would imply lesser amount of catalyst [31].

### Specific activity

Specific activity is the normalization of current per unit surface area. The selected area can either be the Brunauer-Emmet-Teller (BET) surface area or the electrochemically active surface area (ECSA). Generally, ECSA is chosen for SA normalization because it takes into account the active sites available for the catalyst as opposed to BET which relies on nitrogen adsorption and desorption sites which, in reality, may or may not be available for the catalyst [31].

### Tafel slope and exchange current density

The Tafel equation is given by,

$$\eta = m_T \ln j_0 - m_T \ln j$$

The current density,  $j$ , is given by the Butler-Volmer equation, which is the total of the oxidation and reduction reaction currents,

$$j = j_0 \left( e^{\frac{\alpha n F \eta}{RT}} - e^{\frac{(1-\alpha) n F \eta}{RT}} \right)$$

Where,  $\alpha$  is the charge transfer coefficient,  $F$  is Faraday's constant,  $R$  is the universal gas constant, and  $n$  is the number of transferred electrons.  $j_0$ , termed the exchange current density, is another intrinsic parameter which is proportional to the reaction rate measured at equilibrium when the cathodic and anodic currents are equal, i.e., total current = 0. Higher  $j_0$  values indicate lower driving forces to start a given reaction due to enhanced charge transfer reactions. The response sensitivity of the current to an applied overpotential can be gleaned from the Tafel slope,  $m_T$ . It is calculated as follows,

$$m_T = \frac{RT}{n\alpha F}$$

The lower the Tafel slope, the lower the  $\eta$  needed to obtain the same  $j$ , implying faster electron transfer kinetics [31][30]. The Tafel slope can be obtained from voltammograms of Linear Sweep Voltammetry (variation in

current at the working electrode when the potential is varied linearly). E.g.: Figure 11 and Figure 12 show the LSV voltammograms and the corresponding Tafel plots for Pt,  $\alpha$ -Ni(OH)<sub>2</sub>-Pt, and  $\beta$ -Ni(OH)<sub>2</sub>-Pt.

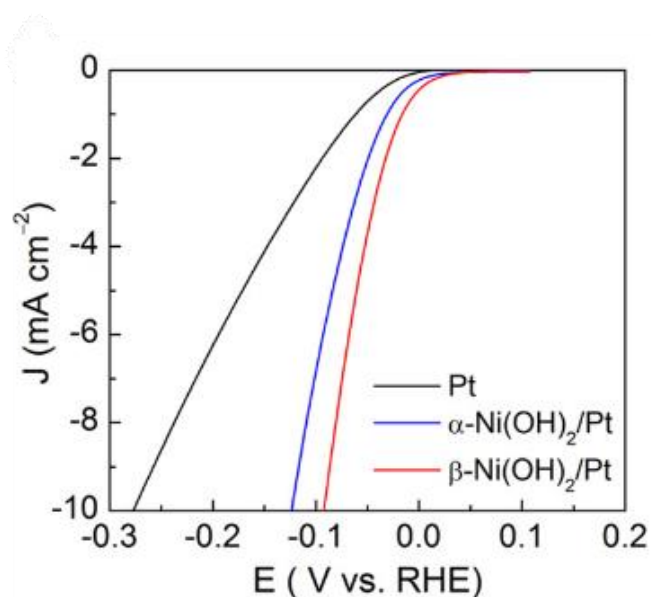


Figure 11: LSV curves for Pt,  $\alpha$ -Ni(OH)<sub>2</sub>/Pt,  $\beta$ -Ni(OH)<sub>2</sub>/Pt (Adapted from [30])

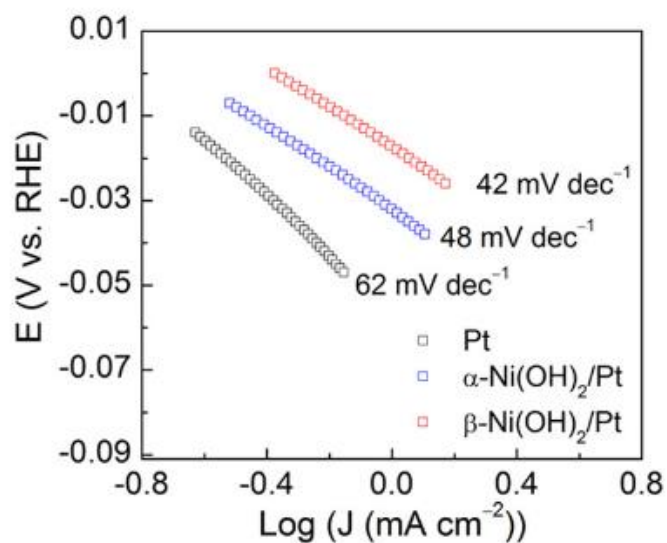


Figure 12: Tafel plots for Pt,  $\alpha$ -Ni(OH)<sub>2</sub>/Pt,  $\beta$ -Ni(OH)<sub>2</sub>/Pt (Adapted from [30])

### Turnover frequency (TOF)

Turnover frequency is the rate of conversion of reactants into products, per active site per second. Numerically, it is calculated using the equation,

$$TOF = \frac{jN_{av}}{nF\Gamma}$$

where,  $j$  is the current density,  $N_{av}$  is the Avogadro number,  $n$  denotes the number of participating electrons,  $F$  represents Faraday's constant, and  $\Gamma$  is the active site concentration [30].

### Faradic efficiency

An electrocatalyst's selectivity is determined from its Faradic efficiency value, which is the ratio of the target gas produced to the theoretical prediction [31].

## Stability

A durable catalyst is required for ensuring higher AEMWE lifetimes. The catalyst stability is affected by material degradation, passivation of the surface, catalyst layer delamination, and corrosion [31]. Metrics such as MEA and catalyst layer lifetime and more recently, the S-number ( $\frac{\text{amount of produced oxygen/hydrogen}}{\text{amount of dissolved catalyst metal}}$ ) are good indicators of a catalyst's stability [28].

## Volcano plot

The catalytic activity in a reaction can be characterized via volcano plots. It involves the calculation of the change in Gibb's free energy of the intermediates formed during OER and HER. It is based on Sabatier's principle that states that the adsorption energy of an ideal electrocatalyst must not be too low nor too high in comparison to the formed intermediate, i.e., the closer the value of  $\Delta G$  is to zero, the better the catalytic activity [30][32]. This implies that the rate of the reaction is low at very weak and very strong adsorptions. Weak adsorption/binding strength indicates the slow formation of the intermediates, whereas a higher adsorption/binding strength means that the release of the formed intermediates would be slow [33][34]. The plot is generally constructed by plotting either the current density or the overpotential against  $\Delta G$  of the intermediates. The HER and OER Volcano plots are displayed in Figure 13 and Figure 14, respectively. It can be observed that Platinum dominates as the HER catalyst. In the non-PGM category, Nickel and Cobalt display good HER activity. In OER, oxides of cobalt and nickel can be seen exhibiting higher catalytic values than their commonly used PGM ( $\text{IrO}_2$ ) counterparts [32].

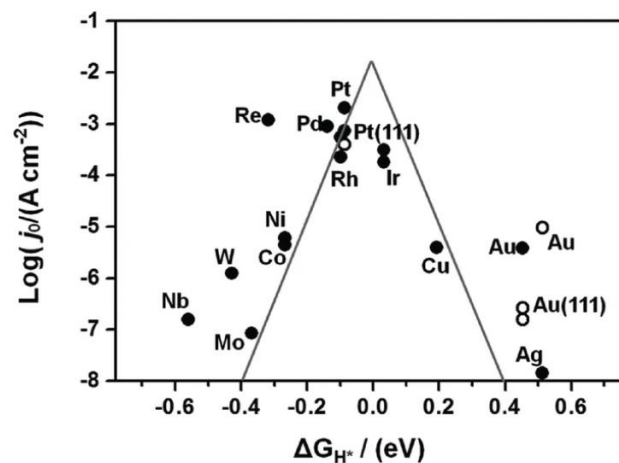


Figure 13: HER volcano plot (Source: [35])

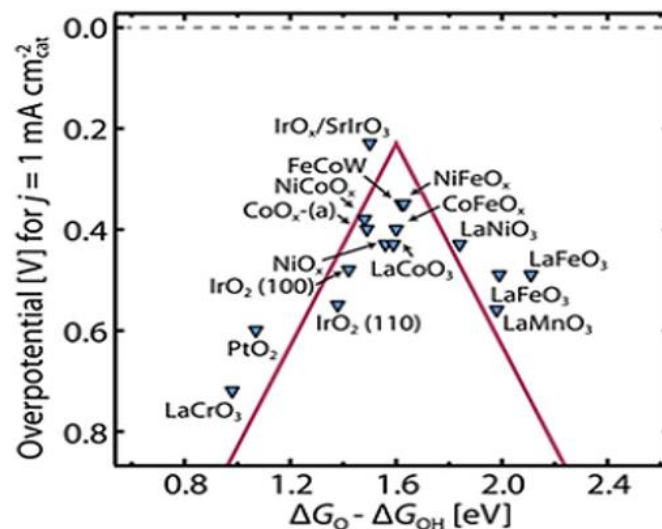


Figure 14: OER volcano plot (Source: [32])

## 2.1.7. ANION EXCHANGE MEMBRANE

The purpose of the membrane is to transport the ions of interest and water, prevent crossover by blocking the gas generated and give anode-cathode distinction. Since  $\text{OH}^-$  are the ions of interest in alkaline water electrolysis, anion exchange membrane are made from polymer backbones attached with positive functional groups [36]. The backbones are usually polyolefin-based – polystyrene, polyethylene, polytetrafluoroethylene, polynorborene; poly(arylene ether)-based – poly(arylene ether ketone), polyphenylene oxide, poly(arylene ether sulfone); or backbones having cationic moieties – poly(phosphazene), poly(benzimidazole). The positive moieties are made from alkaline-stable groups like benzyl trimethylammonium, tertiary diamines, quaternary ammonium, imidazolium, cobaltocenium, phosphonium, guanidinium, etc. Quaternary ammonium is popular owing to its high ionic conductivity [28].

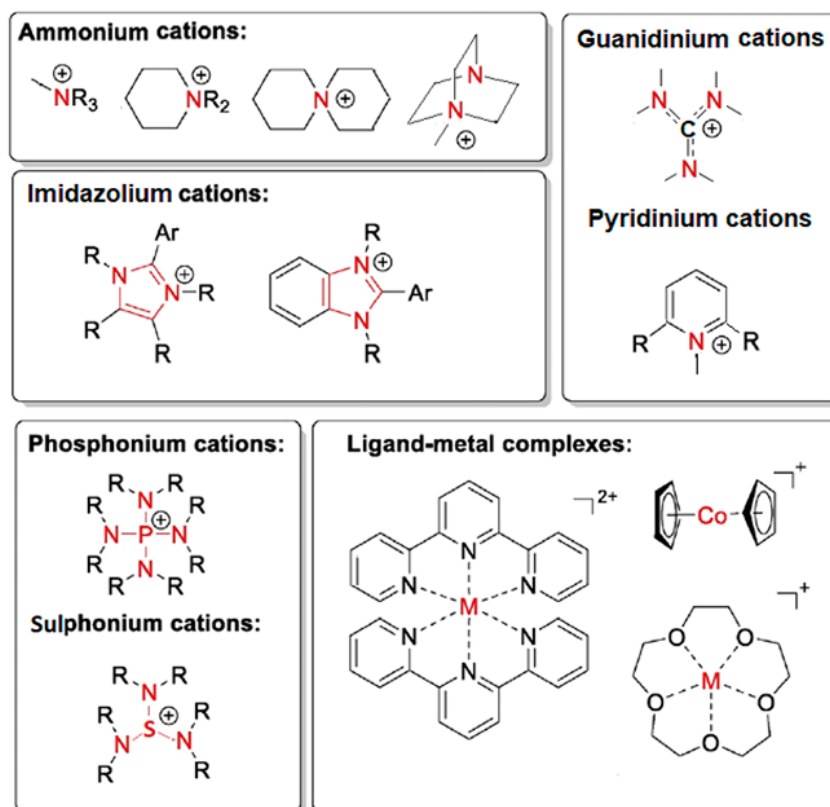


Figure 15: Common alkaline-stable AEM cations (Reproduced from [28])

Key membrane performance metrics include its thickness, water uptake, swelling ratio, ion conductivity, ion exchange capacity (maximum amount of ions that can be exchanged), and its mechanical, electrochemical, and thermal stabilities. Some well-known commercial anion exchange membranes include FAA3 by Fumatech, the AEMION series offered by Ionomr, TM1 by Orion, and Sustainion membranes by Dioxide Materials [37]. Of these, till date, the best performance has been achieved by Sustainion 37-50 which maintained a stable  $1 \text{ A/cm}^2$  current density at an applied voltage of 1.85 V over 10,000 cycles with a degradation rate of just  $1 \mu\text{V/hr}$  [38]. The polymer chemistry of Sustainion is based on poly(4-vinylbenzyl chloride-co-styrene) chemistry (see Figure 16). The presence of styrene makes these membranes really brittle in their dry state. To combat this, the company offers “classic Sustainion” which has a water-soluble plasticizer [37].

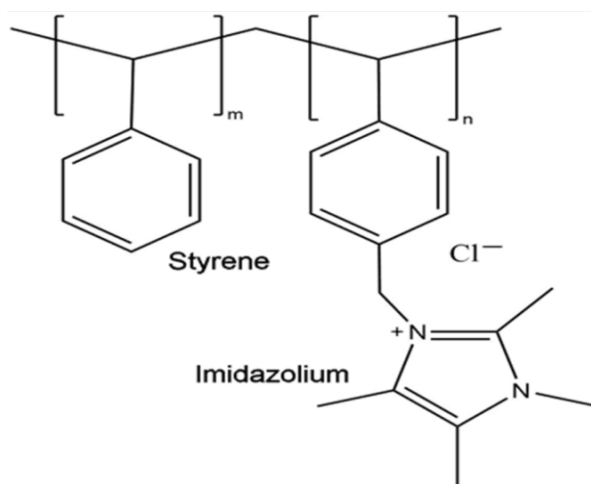


Figure 16: Sustainion structure (Source: [39])

The major drawback that must be addressed while designing an AEM is its alkaline stability. When coupled with the fact that these membranes are run at temperatures  $\geq 40^\circ\text{C}$ , alkaline degradation is exemplified following the van't Hoff rule which expounds a doubling of the rate of a chemical reaction for every  $10^\circ\text{C}$  raise in temperature [37]. Some of the degradation mechanisms identified include nucleophilic addition and displacement (pyridinium), ring opening (N-spirocyclic ammonium, imidazolium), Hofmann  $\beta$ -elimination substitution, nucleophilic  $\text{S}_{\text{N}}2$  benzyl substitution,  $\text{S}_{\text{N}}2$  methyl substitution, dehydrofluorination of the backbone, etc. Of these, Hofmann elimination and nucleophilic substitution are observed in quaternary ammonium containing AEMs (see Figure 17) [28].

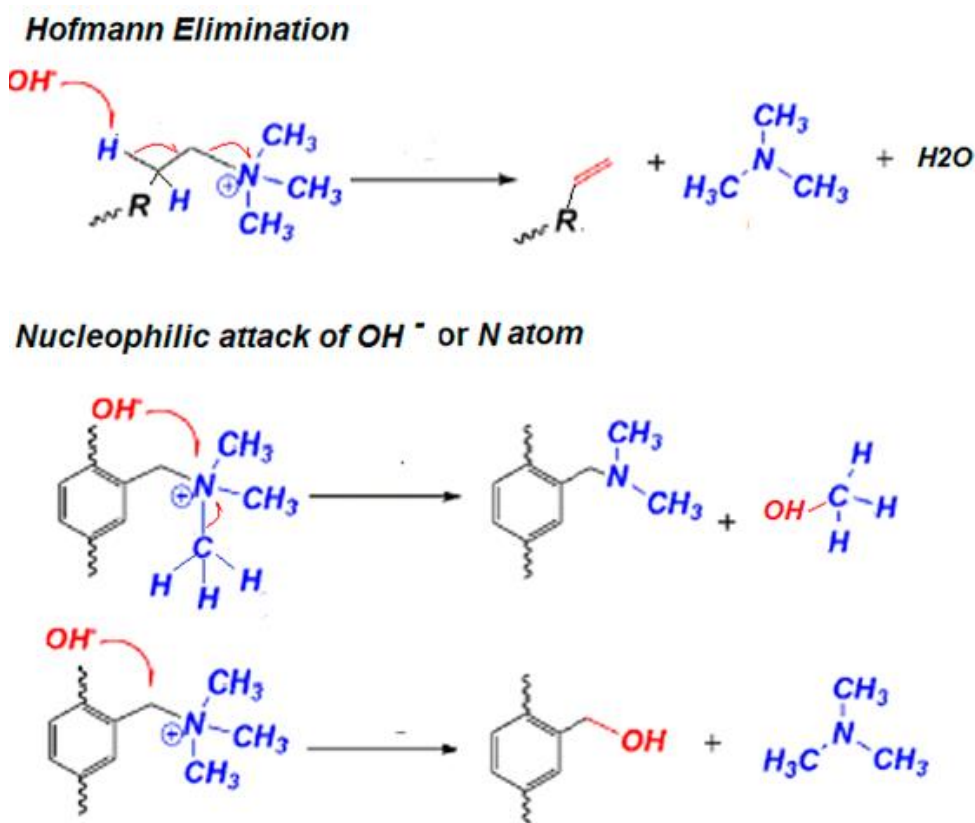


Figure 17: Alkaline degradation mechanisms in QA groups (Source: [28])

### 2.1.7.1. Parameters affecting AEMWE

The cell output is influenced by temperature, flow rate, electrolyte concentration, and the applied voltage.

Higher temperatures lead to increased OH<sup>-</sup> mobility, thereby decreasing the charge transfer resistance, leading to better cell performance. But because the glass transition temperature of the commonly used AEM polymers is ~60°C, operating temperatures must be maintained below this limit.

Increasing the flow rate removes the hydrogen and oxygen bubbles formed on the GDL surface, thus reducing the charge transfer and ohmic resistances. Conversely, very high flow rates (typically greater than 40 mL/min) reduce the contact between the OH<sup>-</sup> ions and the catalyst surface, increasing the ohmic resistance.

Higher electrolyte concentrations also enhance the cell's performance. Increasing concentrations imply higher amounts of OH<sup>-</sup> ions available and a corresponding decrease in the charge transfer resistance.

When it comes to the applied voltage, increasing the voltage increases the energy available for crossing the activation barriers for electron transport via the external circuit and OH<sup>-</sup> transport via the membrane. It is observed that charge transfer resistance dominates in the lower voltage range (1.5-1.7 V) and ohmic resistance is the key player at higher voltages of 1.8-2.2 V. Above 2.1 V, the ohmic resistance is observed to increase sharply, indicating catalytic degradation or bubble formation [40].

## 2.2. STATE-OF-THE-ART AEMWE ELECTROCATALYSTS

### 2.2.1. DESIGN STRATEGIES

Porosity is a coveted property in catalyst design as it leads to increased active sites for adsorption, aids fast bubble detachment and provides supplementary bubble flow channels. This is by virtue of the increased surface roughness that generates superaerophobicity, thus reducing the bubble adhesion. Intrinsic activity can also be increased by controlling the binding energy of the active sites by adding intermediates, tuning their electronic structures, and developing dual active sites. Increasing the wettability via phase engineering and superhydrophilicity is another technique that increases site accessibility. To address the stability requirement, self-supported electrodes that enhance the substrate-catalyst dynamics and catalyst encapsulation by carbon can be adopted. Finally, self-supported catalysts developed on conductive substrates (Ni foam, carbon cloth, carbon fiber, Cu foam, etc. [31]) lead to rapid mass and charge transfer kinetics [41].

**Alloying:** Alloying is a simple design technique which includes adding non-metallic inclusions in metals via vapor deposition, melting, or sintering; or the diffusion of the atoms of two or more metals. Choosing synergetic metal compositions can tailor selectivity and activity. The surface area and mechanical strength are also enhanced through refined grain size. Also, combining non-precious metals with precious metals can reduce the amount of either metal used, thus reducing the cost [42].

**Amorphization:** Modulating the amorphous phases at short-range atomic scales increases the active site density of a catalyst [30][42].

**Facet engineering:** A catalyst's performance varies depending on its exposed surface's facet because of the variance in the adsorption capacity. Preferentially developing the facet required for targeted reactions can reduce the catalyst amount needed [30][42].

**Nanoarchitecture:** Hollow structures, core-shell structures, nanowires, nanosheets, nanoparticles, etc. are some of the morphologies that fall under nanoarchitecture. This design strategy is deemed the most effective as there is a tremendous increase in the ECSA owing to the increase in the active sites and better electrolytic contact [30][42].

**Atomic doping:** Another widely adopted strategy is doping where via the inclusion of non-metallic or metallic elements in the catalyst lattice, its electronic structure and ergo its properties are modified [30].

**Defect engineering:** Intrinsic defects including plane defects, line defects, volume defects, and point defects, form dangling groups that alter the surface and electronic properties (e.g., electronic density), thereby increasing chemical reactivity [30].

**Interface engineering:** In hybrid materials made up of two or more elements, also referred to as heterostructures, the interface exhibits distinct chemical and physical characteristics that dictate a catalyst's capacity to adsorb, convert, and transfer the intermediates, adsorbents, and electrons. Experimental observations of the electronic property modulations and enhanced electron transfer at the interface, signify the need for better interface creation [42].

**Polymorph engineering:** Polymorphs are varying crystal forms of the same compound. As explained, modifying the atomic scale arrangement (in this case, transforming the crystalline phase) leads to increased catalytic activity.

From an electrochemical design perspective, Kanokkanchana et al. [43] have published an extensive review and suggest catalyst design strategies for effective OER, HER, ORR, etc.

### *2.2.1.2. PGM-based electrocatalysts:*

For both acidic and alkaline electrolytes, Platinum dominates as the HER catalyst. In fact, with a measured ECSA of  $62 \text{ m}^2/\text{g}_{\text{Pt}}$ , commercial 46 wt% Pt/C is considered the benchmark catalyst for evaluating novel electrocatalysts. Combining Pt with Ni, like growing  $\text{Ni}(\text{OH})_2$  clusters on Pt(111) demonstrated an 8-fold intrinsic activity increase due to hydrogen spillover mechanisms. Platinum is also alloyed with other PGMs like Ru. Of particular interest is the  $\text{Pt}_1\text{Ru}_{1.54}$  alloy which exceeded Pt/C performance owing to electronic interactions [28].

Next to platinum, iridium is used widely for its OER performance. Like Pt/C for HER,  $\text{IrO}_2$  sets the benchmark for OER. One particular powder of iridium oxide displayed  $275 \text{ A/g}$  mass activity at a Tafel slope of  $0.35 \text{ V}$ . Recently, Lu et al. [44] developed organically capped Ir nanoparticles that served as a bifunctional catalyst capable of outperforming the Pt and Ir benchmarks. A low cell voltage of  $1.495 \text{ V}$  was needed to produce a  $10 \text{ mA/cm}^2$  current density.

Oxides of Ru ( $\text{RuO}_2$  in particular) are also preferred OER choices [28]. In addition, recent design developments have led to better performing catalysts. E.g., Ru-NG750 and Ru- $\text{Fe}_3\text{O}_4/\text{C}$  have Tafel slopes of  $8 \text{ mV}$  and  $11 \text{ mV}$ , respectively, in  $1 \text{ M KOH}$  [45].

Palladium [46], rhodium [47], and osmium [48] can also be employed as electrocatalysts for acidic and alkaline media, but compared to their counterparts, their usage in alkaline water electrolyser cells is limited.

### *2.2.1.3. Non-PGM based catalysts*

To shift away from PGM, the research focus on transition metals and their various forms, including oxides, phosphides, (oxy)hydroxides and alloys, increased. Especially, Ni, Co, Fe, and Mn are coveted for their use as excellent bifunctional catalysts in alkaline media [49]. In particular, oxides of nickel have shown higher activity, with higher valence states exhibiting better OER activity [50]. Combining Ni, Fe, and Co in a Metal Organic Framework, Abdelhafiz et al. [51], developed OER catalysts and performed experiments in an industrial AEMWE cell under industrially expected current densities of  $750$  and  $1000 \text{ A/cm}^2$  and recorded stable performance for 550 hours. In-situ characterization attributed the performance to metal oxygen vacancy formation and oxygen-metal covalency. The research done on Co, Mn, and Fe can be followed in [52], [53], and [54].

Rare earth elements have also been used, either in combination with both PGM [55][56] and non-PGM [57][58] elements as alloys or polycrystalline oxides, or also on its own as single metal oxides [59].

### **Key takeaway**

Though AEMWE is emphasized for its advantage of non-PGM based catalysts, the shift from PGM to non-PGM catalysts is gradual. Moreover, even non-PGM based catalysts still incorporate some quantities of PGM. Even in the non-PGM realm, developments of Ni, Co, Fe, and Mn stand out, amongst which Ni, Co, and Mn fall under the EU's CRM category.

As discussed, to realize an ideal circular economy, the R0-R7 (short and medium loops) of the 10R0 framework are preferred. Unless there is a major breakthrough in catalyst and/or AEMWE technology, this is not possible. Hence, the R8 and R9 routes of recapturing the material's value must be explored. To this end, the upcoming section deals with the different strategies available.

## 2.3. MATERIAL RETRIEVAL STRATEGIES

In this section, the various industrial and emerging strategies for the recovery of metals are explored. In general, there are three steps involved – pre-treatment, enrichment, and refinement. Pre-treatment is carried out for reducing the particle size, activation, and/or removing the impurities. Enrichment, as the name suggests, leads to a more enriched or concentrated metal form, followed by refinement, in which the metal is recovered from the product of the enrichment phase [60]. The most commonly employed technologies across all three stages are pyro-, hydro-, and bio-metallurgy. Pyro- and hydro-metallurgy are collectively referred to as extractive/chemical metallurgy [61].

### 2.3.1. PYRO-METALLURGY:

Pyrometallurgical methods involve subjecting the feedstock to elevated temperatures for retrieving the metals of interest. Techniques such as chlorination, carbothermic roasting, smelting, pyrolysis, etc. exist [62]. Out of these, the most availed industrial process is smelting. Here, the feedstock is mixed with flux components, reducing agents and metal collectors at temperatures above  $1000^{\circ}\text{C}$  in a furnace to produce precious metals-enriched alloys. The role of the flux is to produce low-viscosity molten phase called the slag which melts the non-metallic catalyst supports. Commonly used fluxes include  $\text{CaO}$  and  $\text{Na}_2\text{CO}_3$ . Collectors are generally base metals such as copper, lead, or nickel that combine with the precious metals to form alloys. The molten phase that contains this alloy is termed the matte phase. Further refining can be used to get the pure metals [63]. The smelting process using copper as the collector is shown in Figure 18.

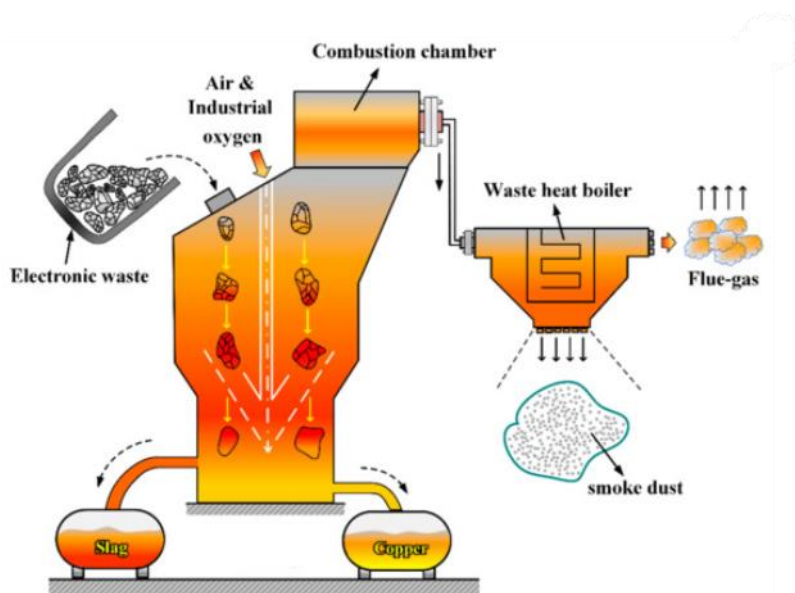


Figure 18: Smelting using copper collector (Adapted from: [64])

The recyclability of spent catalysts is influenced by three main factors: the metal concentration, the nature of the materials supporting the catalysts, particularly the presence of refractory substances and wash coat additives, and the level of impurities that vary with the catalysts' uses. The uncomplicated operation, streamlined processing, and scalability has established pyrometallurgy as the front-runner in industries, alongside hydrometallurgy [63]. But it should be noted that pyrometallurgical processes are highly energy-intensive and lead to the emission of toxic gases [65].

### 2.3.2. HYDROMETALLURGY:

Hydrometallurgy/wet metallurgy is a technique that makes use of solvents for metal recovery via reactions including reduction, oxidation, coordination, replacement, hydrolysis, neutralization, etc. For enrichment, leaching is the most prevalent technique. Acids, bases, salts, water, and/or chelators can be used as the leachants that strip the metals from the feedstock. The metal-rich solution is then refined to recover the metal.

Hydrochloric acid, aqua regia, and sulphuric acid are some of the effective leachants. Hydrometallurgy also plays a major role in metal refinement via precipitation and electrowinning [66]. The processes are depicted in Figure 19.

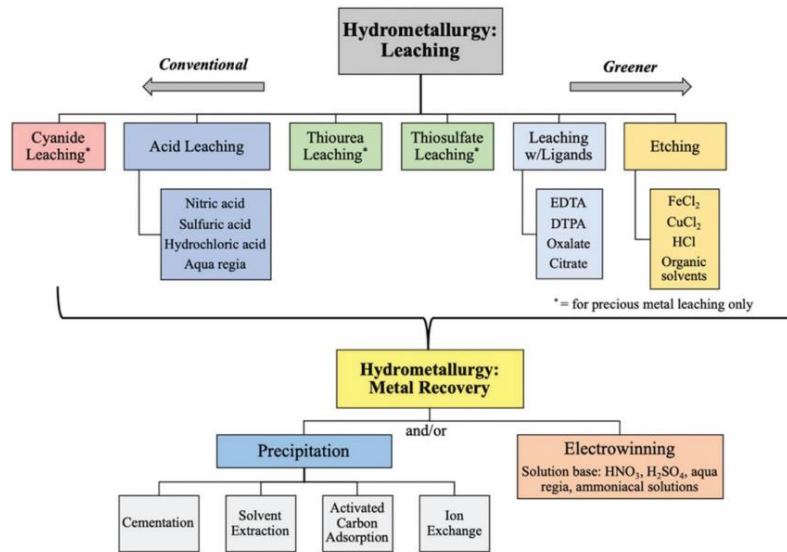


Figure 19: Hydrometallurgical processes (Adapted from: [67])

The main drawback of hydrometallurgical process is the use of copious amounts of highly concentrated acids/bases and the expenses related to the subsequent treatment of this chemical waste [65].

### 2.3.3. BIO-METALLURGY:

As an emerging branch of metallurgy, bio-metallurgy is the least developed of all the techniques. Nevertheless, given its green nature, the field holds a lot of potential. Like the name indicates, bio-metallurgy relies on the interaction between living organisms and metal constituents. The organisms range from various bacteria, fungi, archaea to plants. Bioleaching and bioaccumulation are the main routes availed.

Bioleaching involves the use of acidophiles (organisms that thrive in highly acidic environments) that produce lixivants upon interaction with the feedstock. The commonly used organisms are chemolithotrophs – capable of utilizing inorganic compounds for energy generation, chemoorganoheterotrophs – requiring organic compounds for energy generation, and cyanogenic organisms – capable of generating cyanide (Refer Figure 20) [68].

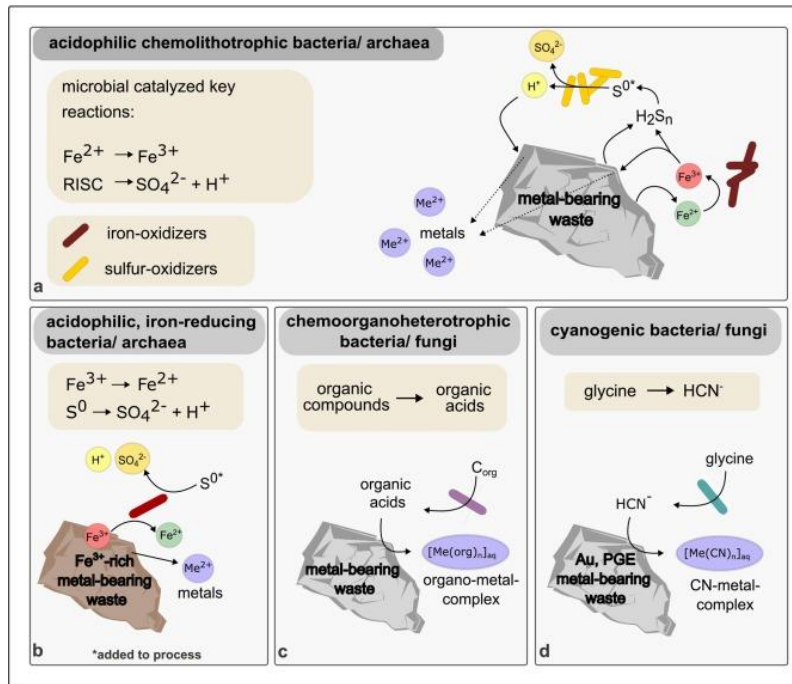


Figure 20: Organisms involved in bioleaching (Source: [68])

Oxidation, reduction, protonation and complexation of the feedstock are the ways in which lixivants are generated [69]. Figure 21 lists the common bioleaching species and the retrieval pathways they follow. Similar to hydrometallurgy, the costs associated with the treatment of the acid wastage is a major disadvantage of bioleaching. An in-depth explanation of the reactions involved in the various leaching pathways are given in the review of Srichandan et al. [65]

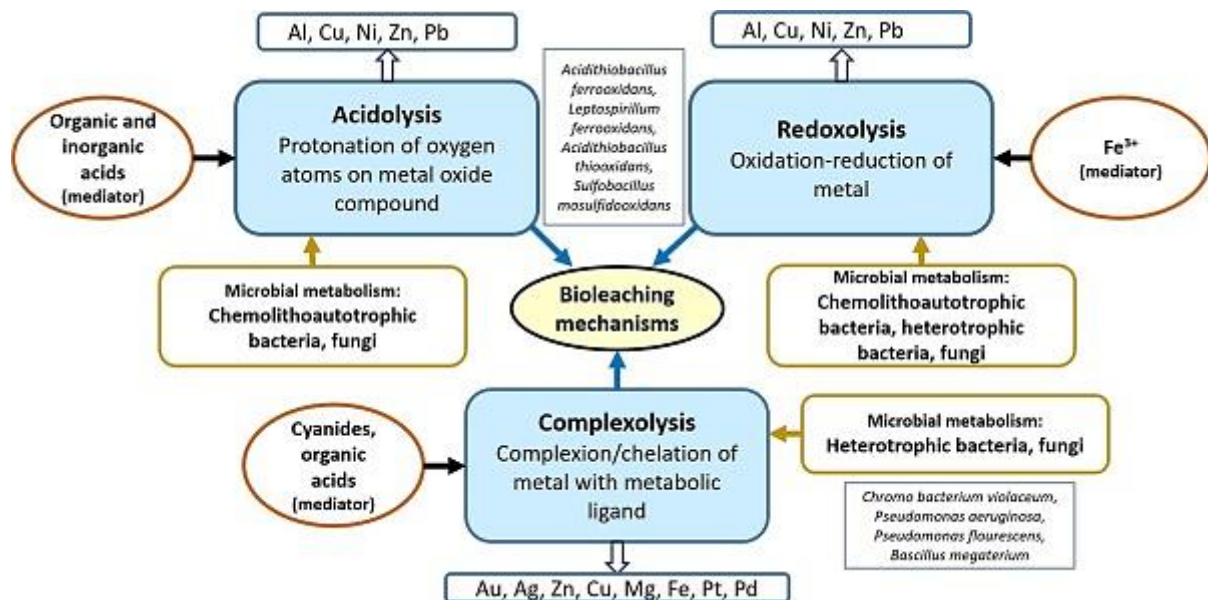


Figure 21: Bioleaching mechanisms (Source: [69])

In bioaccumulation, the importer complexes transport the metals via the lipid layers of the cell wall. Once in the intracellular space, peptide ligands and proteins facilitate the sequestration of the metals. This metabolically active process should not be confused with biosorption which involves the adsorption of metals through the cell wall via chelation, ion exchange, and/or physical interactions [70]. The biosorption and bioaccumulation mechanisms are depicted in Figure 22.

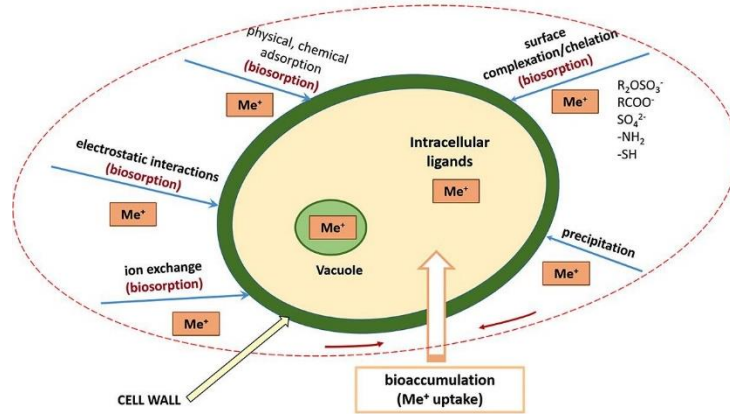


Figure 22: Bioaccumulation mechanisms (Source: [69])

# 3. RESEARCH QUESTION FORMULATION

## 3.1. KNOWLEDGE GAP AND RESEARCH OBJECTIVE

The overarching objective of the current work is to contribute to sustainable aviation. This goal can be achieved by analysing the production level of the broadly accepted green fuel – hydrogen. From meticulous literature evaluation of the trends in PEMWE and state-of-the-art research focus in AEMWE technology, it has been established that hydrogen production by AEMWE is economically favored. Even then, catalysts that are being developed for alkaline electrolysis still make use of elements that have been deemed critical by the EU. Below presented metals are the top five AEMWE electrocatalyst candidates:

1. Platinum
2. Iridium
3. Ruthenium
4. Nickel
5. Cobalt

Current catalyst technology dictates that in the foreseeable future, platinum usage is indispensable. Nickel and cobalt are the frontrunners in transition-metal based OER and HER electrocatalysts. As seen from the volcano plots, Nickel and Cobalt-based catalysts already surpass the performance of Iridium-based candidates for alkaline electrolysis. This thesis therefore covers platinum recovery, followed by the non-PGM-based nickel and cobalt. The strategies discussed for platinum are also widely applicable for the recovery of the other PGM metals.

## 3.2. RESEARCH QUESTION

To attain the objective of environmental-friendly aviation at a fundamental level, the following research question can be used.

**What is the most viable retrieval strategy that mitigates the material demand of Platinum, Nickel, and Cobalt CRMs from AEMWE catalysts within the context of hydrogen in global aviation?**

This broad question can be answered using sub-questions that capture the research work executed.

1. *How much hydrogen would be required to meet the global aviation sector demands from 2035 till 2050?*
2. *How much CRM (Platinum, Nickel, and Cobalt) is exhausted in catalysts as a result of membrane degradation in AEMWEs used for hydrogen production?*
3. *What is the state-of-the-art in the strategies available for CRM retrieval?*

From the formulation of the questions, it is established that this thesis is applicable within a 15-year temporal bound with a global spatial boundary.

The first sub-question is covered by Chapter 5. RETRIEVABLE CRM PREDICTION FROM 2035-2050. Studies by different aerospace organizations are explored and the best prediction is selected.

The second question is addressed by Chapters 4. 4. EXPERIMENTAL WORK and 5. RETRIEVABLE CRM PREDICTION FROM 2035-2050. Availing the state-of-the-art commercial anion exchange membrane, Sustainion X37-50 Grade RT, lab-scale cell tests are performed, and the degradation behaviour recorded using Fourier transform infrared spectroscopy, thermogravimetric analysis, and chronopotentiometry measurements. This can be viewed further in Chapter 4. Chapter 5 delves into the exhausted CRM prediction for platinum, nickel and cobalt based on the hydrogen needs of the global-aviation industry from 2035-2050.

The final sub-question is answered in Chapter 6. **BENEFIT ANALYSIS OF THE CATALYST RECOVERY** by analysing the current industry practices in recycling and weighing them against emerging techniques via a benefit analysis.

# 4. EXPERIMENTAL WORK

To stress the importance of CRM retrieval, the degradation rate of Sustainion X37-50 Grade RT was studied. As evidenced from the literature review, at the time of writing this thesis, Sustainion is the best performing AEM in the market with the ability to maintain a current density of  $1 \text{ A/cm}^2$  over 10,000 hours at 1.85 V. A degradation rate of less than  $1 \mu\text{V/hr}$  was observed [38]. This chapter explains the methodology followed, the variables obtained and provides an interpretation of those variables to better understand membrane degradation.

## 4.1. MATERIALS

Sustainion X37-50 Grade RT, with an ethylene glycol plasticizer – anion exchange membrane with a dry thickness of  $50 \mu\text{m}$ . (Supplier - Dioxide Materials™, USA)

Potassium hydroxide (KOH) – for membrane activation and as the electrolyte in the electrolyser

De-ionized MilliQ water – for membrane storage to prevent membrane dehydration till use.

## 4.2. METHODOLOGY

### 4.2.1. MEMBRANE ACTIVATION

Sustainion in its dry state is present in  $\text{Cl}^-$  (chloride) form. For optimal performance, any ion exchange membrane is soaked in an electrolyte that contains the ion of interest. This is usually the electrolyte that is employed in the cell. For example, to be utilized in  $\text{CO}_2$  electrolysers, the membrane is soaked in sodium bicarbonate ( $\text{NaHCO}_3$ ) solution to be converted to its bicarbonate form ( $\text{HCO}_3^-$ ). For use in AEMWE, the electrolyte of choice is 1M KOH to emulate industrial standards [38].

### 4.2.2. DETERMINATION OF THE OPTIMAL RUNNING CONDITIONS

To determine the best activation time and electrolyte flow rate for Sustainion, three different soaking times - 24 hrs, 48 hrs, and 72 hrs; and 4 different KOH flow rates – 7.6 mL/min, 11.4 mL/min, 15.2 mL/min, and 19 mL/min were tested. (NB: These are the flow rates that corresponds to 40 rpm, 60 rpm, 80 rpm, and 100 rpm of the peristaltic pump employed in the experiments.) The optimal values were determined by means of chronopotentiometry using a lab-scale electrolyser cell. An operating temperature of industrially adopted  $60^\circ\text{C}$  was maintained [38].

### 4.2.3. ELECTROCHEMICAL CHARACTERIZATION

A laboratory-scale  $5 \text{ cm}^2$  electrolyser cell (supplied by Dioxide Materials) with serpentine flow channels for the electrolyte was used for the electrochemical characterization tests. Nickel foam was the material for both the cathode and the anode. Polytetrafluoroethylene (PTFE) gaskets of varying thicknesses provided insulation between the two electrodes. The anion exchange membrane was sandwiched between the anode and the cathode, and the cell was secured with nuts and bolts. The electrolyte (1M KOH) was stored in borosilicate glass containers and refreshed weekly to make sure that the concentration was not diluted with the formation of carbonate compounds. Tubes from the containers went to a peristaltic pump with a maximum of 100 rpm that controlled the electrolyte speed to and from the cathode and anode. The reason for using borosilicate glass was to ensure the durability of the containers when high temperature runs were performed. The containers were placed over heating plates to provide temperature control over the electrolyte, whereas a lab-made heating cell with a thermocouple ensured the precise heating of the MEA. The provision for heating was to maintain the cell at  $60^\circ\text{C}$ . A laptop with a software termed ‘NOVA’ controlled the potentiostat (that applies the required voltage or current) and the booster (for signal amplification). The sense and working electrode leads of the potentiostat were connected to the anode. The inert and counter electrode leads were connected to the cathode. Data acquisition and storage was done via NOVA. The entire set-up is shown in Figure 23. The cross-section of the MEA with the membrane is presented in Figure 24.



Figure 23: Laboratory-scale AEMWE

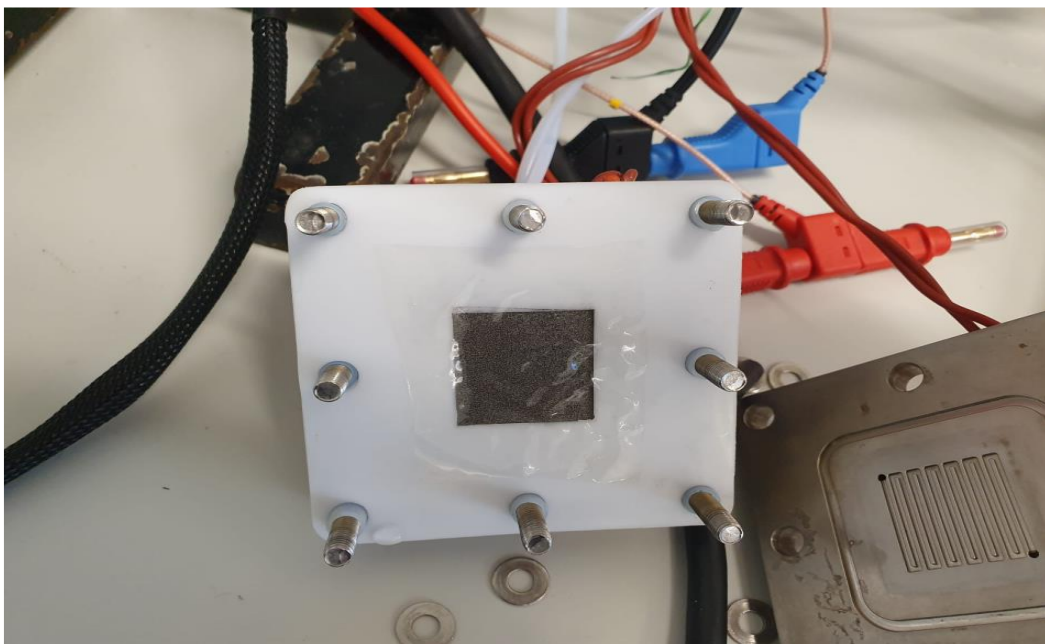


Figure 24: MEA cross-section

#### 4.2.3.1. Chronopotentiometry

Chronopotentiometry is a galvanostatic technique used to determine the ohmic portion of the system's total resistance. For this, the potentiostat applies a current between the counter and the working electrodes. The drop in potential is sensed via the sense electrode [71]. For the optimization tests, a current density of  $300 \text{ mA/cm}^2$  was maintained over 1800 s (30 minutes) and the potential needed to maintain this current was measured for the different flow rates and activation times.

### 4.2.4. MATERIAL CHARACTERIZATION

#### 4.2.4.1. Thermogravimetric analysis (TGA):

Thermogravimetric analysis (TGA) is a technique that measures the degradation temperature,  $T_d$ .  $T_d$  is the measure of a sample's heat resistivity. For membranes used in low temperature electrolyzers, the sample must be thermally stable in the range from RT -  $100^\circ\text{C}$  [72]. Thermogravimetric analyser is the instrument used to deduct the thermal behaviour of the membrane sample. The machine used in this project is Perkin Elmer's TGA4000, which is situated in the Aerospace faculty of TU Delft. The device is shown in Figure 25. A sample of 2-5 mg in mass is placed in a crucible which is then placed in a closed furnace. The temperature range required for the analysis is controlled using the 'Pyris' software. As the temperature progresses, the sample

degrades structurally and forms oxides, eventually displaying weight loss, which gives an overview of its thermal stability [72].



Figure 25: TGA4000 thermogravimetric analyser

After determining the optimal operation conditions, a suitable Sustainion sample is taken out of the activation electrolyte, heated overnight at 120°C to remove the moisture, and placed inside the TGA4000. For comparison, a pristine Sustainion is also tested following the same drying protocol. As done by Luo et al. [73], they are then placed inside the TGA4000 and heated from RT-600°C under a nitrogen atmosphere of 20 mL/min and at a heating rate of 10°C/min.

#### 4.2.4.2. Fourier Transform Infrared (FTIR) Spectroscopy

The principle of FTIR is as follows. When exposing a sample to infrared, certain frequencies are absorbed, and the rest are transmitted. This absorption depends upon the bonds present in the sample, as different bonds have characteristic bond energy associated with them. The spectrum is obtained in the time domain which is then converted to the more useful frequency domain using Fourier Transform [74]. A sample FTIR spectrum of cellulose with the different bonds identified is shown in Figure 26. The peaks in the fingerprint region of the spectrum are characteristic of a molecule as a whole [75].

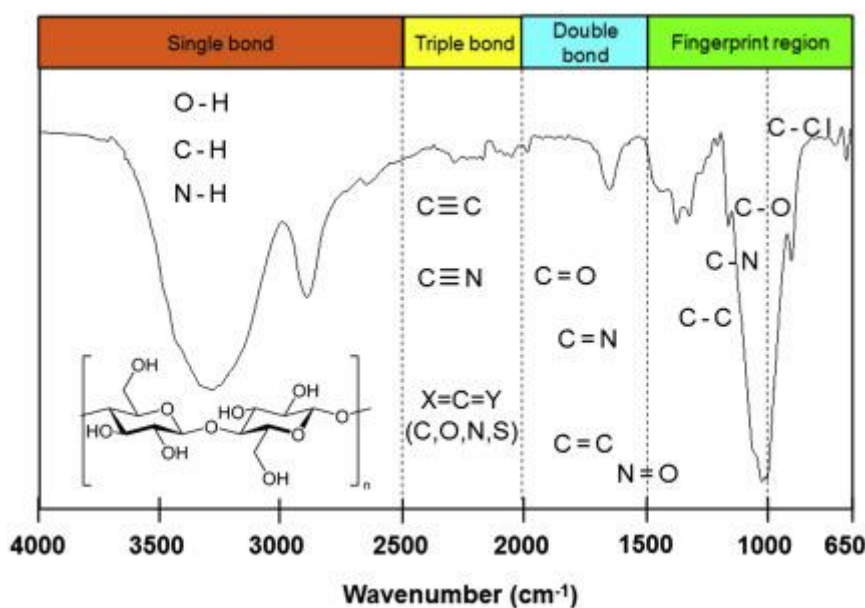


Figure 26: FTIR spectrum of cellulose (Source: [75])

For the present work, the degradation kinetics of Sustainion inside the MEA cell can be learnt. Perkin Elmer Spectrum 100 device situated in the Aerospace faculty of TU Delft (Figure 27) was used. Minimal sample preparation was required. The surface wetness alone was removed using paper towels. The spectrum was recorded by the SpectrumTM 10 software and further analysed.



Figure 27: Spectrum 100 FT-IR spectrometer

## 4.3. RESULTS AND DISCUSSION

### 4.3.1. CHRONOPOTENTIOMETRY CURVES

#### 4.3.1.1. Flow rate selection:

Figure 28 gives an overview of the curves obtained for the different flow rates tested.

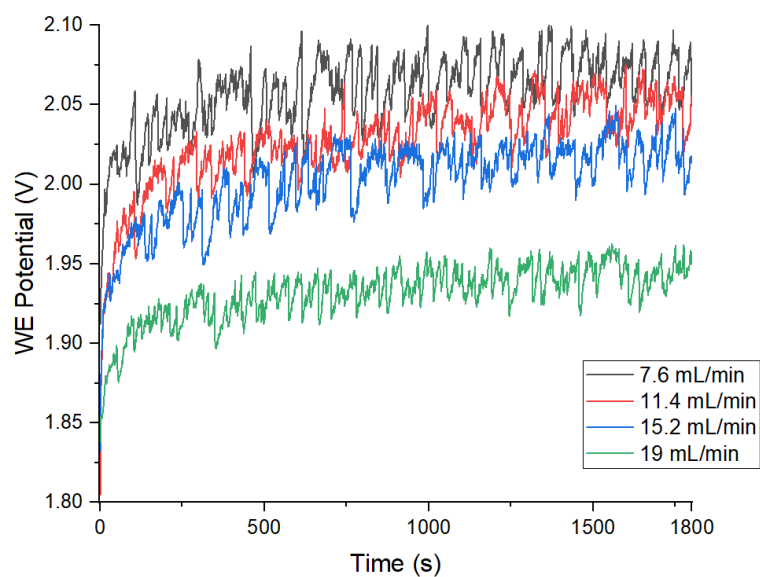


Figure 28: Chronopotentiometry curves for various flow rates

#### 4.3.1.2. Data interpretation

In chronopotentiometry, higher the potential needed to maintain a particular current, higher the internal ohmic resistance of the cell. This helps determine the membrane system that is the least energy intensive. In addition, the stability of the system can be inferred from the noise and how flat the curve is over the tested time. From Figure 28, it is clear that as the flow rate increases, the potential at the working electrode reduces. This is because the bubbles generated on the electrodes' surface is immediately carried away by the electrolyte flow. This not only reduces the bubble overpotential but also provides better contact between the membrane and the electrodes, thus reducing the overall cell resistance [20]. One can also observe that the 19 mL/min curve shows the least noise and most flatness compared to the other flow rate values. An average potential of 1.924 V is required to maintain a 300 mA/cm<sup>2</sup> current density over the 30-minute period. Table 4 provides an overview of the average voltage values obtained for the different flow rates.

Table 4: Voltage obtained from chronopotentiometry for different electrolyte flow rates

FLOWRATE (mL/min)	VOLTAGE (V)
7.6	2.050
11.4	2.013
15.2	1.977
19	1.924

#### 4.3.1.3. Activation time:

Figure 29 displays the CP curves for the various activation times tested.

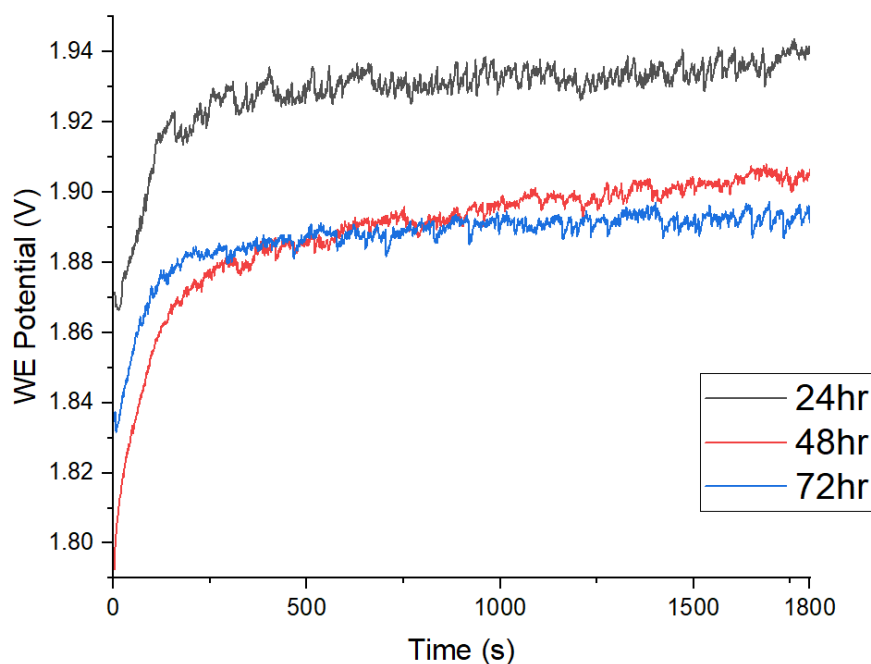


Figure 29: Chronopotentiometry curves for different membrane activation time.

#### 4.3.1.4. Data interpretation

Following the same logic as for the flow rate selection, it is evident that 72hrs-activated membrane shows the best performance. Though the 48hrs-activated membrane closely follows the 72hrs-activated membrane's curve, the performance deteriorates after 10 minutes of operation, whereas the potential required to maintain 300 mA/cm<sup>2</sup> is fairly constant at 1.885 V over the 30-minute testing period for 72hrs-activation. Since, 48 and 72 hrs of activation already produce similar performances, longer activation times were not tested. The average voltage essential for maintaining the 300 mA/cm<sup>2</sup> for the various activation times are shown in Table 5.

Table 5: Voltage obtained from chronopotentiometry for different membrane activation times.

ACTIVATION TIME (hrs)	VOLTAGE (V)
24	1.925
48	1.890
72	1.885

More importantly, the importance of catalyst can be gleaned from the CP curves - Figure 28 and Figure 29. When catalysts are employed, curves that are highly stable even over hundreds of hours and at lower potentials are obtained. An example curve is displayed in Figure 30, where the researchers employed Sustainion anion exchange membrane, Pt/C and stainless steel as the cathode and anode electrocatalysts, respectively. They maintained a stable current density of 1 A/cm<sup>2</sup> over 25 hours at 60°C and 2V [76]. In yet another work, the authors attribute the system stability to the presence of the large amount of the electrocatalysts used [77].

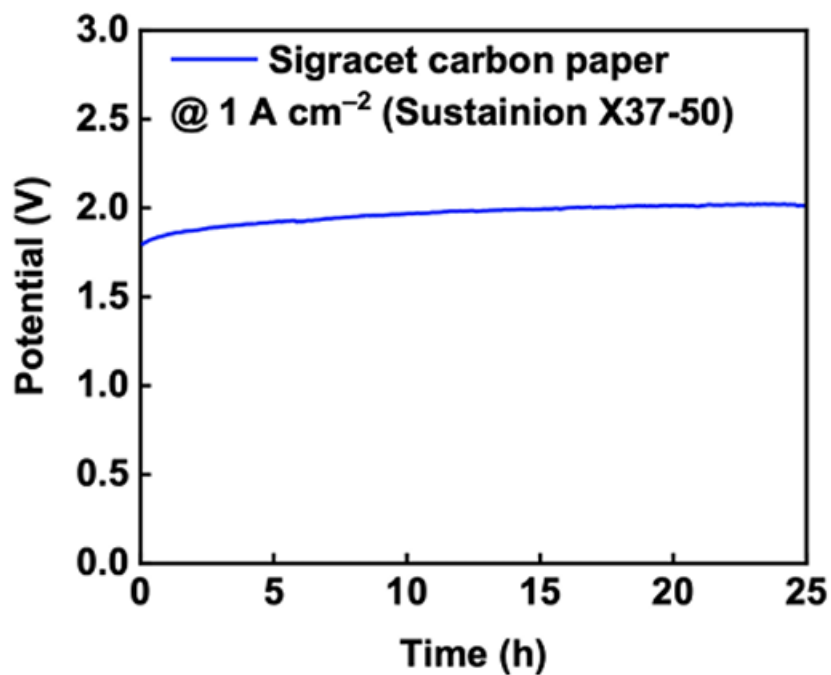


Figure 30: Chronopotentiometry curve for an electrolyser system employing catalysts (Source: [76])

#### 4.3.2. TGA CURVES

A comparison of the TGA curves for pristine and 72-hrs 1M-KOH activated membranes is as shown in Figure 31.

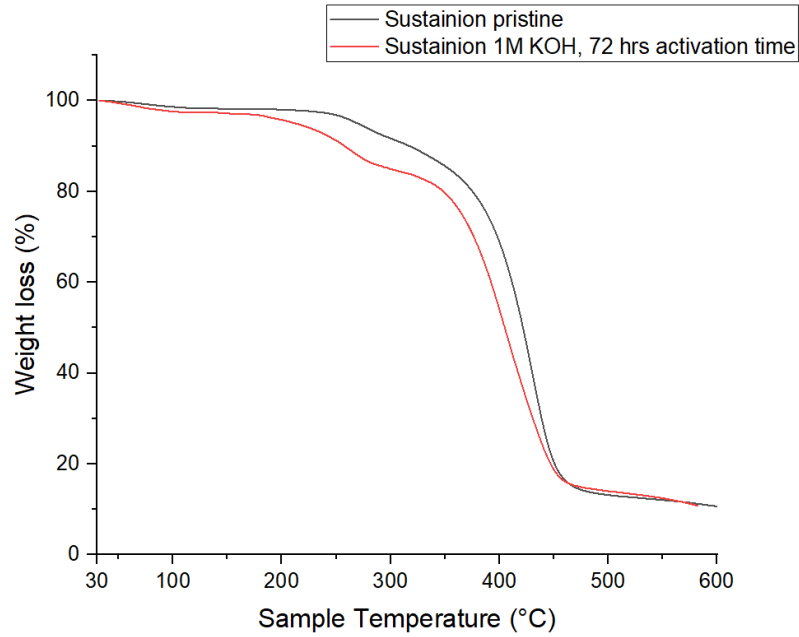


Figure 31: TGA curves of pristine and 72-hrs 1M KOH-treated Sustainion

#### 4.3.2.1. Data interpretation

The curve for the pristine membrane matches those present in literature, with a decomposition of the backbones and ionic groups occurring around 200-480°C. This value is in agreement with those observed for polystyrenes [73]. For the 72hrs-activated membrane, the curve has shifted to lower temperature values of 150-460°C and displays increased weight loss. As evidenced from this shift, it can be deduced that the alkaline environment has caused some membrane degradation.

#### 4.3.3. FTIR SPECTRUM

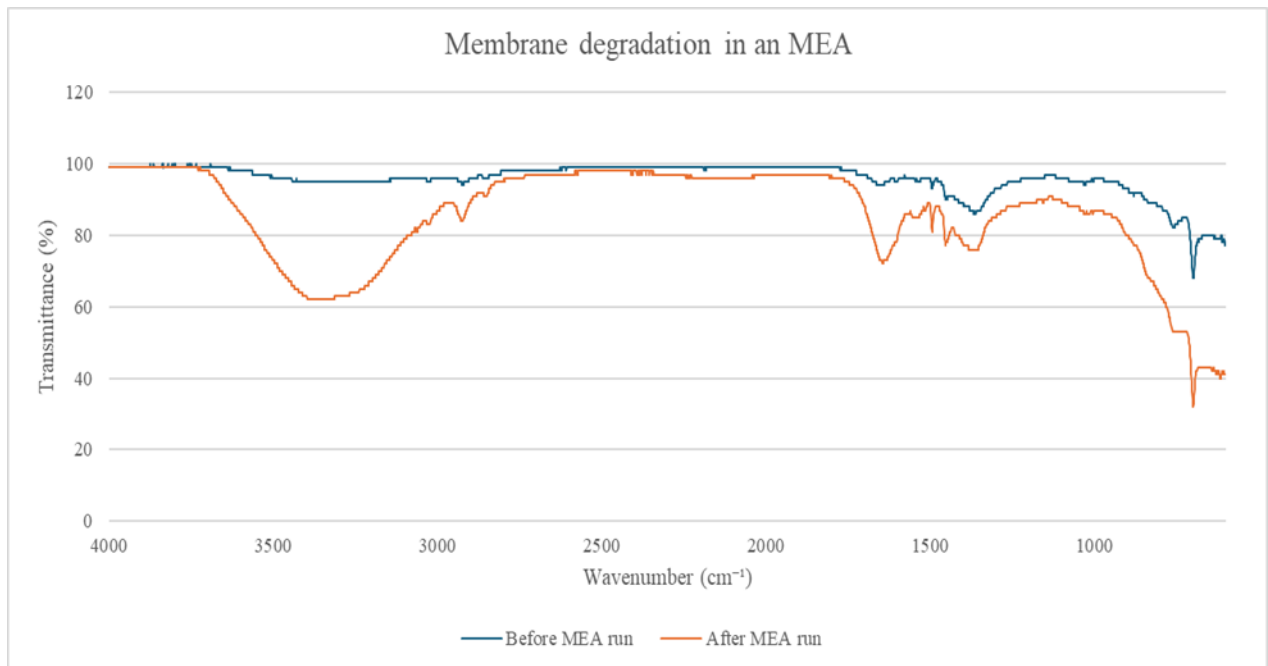


Figure 32: FTIR spectra of the membrane before and after the cell run

#### 4.3.3.1. Data interpretation

For interpreting the spectra obtained (Figure 32), it is compared with the FTIR data of Cook et al. (Figure 33) [78], who studied, amongst various membranes, the membrane degradation of Sustainion after 24 hours immersion in different media.

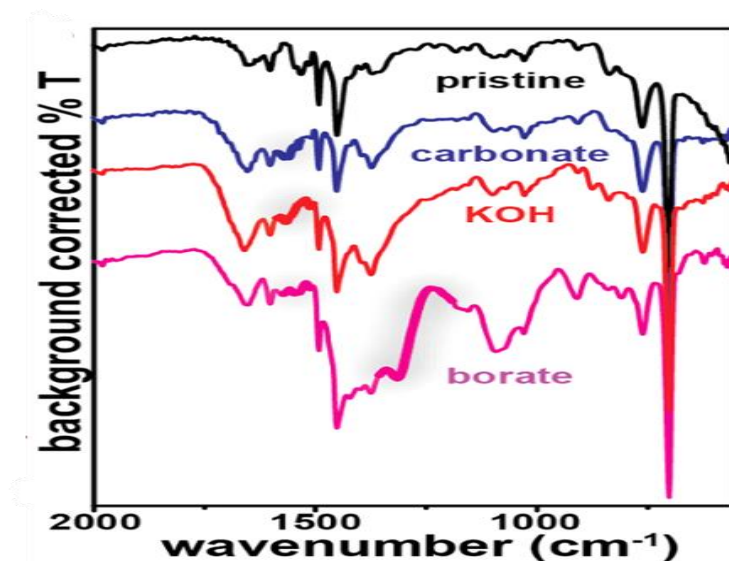


Figure 33: FTIR spectra of Sustainion under different media (Source: [78])

As the FTIR spectrum was taken for the KOH-activated Sustainion membrane, the spectrum displayed in Figure 32 matches closely with the KOH-immersed spectrum in Figure 33 rather than the spectrum for the pristine membrane. The spectrum after the cell run exhibits distinct transmittance reduction in the following regions:

- 3200-3400  $\text{cm}^{-1}$
- 1250-1700  $\text{cm}^{-1}$
- 600-800  $\text{cm}^{-1}$

Assigning characteristic bonds to the peaks from literature [75], the broadened peak at 3200-3400  $\text{cm}^{-1}$  correspond to H-bonded alcohols. The broadening results from the inherent nature of the OH groups to be bound to each other. The C=N of the imidazole group is assigned the 1650  $\text{cm}^{-1}$  peak. The change from 1330-1370  $\text{cm}^{-1}$  can be from changes in the C-N, C=O, O-N=O, and C=N bonds [75][78]. The peaks in the 1475-1600  $\text{cm}^{-1}$  correspond to aromatic C=C bond [75]. The peaks in the fingerprint region (600-800  $\text{cm}^{-1}$ ) are characteristics of polystyrene [79]. The change in transmittance in the regions of 1330-1370  $\text{cm}^{-1}$  and 1650  $\text{cm}^{-1}$  indicate the degradation of the charge-carrying group by means of either electrochemical oxidation or nucleophilic OH<sup>-</sup> attack [78]. The alkaline instability of Sustainion for exposure to 1M KOH even for short durations is evident from the FTIR spectra. The presence of catalysts and different layers in industrial conditions delay this degradation considerably, but it cannot be entirely avoided.

# 5. RETRIEVABLE CRM PREDICTION FROM 2035-2050

The need for recovery strategies can be further emphasized by performing an analysis of the potential recoverable AEMWE electrocatalysts. The parameters necessary for these calculations can be obtained from different sources. The methodology and calculations are covered in this section for predicting the Platinum, Nickel, and Cobalt demands from 2035 till 2050, within the limits of global aviation demands.

## 5.1. METHODOLOGY

In order to determine the amount of CRMs that can be recovered from the End-of-Life AEM electrolyzers used for hydrogen production, the first step was fixing the low-, medium-, and high-demand scenarios. Several works were available, and a well-reasoned one chosen to elect the hydrogen demand till 2050.

Following this, the current catalyst loading values of the electrocatalysts employed in AEMWE were analysed. Per catalyst, various sources have been collected and their respective electrolyser performance examined. The works that were deemed compatible with the current AEMWE technological progress were chosen and their corresponding catalyst loadings tabulated. Logically, the further calculations were carried out for the minimum and maximum loading.

Next, to arrive at realistic calculations, electrolyser stack details, including number of stacks, hydrogen production per day, electrolyser efficiency, etc., of selected products from the AEMWE producer Enapter were studied.

### 5.1.1. HYDROGEN DEMAND PREDICTION

The work of Grimme et al. [80] was selected as the starting point for fixing the aviation hydrogen demand because of its recency (2024) and meticulous compilation of predicted demand from various aerospace organizations. The companies include consulting firms such as McKinsey & Company and Steer, and core aerospace organizations and coalitions including NLR, DLR, and Air Transport Action Group. ATAG predicts a direct demand of 43 MtH<sub>2</sub> and 79 MtH<sub>2</sub> by 2050 and 2060. The European Hydrogen Backbone (EHB) makes a rather conservative 0.27 MtH<sub>2</sub> and 2.04 MtH<sub>2</sub> for 2040 and 2050. By 2050, a study performed by Steer and DLR predicts 6.1 MtH<sub>2</sub>. NLR follows closely with a prediction of 4.9 MtH<sub>2</sub>. The stark contrast in these forecasts underscores the uncertainty and ongoing debate surrounding the adoption pace of hydrogen in aviation. Factors like technological advancements, infrastructure development, and policy support are likely to play key roles in determining which predictions prove most accurate. The demand predicted by different firms are shown in Figure 34.

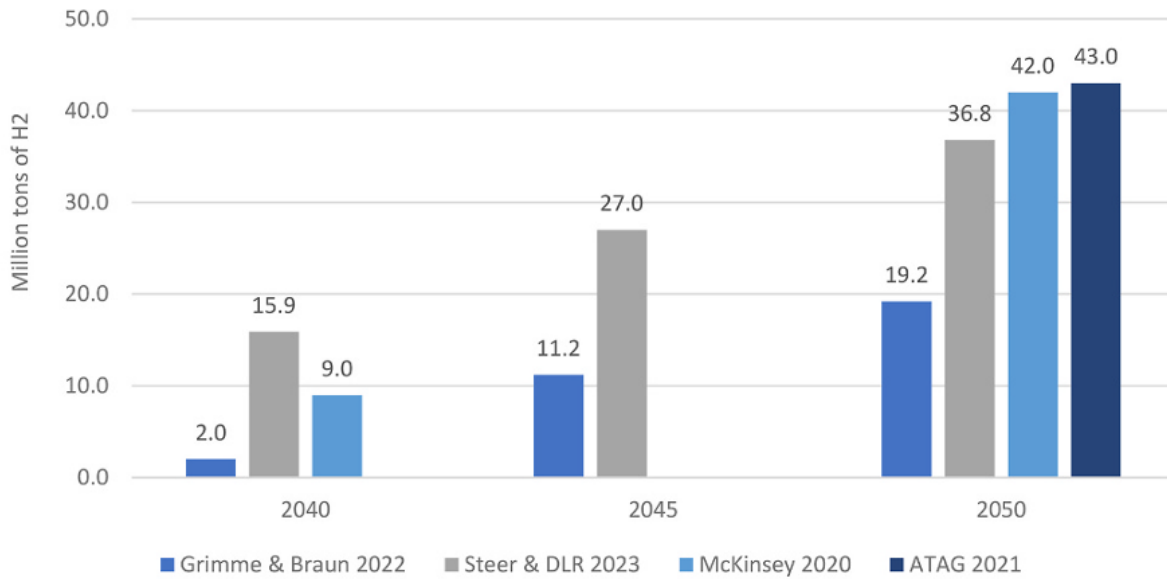


Figure 34: Global direct hydrogen demand prediction by various organizations till 2050 (Source: [80])

The reason for the wide discrepancy between the demand forecast of Grimme’s earlier work, along with co-author Braun, titled “Estimation of potential hydrogen demand and CO<sub>2</sub> mitigation in global passenger air transport by the year 2050” [81] and the other predictions can be attributed to the conservative assumptions regarding hydrogen’s role in long-range flights. Also, McKinsey & Company and the European Commission consider earlier retirement of conventional aircraft (15-18 years) compared to the 22 years in [81], which further elevates the demand. Moreover, for the scenario presented in Figure 34, Grimme and Braun assume a 2040 entry. The authors acknowledge in their original work ([81]) that if the market entry year were taken as 2035, an additional 8 Mt demand would be needed.

Comparing the key assumptions, scenarios, and sensitivity analyses of Grimme and Braun [81], McKinsey & Company [82], and the European Commission’s estimate (edited by DLR and Steer) [83], the demands forecast by European Commission were deemed best-suited for further calculations, as their assumptions align with the developments unfolding in the aviation sector. A notable instance is their entry assumption of 2035 which reflects, amongst many companies, the real-time efforts of Airbus’ ZEROe project – to bring into existence the world’s first commercial hydrogen-powered aircraft from 2035. An important milestone was attained in late 2023, when their hydrogen fuel system reached its full power potential of 1.2 MW. They achieved this by developing hydrogen fuel stacks for powering the electric propulsion system in collaboration with the automotive supplier ElringKlinger.<sup>12</sup>

Moreover, the assumptions for the estimate include deliberations with diversified stakeholders - hydrogen fuel experts, aviation authorities, airports, airlines, aircraft manufacturers, and banks. The following were the assumptions considered:

#### 5.1.1.1. Cost of hydrogen

Due to policies like the EU’s Fit-for-55 package, hydrogen prices are assumed to be on par with conventional fuels by 2035. From a price of 0.053 €/MJ, it is expected to fall to 0.033 €/MJ in 2050. This is including an extra 0.0083 €/MJ for the liquefaction processes at the airports. Other SAFs are presumed to be more expensive owing to the complex production processes.

#### 5.1.1.2. Fleet Size

The report assumes an accelerated replacement of conventional aircraft. Their modelling predicts that by 2040, the global fleet would include 1,885 hydrogen fuel cell aircraft and 5,795 hydrogen turbofan aircraft, out of a

<sup>12</sup> <https://www.airbus.com/en/newsroom/stories/2024-01-first-zeroe-engine-fuel-cell-successfully-powers-on>

total of 9,914 new aircraft. In 2050, out of 50 million global flights, 32 million would employ hydrogen-powered aircrafts.

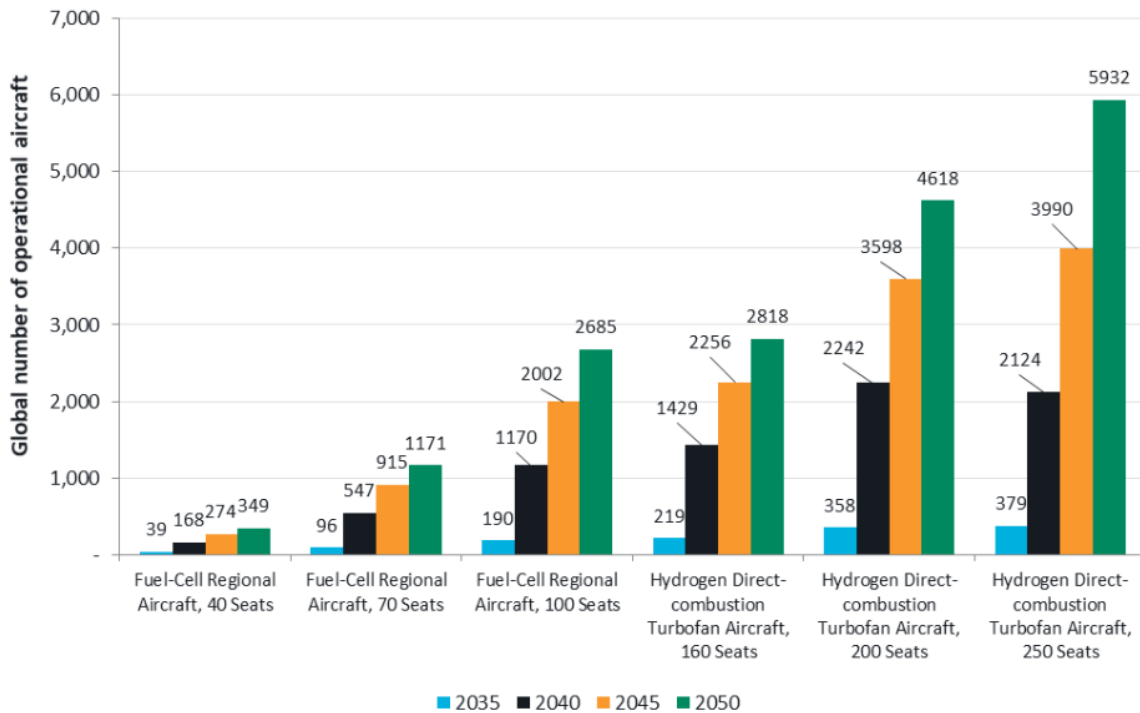


Figure 35: Operational fleet of hydrogen-powered aircraft (2035-2050) (Source: [83])

### 5.1.1.3. Aircraft Retirement

The historically accepted retirement age of 25 years is discarded, and 18 years is selected as the new standard to reflect policy measures such as carbon pricing and financial incentives for retiring conventional aircraft.

**Turboprop Aircraft:** Retirements for turboprop aircraft are expected to increase from over 100 aircraft to almost 300 per year between 2036-2040.

**Regional Jets:** Retirements are projected to reach around 200 aircraft per year from 2035-2040, up from the current 120.

**Narrowbody Jets:** Annual retirement rate is expected to rise to around 800 aircraft compared to the present 300.

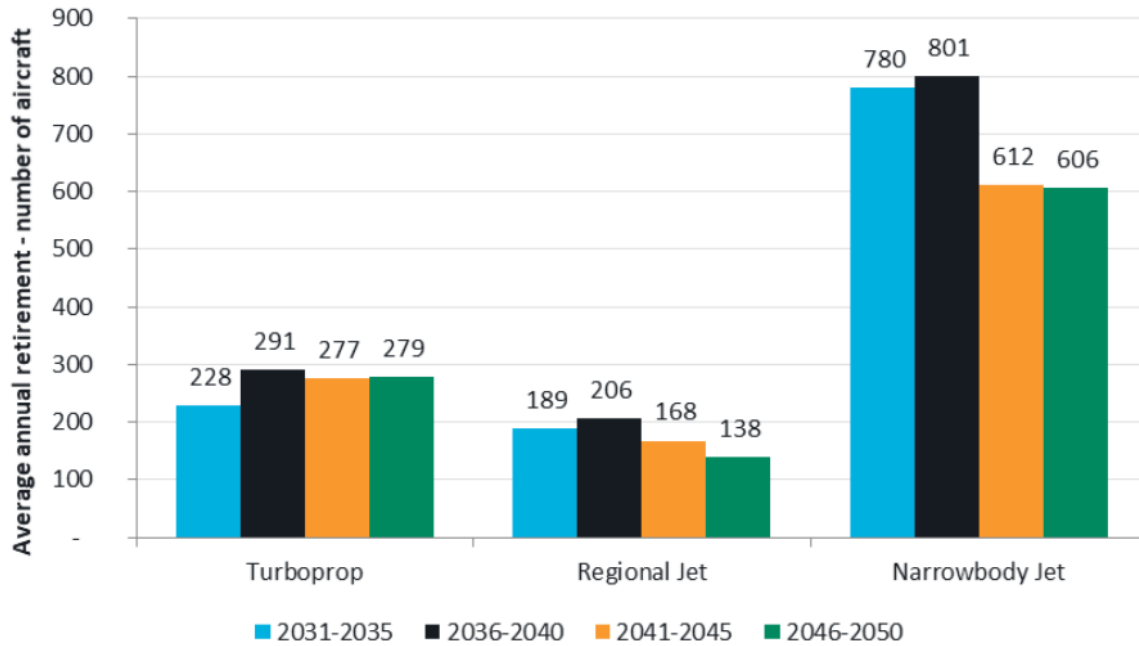


Figure 36: Global flight retirement trend (Source: [83])

#### 5.1.1.4. Airport Infrastructure

Airports are predicted to have distribution and transmission systems for hydrogen via trucks and/or pipelines depending on the individual airport's needs. Initial hydrogen infrastructure is limited to major airports and tankering – refuelling at the home base is assumed to be practised during the initial stages. These assumptions facilitate a reduction in the immediate need for numerous refuelling stations. The report also assumes that logistical and space-related constraints would not be an issue, provided the airports employ off-site storage and mobile refuelling facilities.

#### 5.1.1.5. Aircraft Productivity

Similar to conventional aircraft, hydrogen aircraft is also assumed to have the following annual utilization rates – 2000 flights for regional aircraft with a range of 400 Nm (nautical miles), and 1600 flights for short- and medium-haul turbofan aircraft having a range of 800 Nm plus reserves. Calculating the annual hydrogen demand from these numbers, the report arrives at 600 and 2400 tonnes of annual hydrogen need for regional and short/medium-haul aircraft, respectively.

#### 5.1.1.6. Traffic Growth Rate

The average annual growth rate for air traffic within the EU is taken as 1.9% per year, with a specific growth rate of 1.7% from 2019 to 2040. These values are in line with other major forecasts like the Airbus Global Market Forecast and Boeing's Commercial Market Outlook. For extra-EU traffic, the model assumes a growth rate of 2.1% per year between 2035 and 2050.

#### 5.1.1.7. Policy and Market Assumptions

Measures such as carbon pricing, tax incentives, and public investment in green aircraft technologies are predicted to fasten both the integration of hydrogen infrastructure and the retirement of conventional aircraft, thus leading to accelerated introduction of hydrogen aircraft. The market adoption is assumed to have no selection-bias by airlines. The aircraft would hence be suitable for a wide variety of carriers, including low-cost, charter and network airlines. In a nutshell, a high adoption rate is assumed, provided the operational and commercial characteristics of hydrogen aircraft meet the industry standards.

With the above assumptions, a bottom-up approach was used to determine the hydrogen demand (Figure 37). The report projects a **2.6 Mt, 15.9 Mt, 27 Mt, and 36.8 Mt demand for 2035, 2040, 2045, and 2050.**

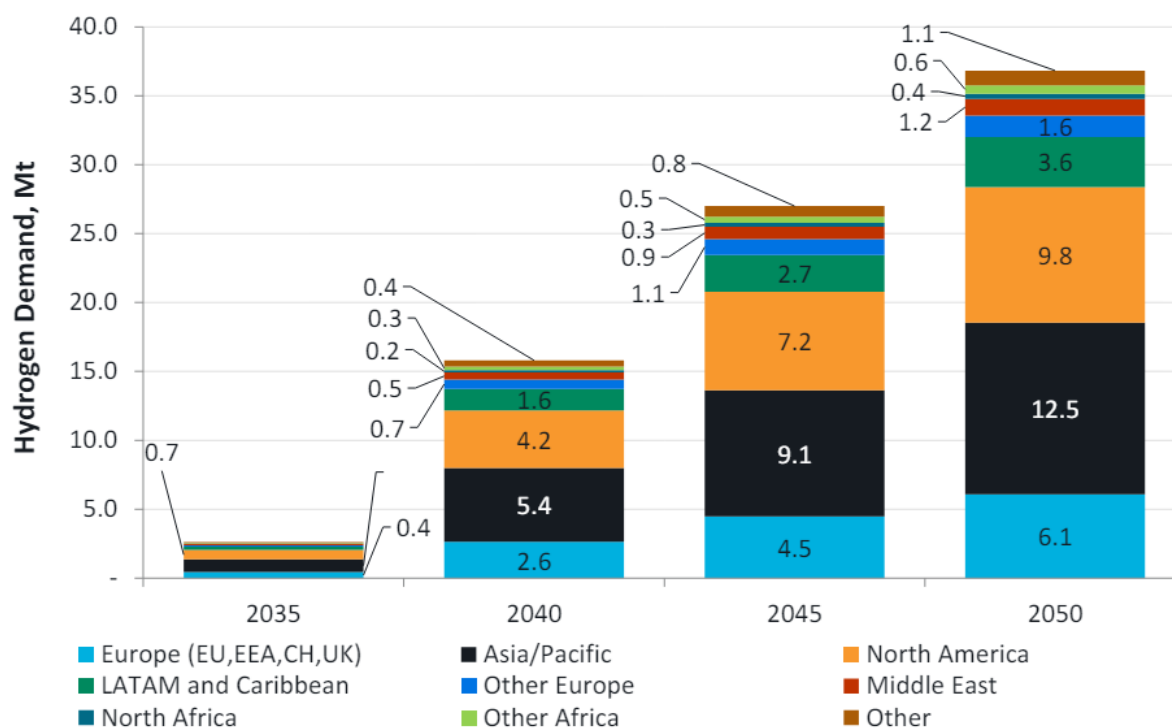


Figure 37: Global hydrogen demand (Source: [83])

### 5.1.2. CATALYST LOADING SELECTION

Now that the hydrogen demand has been established, the catalyst loading must be determined. For this purpose, current OER and HER electrocatalyst loading trends for alkaline water electrolysis was pursued. The commonly assumed value of 2 mg/cm<sup>2</sup> ([84], [85]) could have been chosen, but from the way the electrode and catalyst design is evolving (refer [86], [87]), it was decided to showcase both the extremes. It is crucial to mention that the extremes were chosen only based on the stated literature.

The results per platinum, nickel, and cobalt are summarized in Table 6, Table 7, and Table 8. As expected, most of the works provide the total catalyst loading including the catalyst support, alloyed element, etc. The pure metal content was calculated based on the molecular weight of the compound. From the values, it is clear that some values overshoot and some undershoot the 2 mg/cm<sup>2</sup> assumption. Therefore, as stated, the material demand methodology involves selecting the minimum and maximum loading per CRM. These values are highlighted in the catalyst loading table for each metal.

#### 5.1.2.1. Platinum

Table 6: Platinum loading in literature

CATALYST FORM	OER/HER	Pt loading (mg/cm <sup>2</sup> )	REFERENCE
40 wt% Pt/C	HER	0.1, 0.2, 0.5	[88]
Pt/C	HER	0.5	[89]
Pt/C	HER	1	[20]
<b>PtRu/C</b>	<b>HER</b>	<b>2</b>	[90]
<b>7.1 wt% Pt in Pt-Ni nanowires</b>	<b>HER</b>	<b>0.0018</b>	[86]
Pt/C	HER	0.5	[91]

### 5.1.2.2. Nickel

Table 7: Nickel loading in literature

CATALYST FORM	OER/HER	Ni loading (mg/cm <sup>2</sup> )	REFERENCE
60 wt% Ni <sub>0.9</sub> Mo <sub>0.1</sub> /Vulcan carbon	HER	2.7 (Calculated from 5 mg/cm <sup>2</sup> total catalyst loading)	[92]
Ni nano powder	HER	2	[93]
10% Ti impurities in NiFe <sub>2</sub> O <sub>4</sub>	OER	4.6 (Calculated from 20.3 mg/cm <sup>2</sup> total catalyst loading)	[94]
NiFe <sub>2</sub> O <sub>4</sub>	OER	4.98 (Calculated from 19.8 mg/cm <sup>2</sup> total catalyst loading)	[94]
Ni(OH) <sub>2</sub>	HER	<b>0.00823</b> (Calculated from 0.013 mg/cm <sup>2</sup> total catalyst loading)	[95]
Ni-Fe-Co	HER	1.69 (Calculated from 5 mg/cm <sup>2</sup> total catalyst loading)	[96]
NiAlMo (Ni 39 wt%, Al 44 wt%, Mo 17 wt%)	OER	<b>16.65</b> (Calculated from 42.7 mg/cm <sup>2</sup> total catalyst loading)	[87]

### 5.1.2.3. Cobalt

Table 8: Cobalt loading in literature

CATALYST FORM	OER/HER	Co loading (mg/cm <sup>2</sup> )	REFERENCE
Li <sub>0.21</sub> Co <sub>2.79</sub> O <sub>4</sub>	OER	1.79 (Calculated from 2.5 mg/cm <sup>2</sup> total catalyst loading)	[93]
CoP nanosheets	OER, HER	3.28 (Calculated from 5 mg/cm <sup>2</sup> total catalyst loading)	[97]
<b>Cu<sub>0.5</sub>Co<sub>2.5</sub>O<sub>4</sub></b>	<b>OER</b>	<b>6.06</b> (Calculated from 10 mg/cm <sup>2</sup> total catalyst loading)	[98]
Co <sub>9</sub> S <sub>8</sub> nanowires	HER	0.74 (Calculated from 1.1 mg/cm <sup>2</sup> total catalyst loading)	[99]
Ni-Co-S	OER, HER	1.06 (Calculated from 2.7 mg/cm <sup>2</sup> total catalyst loading)	[100]
<b>CoMoS<sub>4</sub></b>	<b>OER, HER</b>	<b>0.21</b> (Calculated from 1 mg/cm <sup>2</sup> total catalyst loading)	[101]

## 5.1.3. AEMWE SYSTEM SPECIFICATIONS

Calculating the amount of catalyst used in a real AEM electrolyser is the next step. Being the current established commercial AEMWE player, the electrolysers manufactured by Enapter (founded in 2004) were surveyed. The specifications of their two prominent models with different capacities – AEM Flex 120 (120 kW capacity) and AEM Nexus 1000 (~ 1 MW capacity) are given in Table 9.

Table 9: Equipment specifications for AEM Flex 120 and AEM Nexus 1000 (Source: [102], [103])

Specifications	AEM Flex 120	AEM Nexus 1000
----------------	--------------	----------------

Number of stacks	50	420
Number of cells per stack	23	23
Hydrogen production (kgH <sub>2</sub> /day)	53.9	453
Scale (kW)	120	1000
Hydrogen purity (%)	99.95	99.95
Turndown ratio	8:1	33:1
Nominal water consumption (L/hr)	23	190
Specific power consumption (kWh/kgH <sub>2</sub> )	53.3	53.3

In real life, systems having a higher capacity are preferred to reduce the expenses associated. For example, the estimated Balance of Plant (BoP) costs for a 1 MW vs 5 MW AEMWE plant were \$542 and \$291, respectively [84]. Thereby, for the catalyst demand calculation, the 1 MW AEM Nexus 1000 is selected. This electrolyser has 420 stacks [103], each stack having 23 cells.<sup>13</sup> Each cell accommodates an MEA unit. As earlier discussed in the literature analysis chapter, each MEA is home to an anion exchange membrane. Hence, the number of MEA units present in AEM Nexus 1000 is 9660. Multiplying these values by the electrode surface area gives the total surface area in which the catalyst is loaded.

#### 5.1.4. MEMBRANE AREA CALCULATION

The membrane area can be calculated from the current density.

$$J = \frac{\text{Current}}{\text{Area}}$$

The current density of Enapter systems as determined by the Ammonia Energy Association is 0.2 A/cm<sup>2</sup>.<sup>14</sup> The current can be calculated from the nominal power supplied to the system. At this juncture, it is important to note that the voltage is in AC. All electrolysers use DC for stability. This implies the presence of a rectifier that converts the AC to DC before applying it to the stacks. Also, in the datasheet, the nominal power consumption is mentioned to be for the entire system. Based on this knowledge, extra research was carried out and the specifications for a single stack supplied by Enapter was availed. Enapter supplies single stacks that work on DC as well. Comparing the details between the stack that work on DC and AC, the nominal power consumption, hydrogen production, specific power consumption, maximum heat dissipated, stack dimensions, etc. are the same. Only the voltage varies. For the AC stack, 220-230 VAC is the voltage range whereas for the DC stack, 48-60V is nominal. Both of them have a nominal power consumption of 2.4 kW.

In Enapter's maintenance website, the end of life of a stack is said to occur when the cell voltage crosses 2V.<sup>15</sup> Considering that the cells in their stacks are arranged in series following a bipolar design, the voltage for the 23 cells come to around 46V even at EoL.<sup>16</sup> Therefore, to determine the total current, 48V is chosen (rather than 54V – the midpoint between 48 and 60V).

$$\text{Power} = \text{Voltage} \cdot \text{Current}$$

$$2400 = 48 \cdot \text{Current}$$

$$\text{Current} = 50A$$

The area of the membrane is then,

<sup>13</sup> [https://www.enapter.com/kb\\_post/how-many-cells-are-within-one-stack/#:~:text=There%20are%2023%20cells%20in%20each%20stack.](https://www.enapter.com/kb_post/how-many-cells-are-within-one-stack/#:~:text=There%20are%2023%20cells%20in%20each%20stack.)

<sup>14</sup> <https://ammoniaenergy.org/articles/technology-status-anion-exchange-membrane-aem-electrolysis/>

<sup>15</sup> [https://www.enapter.com/kb\\_post/how-is-the-end-of-lifetime-of-enapters-electrolysers-defined/](https://www.enapter.com/kb_post/how-is-the-end-of-lifetime-of-enapters-electrolysers-defined/)

<sup>16</sup> [https://www.enapter.com/kb\\_post/what-is-enapters-aem-technology-and-how-does-it-work/](https://www.enapter.com/kb_post/what-is-enapters-aem-technology-and-how-does-it-work/)

$$0.2 = \frac{50}{Area}$$

$$Area = 250 \text{ cm}^2$$

For a single cell/membrane, the area is,

$$Membrane \text{ area} = \frac{250}{23} = 10.87 \text{ cm}^2$$

The stacks supplied by Enapter are standardized.<sup>16</sup> This means that the membrane area can be multiplied by the number of stacks and cells for AEM Nexus 1000 to determine the total membrane area of the entire unit. The same value is assumed for all the years as future plants are likely to adhere to a fixed electrode and membrane area to avoid incurring costs associated with major equipment modifications.

Finally, a stack's lifetime is given to be >35000 hours [104]. Since all the stacks will not be replaced at the same time, around 20% of stacks are assumed to be replaced every year. Note that even if particular cells in a stack degrade, the stack is still operated. Stack replacement is performed only when the average cell potential supplied crosses 2.0 V and 15% stack degradation is observed.<sup>17</sup>Al

### 5.1.5. LDS, MDS, HDS

It is not prudent to assume that the entire hydrogen demand can be met with the hydrogen produced by AEMWE. Several technological, geopolitical, and economical factors come into play.

Global energy supply security is a major factor. Adopting a single production process will lead to market monopolization by select companies and countries. At a global scale, grid infrastructure is seen as an instrument to increase a territory's power transcending physical boundaries. Though this is more serious in the case of internet infrastructure, the digitization of electricity grids plays a role in increasing the threat. Cross-border electricity connections can shape economic and social environment around the concerned region. One particular instance can be the situation involving China. The country is leveraging its Belt and Road Initiative (BRI) to not only export equipment and components but also to establish Chinese norms and standards internationally. This strategic move includes appointing the president of the International Electrotechnical Commission, enhancing China's influence in global standards setting [105].

There is also the issue of resource availability for the construction of elaborate plants per region. The resource limitation can be monetary, arising from a deficit in the technological development, or material unavailability for manufacturing the AEM components. Assuming global resource sharing for the common goal of a sustainable future, though ideal, is impractical. As a recent example, the Russo-Ukrainian war that began in 2014 led to sanctions being imposed on Russia that targeted the defence, financial, and oil industries [106].

Moreover, hydrogen infrastructure development is dependent on a country's policies and subsidy provisions. If any policy or regulation is revised, it might cause adverse effects if only one production path is used.

Finally, there could be significant breakthroughs in other energy forms which might further bring down the contribution of AEM-based hydrogen or even the total hydrogen. From IEA's "Hydrogen Production and Infrastructure Projects Database", it was gleaned that even within the realm of electrolysis-based hydrogen production, there are over 1500 plants of differing capacities and technologies either under construction or already in operation (excluding demo and feasibility facilities). Including the plants for hydrogen-based fuels, this number crosses 2500.<sup>18</sup> An Excel file detailing all the project details can be downloaded from their webpage.

Taking all these elements into account, conservative scenarios of LDS – **10%**, MDS – **30%**, and HDS – **60%** were applied, i.e., 10, 30, and 60% of the global aviation hydrogen demand would be met by AEMWE-based production. The HDS was purposefully taken higher to account for a highly optimistic case.

<sup>17</sup> [https://www.enapter.com/kb\\_post/how-is-the-end-of-lifetime-of-enapters-electrolysers-defined/](https://www.enapter.com/kb_post/how-is-the-end-of-lifetime-of-enapters-electrolysers-defined/)

<sup>18</sup> <https://www.iea.org/data-and-statistics/data-product/hydrogen-production-and-infrastructure-projects-database>

## 5.2. PLATINUM, NICKEL, AND COBALT RECOVERABLE AMOUNT CALCULATION

Combining the different elements of calculation, the recyclable amount of platinum, nickel, and cobalt were determined for their respective minimum and maximum loading from 2035 till 2050. To comprehend the method of calculation, the LDS, MDS, and HDS 2050 values for the high catalyst loading of platinum is presented below.

2050 predicted global aviation hydrogen demand– 36.8 Mt = 36800000000 kg

LDS – 10% of the total demand – 3680000000 kg

MDS - 30% of the total demand – 11040000000 kg

HDS - 60% of the total demand – 22080000000 kg

Daily hydrogen production rate of AEM Nexus 1000– 453 kg/day

Yearly hydrogen production rate of AEM Nexus 1000– 365 x 453 = 165345 kg/year (assuming uninterrupted service)

To meet the global LDS demand of 3680000000 kg, daily H<sub>2</sub> production =  $\frac{3680000000}{365} = 10082191.78$  kg

To meet the global MDS demand of 11040000000 kg, daily H<sub>2</sub> production =  $\frac{11040000000}{365} = 30246575.34$  kg

To meet the global HDS demand of 22080000000 kg, daily H<sub>2</sub> production =  $\frac{22080000000}{365} = 60493150.68$  kg

Hence, the number of AEM Nexus 1000 systems needed to meet the global demand:

For LDS = 22256

For MDS = 66769

For HDS = 133539

Each system has 420 stacks, and each stack has 23 cells (so, 23 MEA). Combined with the 10.87 cm<sup>2</sup> membrane surface area and the 20% replacement rate assumed, the total surface area that the catalyst needs to cover reaches:

LDS = 22256 x 420 x 23 x 10.87 x 0.2 = 467394695.04 cm<sup>2</sup>

MDS = 66769 x 420 x 23 x 10.87 x 0.2 = 1402205085.96 cm<sup>2</sup>

HDS = 133539 x 420 x 23 x 10.87 x 0.2 = 2804431172.76 cm<sup>2</sup>

For the high Platinum catalyst loading of 2 x 10<sup>-6</sup> kg.cm<sup>-2</sup>, the following values are obtained:

**2050 LDS Platinum recyclable amount** = 467394695.04 x 2 x 10<sup>-6</sup> = **934.79 kg**

**2050 MDS Platinum recyclable amount** = 1402205085.96 x 2 x 10<sup>-6</sup> = **2804.41 kg**

**2050 Platinum recyclable amount** = 2804431172.76 x 2 x 10<sup>-6</sup> = **5608.86 kg**

### 5.2.1. RECYCLABLE AMOUNT PROJECTION

Since the hydrogen demand values of the European Commission report are of a linear nature - 2.6 Mt in 2035, 15.9 Mt in 2040, 27 Mt in 2045, and 36.8 Mt demand in 2050; the LDS, MDS, and HDS recyclable amount of the CRMs were determined using linear curve fitting, using the average between the minimum and maximum catalyst loading, with each curve displaying an R<sup>2</sup> > 0.99 indicating the correctness of the fit. The obtained curves for recyclable Platinum, Nickel, and Cobalt per year from 2035 to 2050 are shown in Figure 38, Figure 39, and Figure 40, respectively.

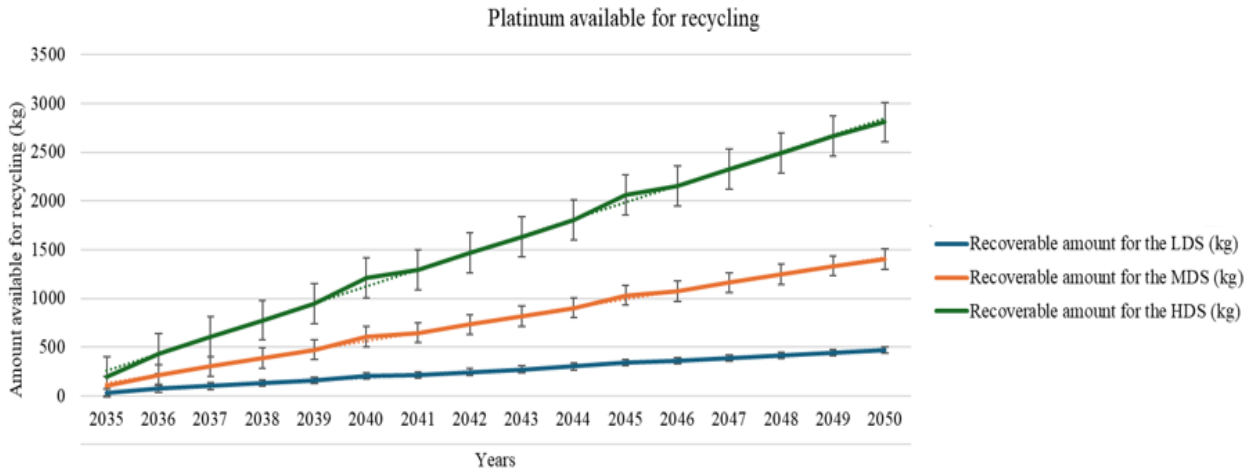


Figure 38: Platinum available for recycling per year from 2035-2050

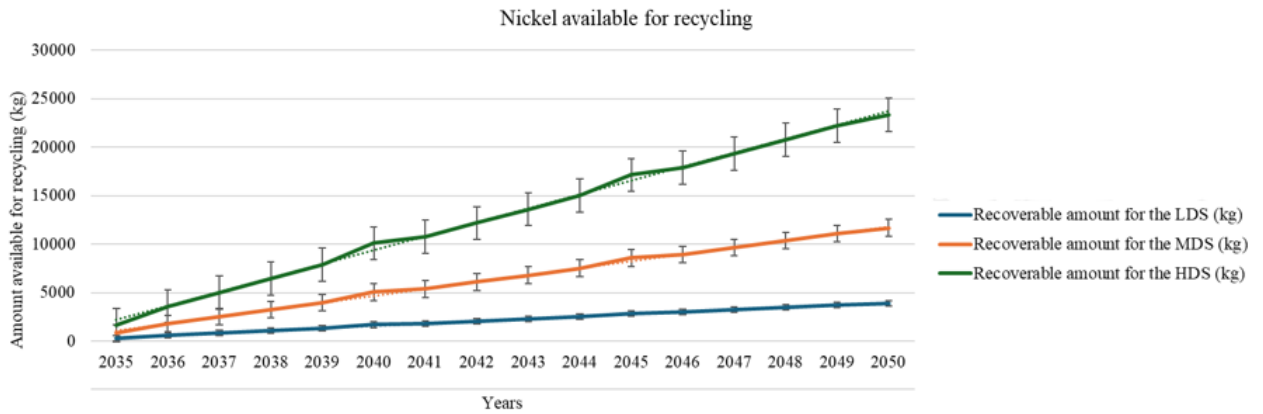


Figure 39: Nickel available for recycling per year from 2035-2050

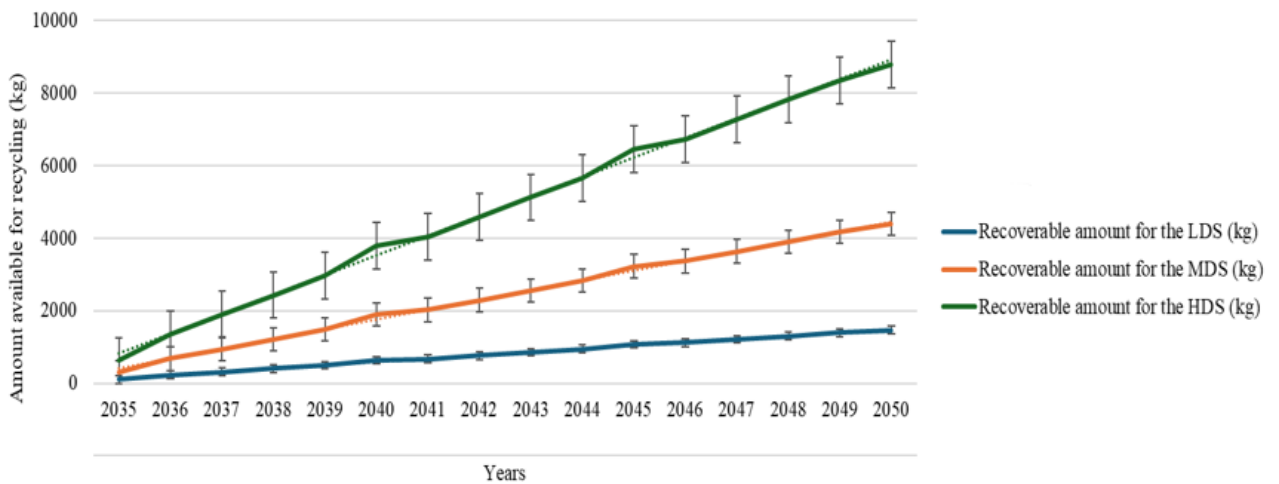


Figure 40: Cobalt available for recycling per year from 2035-2050

For a better comprehension of the numbers, Table 10 summarises the recyclable amount per element in LDS, MDS, and HDS in 2050.

Table 10: Recyclable CRM amounts in 2050

CRM	RECYCLABLE AMOUNT IN 2050 (kg)					
	Low loading			High loading		
	LDS	MDS	HDS	LDS	MDS	HDS
Platinum	0.84	2.52	5.05	934.79	2804.41	5608.86
Nickel	3.85	11.54	23.08	7782.12	23346.71	46693.78
Cobalt	98.15	294.46	588.93	2832.41	8497.36	16994.85

When considering the fact that supply from primary sources have an extremely low yield - about 1-5 grams of platinum + rhodium + gold + palladium in 1 tonne of the ore [107], secondary sources (recycling and recovery of spent catalysts, batteries, and other e-waste) must be availed to meet future CRM demands.

# 6. BENEFIT ANALYSIS OF THE CATALYST RECOVERY STRATEGIES

Ways of material recovery can be reviewed from different fields, of which the ones pertinent to the current work can be attained from the fields of ore mining, spent catalyst and metal recovery from e-waste and automotives. The former comes under primary source extraction and the latter under secondary source extraction. Players were chosen based on market size in extraction and recovery - both primary and secondary sources, from sample reports obtained from Research Dive<sup>19</sup>, IMARC Group<sup>20</sup>, Industry Growth Insight<sup>21</sup>, and Allied Market Research<sup>22</sup>. A conglomeration of the top players was compiled.

- Umicore
- Tanaka
- Heraeus
- Johnson Matthey
- BASF Catalysts
- Boliden
- Materion Corporation
- Anglo American Platinum Limited (Anglo American PLC)
- Glencore International AG
- Impala Platinum Holdings Limited (Implats)

Each company has its proprietary recovery method, but the predominant trend involves combining pyro- and hydro-metallurgical processes. Though the companies' websites provide meagre information about the chemicals involved, looking through their past and recent patents (Table 11) gives valuable insights.

Table 11: Patents related to metal recovery technologies.

COMPANY	INTERESTED TECHNOLOGY	US PATENT NUMBER
Aleon Renewable Metals, LLC.	Nickel and cobalt recover from spent catalysts of Ni-MH and Li batteries	11682801B1
Boliden Aktiebolag	Pyrometallurgical recovery of PGM and precious rich in halogens	4613365A
Boliden Aktiebolag	Electrowinning recovery	4738762A
Boliden Mineral	Nickel, cobalt precipitation	6342189B1

<sup>19</sup><https://www.researchdive.com/8365/precious-metal-e-waste-recovery-market>

<sup>20</sup><https://www.imarcgroup.com/precious-metal-companies>

<sup>21</sup><https://industrygrowthinsights.com/report/global-spent-catalyst-recycling-market/>

<sup>22</sup><https://www.alliedmarketresearch.com/precious-metals-e-waste-recovery-market-A31390>

Boliden Mineral	Metal recycling from waste with high organic content	20050284261A1
Boliden Mineral AB	Leaching acid purification	6406676B1
Boliden Mineral AB	Metal recovery from sulfuric acid leachant	6383255B1
Heraeus Deutschland & GMBH & Co. KG	Activated coal supported PGM catalysts incineration	10393374B2
Johnson, Matthey & Co., Limited	PGM recovery from aqueous phase	4123500A
Johnson Matthey Public Limited Company	PGM recovery from catalyst	4511539A
Johnson Matthey Public Limited Company	PGM recovery from scrap	4427442A
Johnson, Matthey & Co., Limited	PGM recovery from wash-coated catalysts	4074865A
Johnson Matthey Public Limited Company	Pt/C recovery from heterogeneous and homogeneous catalysts	7122167B2
Johnson Matthey Public Limited Company	PGM precipitation with polyamine	5165901A
Umicore	Nickel and cobalt recycling from batteries	7169206B2
Umicore	PGM concentration from fluorine-rich fuel cell recycling	8101304B2
Umicore	Nickel and cobalt recovery from lithium batteries	10164302B2
Umicore	PGM recovery from silicon carbide-rich catalysts	11879164B2
Umicore	PGM recovery from spent homogeneous catalysts	9249477B2

From research, two major recycling routes were identified – an integrated process where both PGM and base metals are recovered, and one that was dedicated purely to either precious metal recovery or base metal recovery. The latter mostly catered to metal extraction from ores and battery recycling, especially from lithium and nickel metal hydride batteries. For better insight of how the processes look like, process flowcharts of various companies are presented in APPENDIX A. Major recycling companies tailor the recycling recipe based on the feedstock received. The feedstock can include sweeps, hydrometallurgical residue, tank house slimes, copper cement, matte, flue dust, PM-containing slag, dross, electrolyser and fuel cell catalysts and/or MEA, bullions, incineration bottom ashes, integrated chips, Central Processing Unit, connectors, cell phones, smaller IT devices, PCBs, laptops and screens, spent industrial and automotive catalysts.<sup>23, 24, 25, 26, 27, 28, 29, 30, 31</sup>

<sup>23</sup> <https://pmr.umicore.com/en/recyclables/incineration-bottom-ashes/>

<sup>24</sup> <https://pmr.umicore.com/en/recyclables/e-scrap/>

<sup>25</sup> <https://pmr.umicore.com/en/recyclables/spent-industrial-catalysts/>

<sup>26</sup> <https://pmr.umicore.com/en/recyclables/spent-automotive-catalysts/>

<sup>27</sup> <https://pmr.umicore.com/en/recyclables/other-materials/>

<sup>28</sup> <https://pmr.umicore.com/en/industrial-by-products/>

<sup>29</sup> <https://www.umicore.com/en/newsroom/news/fuel-cells-challenges-for-circularity/>

<sup>30</sup> <https://www.boliden.com/sustainability/case-studies/largest-electronic-material-recycler-in-the-world/>

## 6.1. INDUSTRIAL RECYCLING METHOD

To showcase the intricacies of industrial recycling process, the approach of Umicore – a prominent recycler is discussed.

Their recycling process starts with sampling and assaying. Here, the material that arrives from diverse sources are individually tested in facilities near the Hoboken plant. An à la carte approach is applied for creating a recycling recipe with maximum recovery.<sup>32</sup>

Following this, the feedstock is sent to the Precious Metals Operations. Three main processing steps are present: the smelter, the copper leaching and electrowinning plant. Raw materials are optimally introduced into the process based on their analytical fingerprint, physical characteristics, and precious metals content. The smelter uses Isa smelt submerged lance combustion technology. Fuel and oxygen-enriched air are injected in a molten bath from which precious metals are collected in a copper bullion. Other metals are collected in a lead slag and sent to the Base Metals Operations. After copper is leached out in the electrowinning plant, the remaining precious metals residue is refined in the precious metals refinery. The precious metals refinery combines classical methods like cupellation with proprietary processes, enabling the treatment of various ratios of precious metals and platinum group metals at the Hoboken facility.<sup>32</sup>

The lead slag collected undergoes three main processes in the Base Metals Operations step: the blast furnace, the lead refinery, and the special metals plant. The blast furnace reduces the oxidized lead slag along with high lead-containing third-party raw materials, forming impure nickel speiss, lead bullion, copper matte, and depleted slag. The impure lead bullion contains most of the non-precious metals and is further processed in the lead refinery to produce pure lead and special metals residues. These residues are refined in the special metals refinery to produce high-quality metals and intermediates. Nickel is leached from the nickel speiss and converted into nickel sulphate. The remaining precious metals residue is sent to the precious metals refinery. The copper matte is recycled back to the smelter, and the depleted blast furnace slag is repurposed to be used in concrete industry or as dyke fortification material.<sup>32</sup> The complete flowchart is depicted in Figure 41.

### Major flowsheet investments

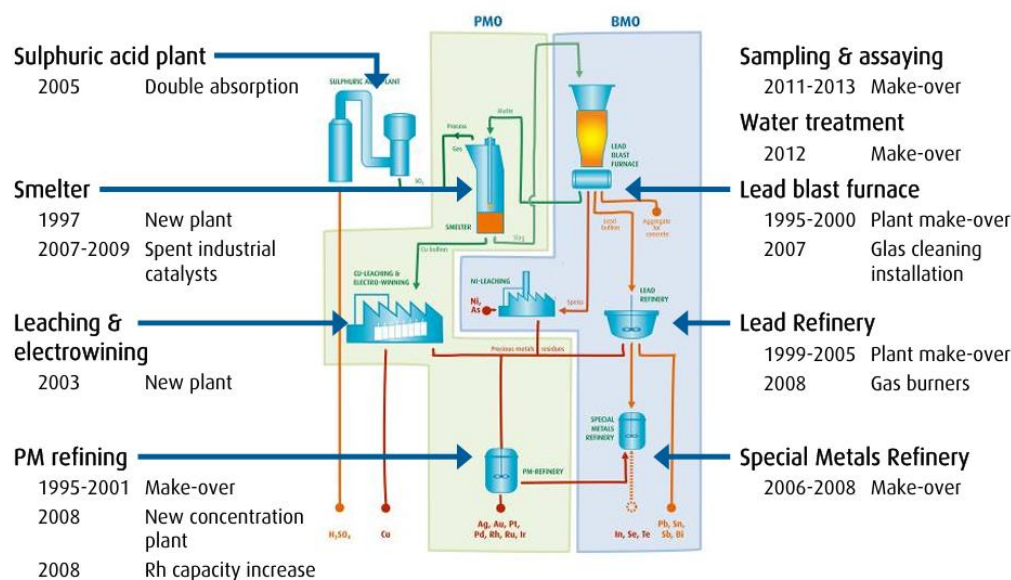


Figure 41: The Umicore recovery process (Source: [108])

<sup>31</sup>[https://www.heraeus.com/en/hpm/recycling\\_solutions/recycling/precious\\_metal\\_scrap/precious\\_metal\\_scrap.html](https://www.heraeus.com/en/hpm/recycling_solutions/recycling/precious_metal_scrap/precious_metal_scrap.html)

<sup>32</sup><https://pmr.umicore.com/en/about-us/process/>

An overview of other prominent processes can be seen in APPENDIX A.

### 6.1.1. PYRO-METALLURGICAL PROCESS

Pyrometallurgy gained impetus after World War II to aid country rebuilding and economy expansion. Several groups emerged for learning the physical chemistry behind these processes [109]. As a result, pyrometallurgy for metal recovery is highly advanced. From the patents US7169206B2, US8101304B2, US9249477B2, and US11879164B2 pertaining to battery and catalyst recycling, smelting was determined to be industry preferred. The various additives added to form the metallic bath can also be determined from the mentioned patents. For instance, for fluorine-containing fuel cell recycling, US8101304B2 recommend inorganic additives of IA, IIA, and IIIA group, i.e., mono-, di-, and trivalent metals to bound the fluorine. The compound can be in the form of hydroxides, carbonates, nitrates, sulphates, phosphates, hydrogen phosphates, oxalates, and formates. The patent goes in so far as to recommending hydroxides and carbonates as highly preferred choices. Patent US7169206B2 gives a slag composition having a minimum of 20 wt. % Fe and a maximum of 20 wt. % of Co or Ni and 4-20 wt. % coke as the reducing agent. Slag formers identified from the patents include  $\text{CaCO}_3$  (limestone),  $\text{SiO}_2$  (silica),  $\text{Al}_2\text{O}_3$  (alumina),  $\text{CaO}$ , and  $\text{MgO}$ . Copper, lead, silver, nickel, cobalt, and iron are mentioned as prominent collectors used for matte phase creation. The work of Liu et al. [110] mentions a smelting processing time of 4 hours and a temperature of  $1500^\circ\text{C}$  as being the optimum for platinum recovery (98%) from spent catalysts. For nickel, a smelting temperature of  $1525^\circ\text{C}$  and 2 hours yields 96.82% recovery [111]. Applying Ausmelt furnace technology, Cobalt recoveries ranging from 91-98% have been reported for a temperature range of  $1300\text{-}1400^\circ\text{C}$  [112]. In another work, Ni and Co recoveries of 98.39% and 98.83% were recorded using copper slag at  $1450^\circ\text{C}$  for 30 minutes [113].

### 6.1.2. HYDROMETALLURGICAL PROCESS

From Umicore's flowsheet for their lithium and nickel metal hydride battery recycling (shown in Figure 42) and other flowsheets presented in APPENDIX A, HCl is identified as a common leaching agent for nickel and cobalt recovery. The mention of nickel being leached in its sulphate form from the speiss in Umicore's precious and base metal recovery operations also implies sulphuric acid as a potential lixiviant.<sup>32</sup>

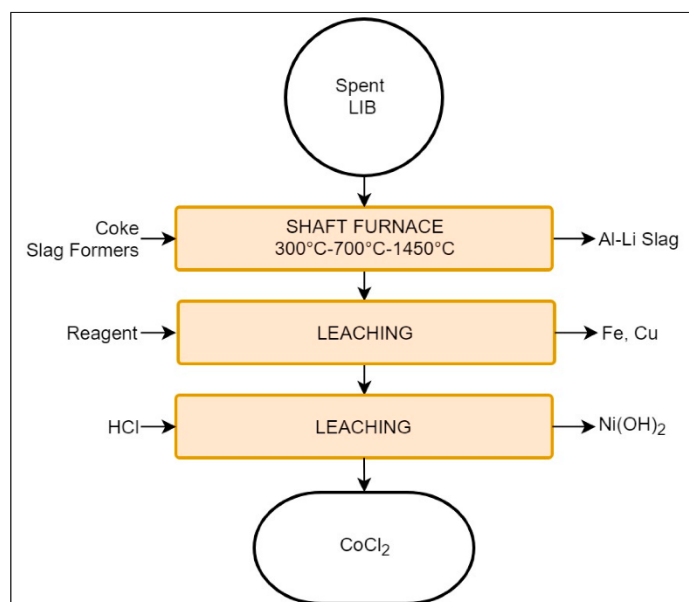


Figure 42: Umicore Lithium battery recycling route (Source: [114])

## 6.2. OPTIMIZATION ROUTES

For a greener economy, there are three levels of implementation which leads to waste reduction, reuse, or elimination:

- Level 1 – source reduction
- Level 2 – internal recycling
- Level 3 – External recycling or biogenic cycles [115].

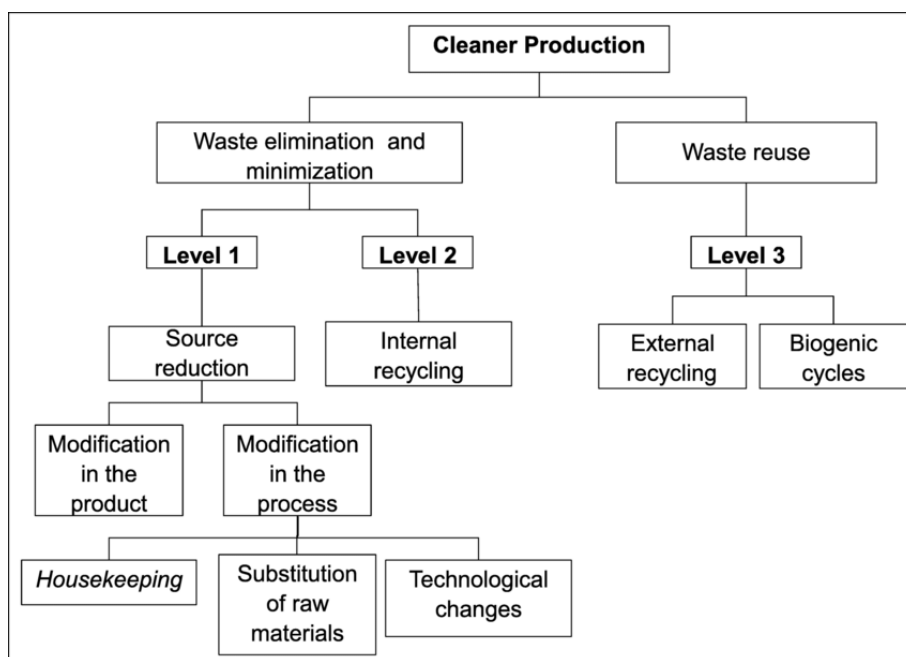


Figure 43: Clean production strategies (source: [115])

Here, the ecological footprint of recycling plants is predominantly tackled by recommending changes to the current technological practices.

### 6.2.1. PYROMETALLURGICAL PROCESS OPTIMIZATION

A patent on battery recycling, US7169206B2, mentions coke as a reducing agent. The papers on WEEE recycling process [116], [117] mention that this requirement is partially fulfilled by the organics present in plastics. As a niche improvement, the implementation of biochar is put forth. This can also be used to replace the graphite electrodes used in electric arc furnaces. Biofuels extracted from agricultural yield like corn, rice husk, sugar, etc., or aquatic feedstock, or inedible biomass of lignocellulosic origin can also be implemented in the molten phase. More optimization strategies including the application of induction furnaces, Seebeck-based thermoelectric systems, CCUS, gas-scrubbing, etc. in the review by Kentaro et al. [118] Hydrogen as a reductant is also a viable alternative [119]. Hydrogen has the capability to reduce hot metal oxides/sulfates/carbonates of metals, to their metallic form. The use of hydrogen as an activator for Adams' catalyst ( $\text{PtO}_2 \cdot \text{H}_2\text{O}$ ) is well-known. The catalyst gets reduced by the hydrogen to its elemental form  $\text{Pt}(0)$  which is the actual catalyst [120]. Likewise, the kinetics for cobalt and nickel reduction from their oxides by hydrogen can be seen in [121] and [122] respectively.

In addition to using hydrogen as a reducing agent, it can also be used to generate the entire energy requirement of the PMT process. An LCA conducted on the PMT vs HMT recovery of spent ternary Li batteries in China calculated a 38.02% reduction in fossil energy consumption and a 29.41% in the global warming potential by the year 2060 for a scenario where hydrogen is used as the energy source [123]. The exact HMT and PMT recovery processes they analysed is given in Figure 44. Other alternative energy options include solar, wind, etc. [119]

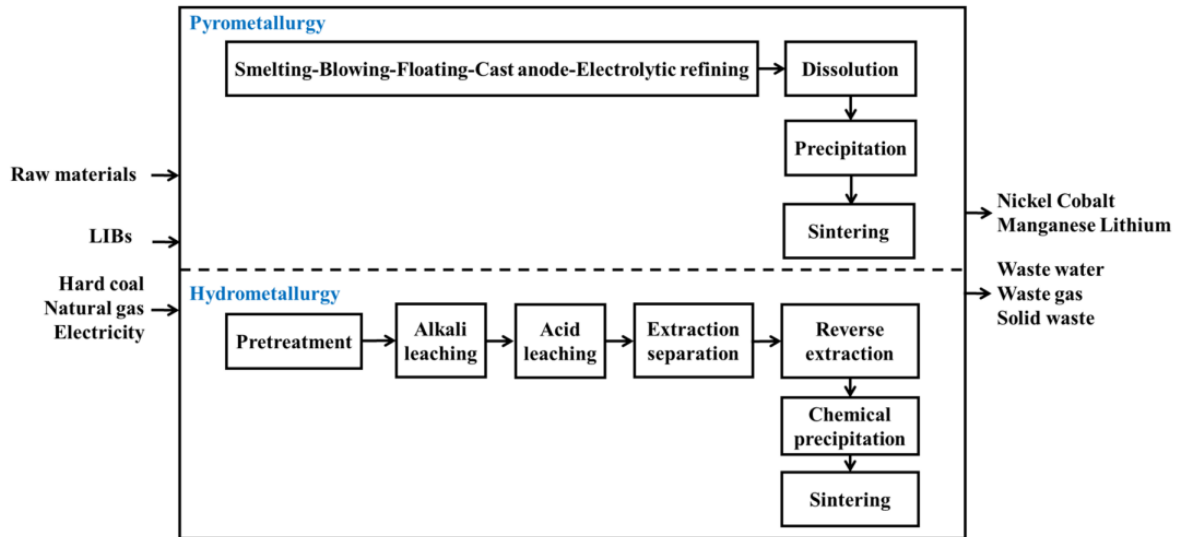


Figure 44: PMT and HMT processes utilized in the LCA (Source: [123])

Microwave-assisted pyrometallurgy can reduce the energy consumption significantly as the expensive torches used to attain higher temperatures can be replaced. The radiation enables localised heating of the metals, and the time of the process is also highly reduced. The procedure is as shown in Figure 45. Availing this technology, Tang et al. [124] got a 98.59% Pt recovery yield in 2 hours at 1250°C (set by microwave radiation). Fu et al. [125] recovered Lithium, nickel and cobalt from Li ion batteries using MW-assisted carbothermic reduction. When exposed to 500 W for 30 minutes and then leached using 1M aqua regia at 15 g/L pulp density, Ni and Co recoveries of 97.65% and 97.85% were recorded.



Figure 45: Microwave assisted smelting (Source: [124])

Likewise, ultrasound can also be availed. Both electro- and mechano-acoustic systems have been used for their streaming (occurrence of steady flow as a result of the ultrasonic absorption), radiation pressure (pressure exerted by the waves around any object - even different volumes of the same medium) they encounter, and cavitation (bubble formation when the pressure crosses the cavitation threshold) properties. From an equipment standpoint, these systems have aided in dust removal from the high temperature exhaust gasses, enhanced combustion via improved mass transfer and mixing in the molten phases, better fuel combustion rate by fuel vapor-oxidant mixing (especially at resonant frequencies), degassing the slag phase via cavitation, and controlling slag foaming. Coming to the metals, they are used for atomization (creating fine droplets from liquified metals) to create fine metal powders, structurally modifying the solidifying metals, etc. [126]

## 6.2.2. PYROMETALLURGY ELIMINATION/ HYDROMETALLURGY OPTIMIZATION

The patent US 7169206B2 points out the operational costs associated with solvent recycling and further refining as the drawback of HMT. The patent was filed in 2005. Over the past 2 decades, developments in solvent technology mitigates this drawback. This can also be evidenced by the venture of Australian-based Podium Minerals. The company is exploring purely hydrometallurgical routes for PGM recovery. Even at atmospheric leaching conditions, it reported > 90% recovery rates for Platinum<sup>33</sup>. A more well-known route is the Kell process (Figure 46). Using a modified pressure oxidation step, Cu, Ni and Co can be removed. The PGM residue obtained is then heated to make the following chlorination step easier. The route allows for a >95% recovery of Pt, Pd, Au, Ni, Co, Rh, and Cu [127]. Though the process has been around since the 90s, presently it is implemented by Sedibelo Platinum Mines Limited in South Africa<sup>34</sup>.

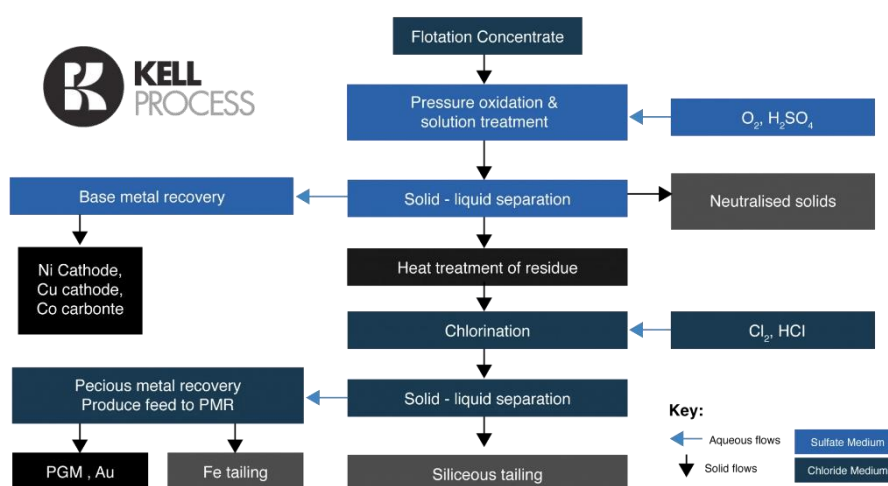


Figure 46: Kell's process (Source: Sedibelo Resources<sup>34</sup>)

In another case, LCA conducted by Guo et al. [123] illustrated that HMT consumed 17.8% less energy than PMT, in the case of Li battery recycling.

Like in pyrometallurgy, microwave and ultrasound can also be applied to HMT processes. Patil et al. [128] attained an 85% Co recovery rate when leaching LiCoO<sub>2</sub> under 180 W irradiation for 25 min with a mixture of ascorbic and citric acids. Parhi et al. [129] extracted 99.2% Ni within 5 minutes of 1000 W irradiation from spent desulphurization catalyst using sulphuric acid as the leachant. Jafarifar et al. [130] irradiated catalysts containing Pt and Re at 150 W for 5 minutes and recovered 98.3% of Pt using aqua regia at a solid/liquid ratio of 2. The same process without the irradiation yielded <70% recovery efficiency. The effect of weight, temperature (adjusted by microwave), and time on Platinum recovery from spent CCR (Continuous Catalyst Regeneration) platforming catalysts was carried out by Shauma et al. [131] using aqua regia. The results are presented in Table 12.

Table 12: Platinum recovery at various temperatures (Adapted from [131])

Catalyst wt. (g)	Recovery at different temperatures (%)				
	180°C	190°C	200°C	210°C	220°C
0.04	36.88	37.34	38.28	39.06	39.06
0.06	51.41	55.00	57.19	57.34	61.25
0.08	83.13	86.56	87.81	89.53	91.88
0.10	86.09	90.16	91.09	93.13	94.06

<sup>33</sup> <https://www.miningweekly.com/article/smelterless-low-energy-platinum-processing-concept-advances-further-in-australia-2023-03-31>

<sup>34</sup> [sedibeloresources.com/kell-process/](https://sedibeloresources.com/kell-process/)

Ultrasound can improve the mass transfer and diffusion kinetics of the leachants, enhance solubility of the metals, hence increasing the leaching efficiency. The mechanical, thermal and cavitation effects of the ultrasound play key roles in this. Research in this area is pretty extensive as evidenced by the review work of Bao et al. [132] Some relevant examples include the usage of 30 kHz waves at 90°C for 50 minutes to retrieve 95% Ni from spent catalysts with HNO<sub>3</sub>, 37 kHz at 40°C for 35 minutes retrieving 100% Ni and Co from spent Li-ion batteries with lemon juice-H<sub>2</sub>O<sub>2</sub> as the leachant [133], and disintegration of Pt from Pt/Al<sub>2</sub>O<sub>3</sub> catalysts using aqua regia in the presence of ultrasonic waves (details not specified) getting a 50.2% platinum concentration after 10 minutes [134]. Hongying et al. [135] recovered 97.17% Pt from dehydrogenation spent catalysts using 400 W ultrasound at 90°C for 150 minutes using a HCl-H<sub>2</sub>O<sub>2</sub>-NaClO<sub>3</sub>-AlCl<sub>3</sub> leachant system.

Adjustments can also be made to adapt to current solvent technology. Some unconventional solvents include alkaline glycine, iodide systems, bromide systems, chloride systems, thiocyanate, thiourea, thiosulfate, etc. [136] From literature survey, it was inferred that the use of non-aqueous solvents, i.e., ionic liquids, deep eutectic solvents, is the current trend (Refer Table 13). Organic solvents are also good choices but their volatile nature is a major drawback [137]. Another interesting strategy is the use of subcritical water. Khan et al. [138] were able to retrieve 96.38% and 99.96% of Ni and Co from nickel-cadmium batteries using PVC-mixed subcritical water at 300°C and 120 minutes reaction time.

Table 13: Novel solvents used in hydrometallurgy

Metal	Chemicals	Solvent technology	Recovery efficiency (%)	Reference
Platinum	HCl + H <sub>2</sub> O <sub>2</sub> + polySILP	Ionic liquid	86	[139]
	Diaion PA308	Ion exchange resin	99.4	[140]
	Trioctylphosphine oxide + 1-butanol	Hydrophobic deep eutectic solvent	98.9	[141]
	Tetraoctylammonium bromide+Hexanoic acid	Deep eutectic solvent	99.8	[142]
Nickel	0.4M EDTA	Chelating agent	72.7	[143]
	trialkylmethylammonium chloride + decanoic acid	Hydrophobic deep eutectic solvent	>99	[137]
	Subcritical water	Subcritical water extraction	Not provided	[144]
	Subcritical water + PVC	Subcritical water extraction	96.38	[138]
	[P <sub>44414</sub> ][Cl]-NaCl-H <sub>2</sub> O	Ionic liquid	Not provided	[145]
	[P <sub>8888</sub> ][Oleate]	Ionic liquid	100	[146]
Cobalt	Subcritical water + PVC	Subcritical water extraction	99.96	[138]
	1:2 choline chloride:formic acid	Deep eutectic solvent with microwave-assistance	>99	[147]
	trialkylmethylammonium chloride + decanoic acid	Hydrophobic deep eutectic solvent	>99	[137]
	p-toluene sulfonic acid+choline chloride	Deep eutectic solvent	>90	[148]
	p-toluene sulfonic acid+ polyethylene glycol	Deep eutectic solvent	>90	[148]
	[P <sub>44414</sub> ][Cl]-NaCl-H <sub>2</sub> O	Ionic liquid	Not provided	[145]
	[P <sub>8888</sub> ][Oleate]	Ionic liquid	100	[146]

### 6.2.3. BIO METALLURGY

It is widely accepted that biology-based routes have the least emissions of all the technologies. Though many mining companies use these techniques for the leaching of ores, at present, bio recovery for recycling purposes is still nascent. This drawback notwithstanding, biotechnological developments with regards to Pt, Ni and Co which can be implemented at a larger scale in the future are explained in detail.

Bioleaching (using lixivants generated by biological means) is an attractive option for a profound reduction in carbon footprint. Both one-step and two-step bioleaching can be utilized. The main advantage of two-step bioleaching is that microbial death by the catalysts' toxicity can be prevented. But a single-step process, if optimized, can be economically and environmentally more beneficial. A few works done in the bioleaching of platinum, nickel and cobalt from secondary source are summarized in Table 14.

To understand the process, the work of Park et al. [149] is explained in detail. The team used a two-step leaching process for the recovery of Pt, Pd and Rh from spent automotive catalysts. With the help of *Chromobacterium violaceum* bacteria, they acquired cyanide which was then employed for the extraction. Out of the various conditions tested, the optimal temperature and cyanide concentration were determined to be 150°C and 1000 mg/L leading to a Pt recovery rate of 92.1%. To produce sodium cyanide, 1g/L of glycine precursor, >5 N NaOH traps, and a pH value of 11 were determined to be optimal. Overall, the cyanide production and accumulation in the NaOH trap reaches a maximum before the completion of 2 days, after which the stationary phase starts, and production rate degrades.

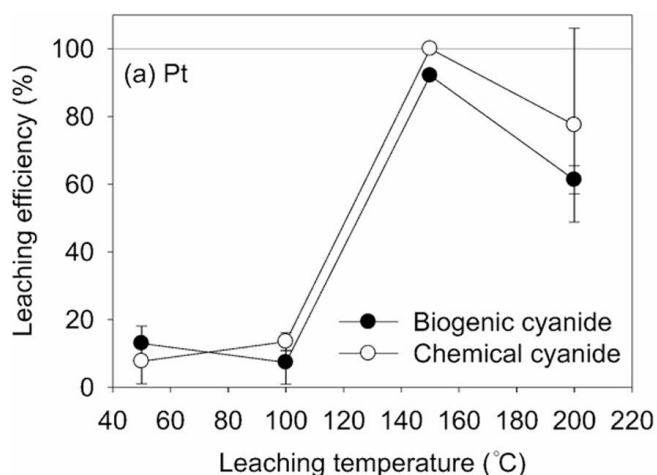


Figure 47: Platinum recovery rate at 150°C using NaCN from *Chromobacterium violaceum* (Source: [149])

Table 14: Bioleaching advances in Platinum, Nickel, and Cobalt recovery

Metal	Organism	Species	Leaching conditions	Recovery efficiency (%)	Reference
Platinum	<i>Chromobacterium violaceum</i>	Bacteria	Two-step leaching 150°C pH 11 NaCN	92.1	[149]
	<i>Bacillus megaterium</i>	Bacteria	Two-step leaching pH 9 Pre-treatment - <45 µm particles after ball-milling and sieving HCN	50	[150]
	<i>Pseudomonas fluorescens</i>	Bacteria	Two-step leaching pH 10 HCN	58	[150]

			Pre-treatment - <45 $\mu\text{m}$ particles after ball-milling and sieving		
	<i>Bacillus megaterium</i>	Bacteria	Two-step HCN leaching 30°C pH 9 Pre-treatment - <75 $\mu\text{m}$ particles after decoking, ball-milling, and sieving	15.7	[151]
	<i>Pseudomonas plecoglossicida</i>	Bacteria	Two-step cyanide leaching pH 7.2	0.2	[152]
Nickel	<i>Penicillium simplicissimum</i>	Fungi	One-step oxalic and citric acid leaching 30°C pH 3	100	[153]
	<i>Aspergillus niger</i>	Fungi	One-step oxalic and citric acid leaching 30°C pH 2	>95	[153]
	<i>Thiobacillus ferrooxidans</i> + <i>Thiobacillus thiooxidans</i>	Bacteria	Two-step ferric iron and sulfuric acid leaching 30°C pH 4	>90	[153]
	<i>Guyarkeria halophila</i> VKM B-2757D + <i>Acidithiobacillus</i> sp. KZ-02	Bacteria	Subsequent formic and sulfuric acid leaching pH 5-5.4 28°C	69.75	[154]
Cobalt	<i>Aspergillus niger</i>	Fungi	Citric and oxalic acid leaching pH 1 30°C	86	[155]
	<i>Penicillium chrysogenum</i> KBS3	Fungi	Ferulic acid leaching pH 3.3-3.7 30°C	60	[155]
	<i>Aspergillus niger</i>	Fungi	Ultrasound-enhanced, citric, oxalic, malic, and tartaric acid pH 6 28°C	71	[155]
	HQ0211 (patented)	Bacteria	pH 1.5 45°C	96.5	[155]
	<i>Acidithiobacillus thiooxidans</i> + <i>Acidithiobacillus ferrooxidans</i>	Bacteria	Ferric iron and sulfuric acid leaching pH 2 30°C	91	[155]
	<i>Acidiphilium multivorum</i> + <i>Leptospidillum ferriphilum</i>	Bacteria	Reduction and oxidation of iron species pH 2.05 30°C	>99	[156]

Many other mechanisms such as siderophore leaching (e.g., platinum and palladium recovery from PGM ore [157]) is also gaining impetus. Use of ultrasound for bioleaching, termed sonobioleaching was explored in the late-90s and early 2000s for nickel leaching from its ores [158][159]. The waves help in removing carbon dioxide and oxygen, accelerate the nutrient process intake, increase mass transfer inside and outside the cells, etc. thereby providing an optimal environment for the organisms [159]. Using *Aspergillus niger*, a nickel recovery of 95% was achieved in a one-step leaching process using 20 kHz ultrasonic pretreatment of the biomass for 30 minutes using an intensity of 1.5 W/cm<sup>2</sup> by Panchanadikar et al. [158] When they increased the intensity to 2.25 W/cm<sup>2</sup>, the same could be achieved with 15-minute exposure [159]. Using a modified version of this process, Anjum et al. [160] extracted 71.1% of cobalt from black shale.

Biosorption using bacteria, fungi, algae, proteins, and even plants have been studied. Those pertinent to the metals of interest are presented in Table 15.

Table 15: Biosorption of Platinum, Nickel, and Cobalt

Metal	Organism/Compound	Species	Efficiency, in terms of the adsorption capacity (mmol/g)	Reference
Platinum	Chitosan derivatives – carboxymethyl groups	Not applicable	0.006	[161]
	Chitosan derivatives – glycine groups	Not applicable	0.628	[161]
	<i>Desulfovibrio desulfuricans</i>	Bacteria	0.32	[161]
Nickel	<i>Candida</i> spp.	Fungi	0.797	[162]
	Nickel adapted <i>Candida</i> spp.	Fungi	0.525	[162]
	<i>Stenotrophomonas</i> MB339	Bacteria	0.00852	[163]
	<i>Escherichia coli</i> JM109	Bacteria	0.015	[70]
Cobalt	<i>Escherichia coli</i> JM109, BL21-DE3, MC4100, ARY023	Bacteria	0.000204	[70]
	<i>Deinococcus radiodurans</i> R1	Bacteria	0.000204	[70]
	<i>Mortierella</i> Coem. (1863) SPS403	Fungi	17.61	[164]
	<i>Rhizopusarrhizus</i> A.Fisch. (1892)	Fungi	0.124	[164]

Genetic engineering can improve the metal selectivity of organisms. Gene manipulation (e.g., *nixA*), enzyme overexpression (e.g., serine acetyltransferase), genome replication, gene deletion, etc. have been used to increase the bioaccumulation. Taking Ni as an example, overexpression of the serine acetyltransferase enzyme and manipulation of the *nixA* gene have led to increased Ni<sup>2+</sup> bioaccumulation. Likewise, bio-engineered *E. coli* and *Deinococcus radiodurans* R1 strains have successfully removed cobalt and nickel [165].

## 6.3. BENEFIT ANALYSIS

### 6.3.1. METHODOLOGY

Per each CRM, the process that is the currently used is weighed against the processes that yield the maximum recovery in emerging technologies – bioleaching, ultrasound and microwave-based metallurgy, and novel solvents in hydrometallurgy. Because each technology has its unique performance indicators, for a comparison amongst the varying PMT, HMT, and BMT techniques, the common factors of temperature, time, pH, and recovery efficiency are used for the optimal process selection.

Detailed benefit analyses involve the evaluation of key performance indicators (KPIs) such as the global warming potential (the energy absorbed by a ton of emitted gas relative to a ton of emitted carbon dioxide<sup>35</sup>), ecotoxicity, human toxicity, costs, etc. Though these values are readily available for conventional HMT, PMT, and BMT, for the emerging processes that are still at a laboratory scale, these values do not hold much relevance. Also, for BMT, the calculation must include the resources to cultivate the bio-organisms. It is also important to note that the factors considered here directly contribute to several important KPIs, including but not limited to energy consumption, overall costs, profits, and carbon footprint. Temperatures closer to room temperature implies an energy-efficient process because of the avoidance of sophisticated heating and cooling equipment that uses expensive temperature-resistant materials. As an example, in conventional pyrometallurgy, an estimated 300 MJ/kg is needed for the recovery of the precious metals from LiB feedstock. Employing a microwave wattage of 1000 W, the energy is drastically reduced to 2.5MJ/kg [129]. Similarly, neutral pH (pH 7) can also reduce equipment costs by eliminating frequent maintenance checks, equipment replacement, and choosing common materials over highly corrosion-resistant ones. A higher recovery rate and lesser time for recovery also lead to reduced power consumption and enables a higher feedstock recycling rate.

### 6.3.2. SCORING SCHEME

A 1-5 scoring scheme (Table 16) is applied to the factors. All the factors are given equal weightage by virtue of their aforementioned importance. This means that the final composite score per process can be calculated by averaging the individual factor scores.

Table 16: Benefit analysis scoring scheme

Value	Temperature (°C)	Time (minutes)	pH	Recovery efficiency (%)
1	$T > 1000$	Time $> 270$	pH $\leq 0.0$ , pH $\geq 14.0$	Efficiency $< 90.0$
2	$500 < T \leq 1000$	$150 < \text{Time} \leq 270$	$0.0 < \text{pH} \leq 2.0$ $12.0 < \text{pH} \leq 14.0$	$90.0 \leq \text{Efficiency} < 95.0$
3	$250 < T \leq 500$	$90 < \text{Time} \leq 150$	$2.0 < \text{pH} \leq 4.0$ $10.0 < \text{pH} \leq 12.0$	$95.0 \leq \text{Efficiency} < 97.5$
4	$50 < T \leq 250$	$30 < \text{Time} \leq 90$	$4.0 < \text{pH} \leq 6.9$ $7.0 < \text{pH} \leq 10$	$97.5 \leq \text{Efficiency} < 100$
5	$20 \leq T \leq 50$	Time $\leq 30$	pH = 7.0	Efficiency = 100

In processes where a certain factor is irrelevant, no score is given to that factor and the average of the other factors is considered the final score. For example, metallic bath (slag, matte, etc.) in PMT do not have a pH. Similarly, for the MW-assisted HMT for Platinum [130], Nickel [129], and Cobalt [128], the authors do not explicitly mention the process temperatures but rather specify the wattages (150 W, 1000 W, and 180 W, respectively, for Platinum, Nickel, and Cobalt). Since the precise temperature depends on a number of factors such as the specific heat capacity of the process chemicals determined by the quantities of the leachants used, and the composition and the mass of the feedstock, and the instrument specifications including wattage, maximum temperature attainable, and the time in which that maximum temperature can be reached, approximation was not deemed a prudent option.

### 6.3.3. OPTIMAL RETRIEVAL PROCESS DETERMINATION

Now that the scoring system is established, the optimal retrieval strategies for the CRMs can be determined. The factors and their respective scores for Platinum, Nickel, and Cobalt are tabulated in Table 17, Table 18, and Table 19.

<sup>35</sup> <https://www.epa.gov/ghgemissions/understanding-global-warming-potentials>

### 6.3.3.1. Platinum

Table 17: Viable strategy determination for Platinum

Process		Temperature (°C)	Time (minutes)	pH	Recovery efficiency (%)	Final score	Reference
PMT	Value	1500	240	Not applicable	98	<b>2.33</b>	[110]
	Score	<b>1</b>	<b>2</b>	-	<b>4</b>		
MW-assisted PMT	Value	1250	120	Not applicable	98.59	<b>2.67</b>	[124]
	Score	<b>1</b>	<b>3</b>	-	<b>4</b>		
HMT	Value	150	120	-1.08	96	<b>2.75</b>	[166]
	Score	<b>4</b>	<b>3</b>	<b>1</b>	<b>3</b>		
HMT – novel solvent technology	Value	25	~120	1 (0.1 mol/dm <sup>3</sup> HCl)	99.8	<b>3.5</b>	[140]
	Score	<b>5</b>	<b>3</b>	<b>2</b>	<b>4</b>		
MW-assisted HMT	Value	Not applicable	5	2	98.3	<b>3.67</b>	[130]
	Score	-	<b>5</b>	<b>2</b>	<b>4</b>		
US-assisted HMT	Value	90	150	1.56	97.17	<b>3</b>	[135]
	Score	<b>4</b>	<b>3</b>	<b>2</b>	<b>3</b>		
BMT	Value	150	60	11	92.1	<b>3.25</b>	[149]
	Score	<b>4</b>	<b>4</b>	<b>3</b>	<b>2</b>		

### 6.3.3.2. Nickel

Table 18: Viable strategy determination for Nickel

Process		Temperature (°C)	Time (minutes)	pH	Recovery efficiency (%)	Final score	Reference
PMT	Value	1450	30	Not applicable	98.39	<b>3.33</b>	[113]
	Score	<b>1</b>	<b>5</b>	-	<b>4</b>		
MW-assisted PMT	Value	900	30	Not applicable	97.65	<b>3.67</b>	[125]
	Score	<b>2</b>	<b>5</b>	-	<b>4</b>		
HMT	Value	90	1080	11	99.99	<b>3</b>	[167]
	Score	<b>4</b>	<b>1</b>	<b>3</b>	<b>4</b>		
HMT – novel solvent technology	Value	22	375	1-2	100	<b>3.25</b>	[146]
	Score	<b>5</b>	<b>1</b>	<b>2</b>	<b>5</b>		
MW-assisted HMT	Value	Not applicable	5	-0.55 (from 10 (v/v) % H <sub>2</sub> SO <sub>4</sub> )	99.2	<b>3.33</b>	[129]
	Score	-	<b>5</b>	<b>1</b>	<b>4</b>		
US-assisted HMT	Value	40	35	2.26 (average of pH 2 and pH 3)	100	<b>4.25</b>	[133]
	Score	<b>5</b>	<b>4</b>	<b>3</b>	<b>5</b>		
BMT	Value	30	30240	3	100	<b>3.5</b>	[153]
	Score	<b>5</b>	<b>1</b>	<b>3</b>	<b>5</b>		
US-assisted BMT	Value	37 (actual leaching)	20160	2.7	95	<b>2.75</b>	[158], [159]
	Score	<b>4</b>	<b>1</b>	<b>3</b>	<b>3</b>		

### 6.3.3.3. Cobalt

Table 19: Viable strategy determination for Cobalt

Process		Temperature (°C)	Time (minutes)	pH	Recovery efficiency (%)	Final score	Reference
PMT	Value	1450	30	Not applicable	98.83	<b>3.33</b>	[113]
	Score	<b>1</b>	<b>5</b>	-	<b>4</b>		
MW assisted PMT	Value	900	30	Not applicable	97.85	<b>3.67</b>	[125]
	Score	<b>2</b>	<b>5</b>	-	<b>4</b>		
HMT	Value	90	1080	3	100	<b>3.25</b>	[167]
	Score	<b>4</b>	<b>1</b>	<b>3</b>	<b>5</b>		
HMT – novel solvent technology	Value	22	250	-0.9	100	<b>3.25</b>	[146]
	Score	<b>5</b>	<b>2</b>	<b>1</b>	<b>5</b>		
MW-assisted HMT	Value	Not applicable	25	1.91	85	<b>2.67</b>	[128]
	Score	-	<b>5</b>	<b>2</b>	<b>1</b>		
US-assisted HMT	Value	40	35	2.26 (average of pH 2 and pH 3)	100	<b>4.25</b>	[133]
	Score	<b>5</b>	<b>4</b>	<b>3</b>	<b>5</b>		
BMT	Value	30	10080	2.05	>99	<b>3.25</b>	[156]
	Score	<b>5</b>	<b>1</b>	<b>3</b>	<b>4</b>		
US-assisted BMT	Value	28	34560	1.51	71.1	<b>2.25</b>	[160]
	Score	<b>5</b>	<b>1</b>	<b>2</b>	<b>1</b>		

For Platinum, MW-assisted HMT process followed by Jafarifar et al. [130] emerges as the best recycling option. This is immediately followed by novel solvent-assisted HMT. When comparing their recycling efficiencies, the method with the solvent has an upper hand, but the processing time of ~120 minutes results in lesser recycling rate which is usually not preferred by industries for combating the increasing recycling demands.

For Nickel and Cobalt, US-assisted HMT is highly optimal with a good score of 4.25. The fact that it uses a readily available and environmentally-friendly leachant – lemon juice, makes it a coveted process. It is important to note that the BMT (conventional and US-assisted) methods that have acceptable recovery yields are one-step leaching processes with processing time in days [153][156][158][159][160]. If the processes can be modified to become two-stepped, then the actual recovery time would be drastically reduced. Considering this, if the scores are recalculated for BMT and US-assisted BMT without taking the process time into account, a score of 4.33 and 4.00 are observed for Nickel and Cobalt recovery using conventional BMT routes [153][156].

### 6.3.4. CRM RECOVERY FROM 2035-2050

To recapitulate, with the chosen scoring scheme, the process availed by Jafarifar et al. [130] for Platinum recovery with an aggregate score of **3.67** and that of Rahimi et al. [133] for Nickel and Cobalt recovery with a score of **4.25** are the viable options. The associated recovery efficiencies of Platinum - 98.3%, Nickel – 100%, and Cobalt – 100% can be used to determine the amount of CRMs that can be recovered from 2035-2050. The values are displayed in Figure 48, Figure 49, and Figure 50. In 2050 specifically, the CRM amount that would be recovered is tabulated (Table 20).

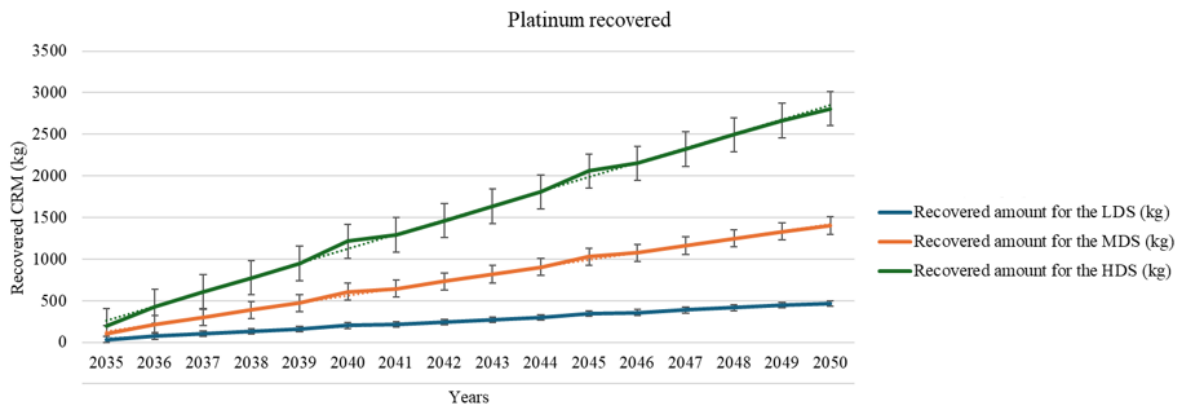


Figure 48: Platinum recovered using MW-assisted HMT

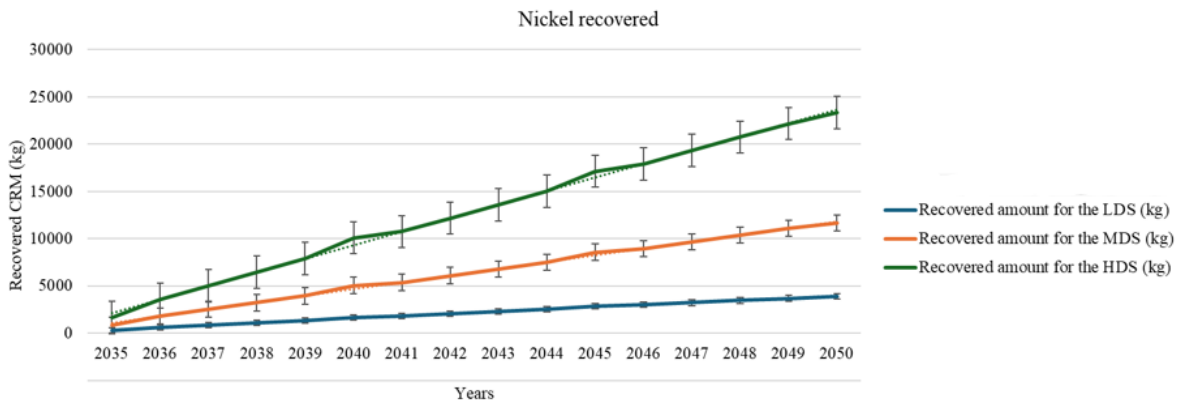


Figure 49: Nickel recovered using US-assisted HMT

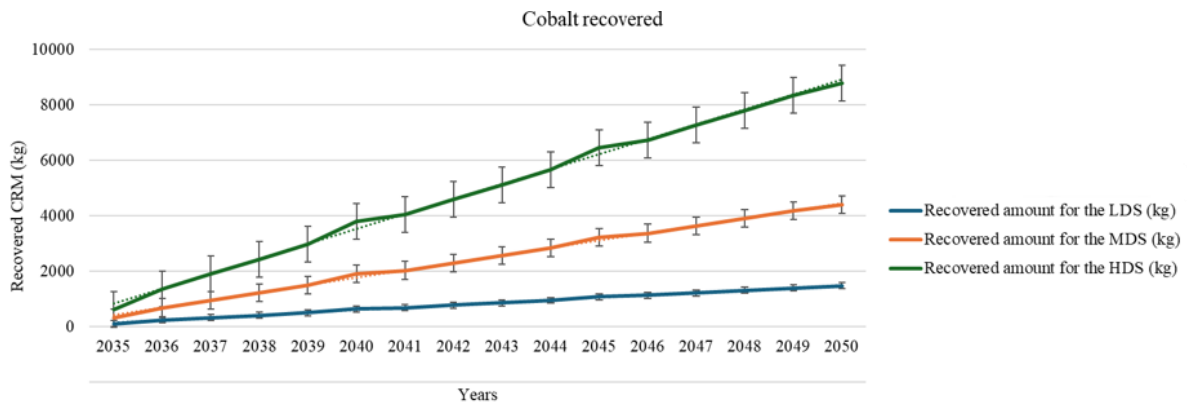


Figure 50: Cobalt recovered using US-assisted HMT

Table 20: Recycled CRMs for 2050

CRM	RECYCLED AMOUNT IN 2050 (kg)					
	Low loading			High loading		
	LDS	MDS	HDS	LDS	MDS	HDS
Platinum	0.82	2.48	4.96	918.89	2756.73	5513.51
Nickel	3.85	11.54	23.08	7782.12	23346.71	46693.78
Cobalt	98.15	294.46	588.93	2832.41	8497.36	16994.85

## 6.4. OTHER RECOMMENDATIONS

It is important to mention the imminent expansion of current recycling plants to account for the growing e-waste. As an example, Umicore, which launched its Battery Recycling Solutions in 2022, plans to be Europe's largest battery recycling plant with a 150,000-tonne capacity by 2026. Using pyrometallurgy, they generate a metal alloy of copper, nickel and cobalt and lithium-concentrate. Further lean hydrometallurgy recovers individual metals which can be reused in batteries, thus closing the material loop of the battery value chain.<sup>36</sup> Future AEMWE plants that incorporate either PGM-based catalysts or purely base-metal catalysts (assuming catalyst technology reaches such a stage) can close the loop by collaboration with the recycling companies. An example of such a coalition would be the one between Audi and Umicore, where they entered closed loop battery recycling operations in January 2020 after initial testing phases. The feedstock is the cell modules of the Audi e-tron model car from which nickel and cobalt can be recovered.<sup>37</sup>

Finally, it should be noted that implementing any of the suggested strategies would lead to the incurrence of capital and operational expenses (CAPEX and OPEX). Detailed feasibility, Cost Benefit Analysis (CBA), and Life Cycle Assessment (LCA) studies at an industrial scale must be carried out taking the company size into account.

---

<sup>36</sup> <https://www.umicore.com/en/newsroom/news/umicore-battery-recycling/#:~:text=Our%20proprietary%20process%20is%202020,end%2Dof%2Dlife%2Dbatteries.>

<sup>37</sup> <https://www.umicore.com/en/newsroom/news/battery-recycling-audi-and-umicore-start-closed-loop-for-cobalt-and-nickel/>

## 7. CONCLUSION

For achieving the main objective of contributing to sustainable aviation by tackling material demand issues at the fuel manufacturing level, the study started with the formulation of the research question - **What is the most viable retrieval strategy that mitigates the material demand of Platinum, Nickel, and Cobalt CRMs from AEMWE catalysts within the context of hydrogen in global aviation?**

Using the estimated hydrogen demands of 2.6, 15.9, 27, 36.8 Mtonnes for the years 2035, 2040, 2045, and 2050, respectively provided by the European Commission, the amount of Platinum, Nickel, and Cobalt that can be retrieved from 2035-2050 was calculated. Using the specifications of Enapter's 1 MW capacity AEM Nexus 1000, the following values were obtained for Platinum, Nickel, and Cobalt, respectively, in a high catalyst loading and high demand (60%) scenario in 2050 - 5608.86 kg/year, 46693.78 kg/year, and 16994.85 kg/year.

Reverting to the main objective of sustainable aviation, various retrieval routes in pyrometallurgy, hydrometallurgy, and bio metallurgy were analysed. Current developments such as employing new solvents in hydrometallurgy, use of microwave and ultrasound to enhance the recovery kinetics across the three major metallurgy domains, etc. were discussed. From the benefit analysis performed, MW-assisted HMT using aqua regia for platinum retrieval, and US-assisted HMT with lemon juice/H<sub>2</sub>O<sub>2</sub> for nickel and cobalt scored higher – 3.67 (platinum), 4.25 (nickel), and 4.25 (cobalt) out of a potential 5, indicating their potential for replacing older techniques. The recovery rates employing these strategies would be 98.3%, 100%, and 100% for Platinum, Nickel, and Cobalt, respectively. It was also deduced that for Nickel and Cobalt, the conventional BMT routes performed well with scores of 4.33 and 4 out of a potential 5, if the long process times were not considered in the aggregate score calculation. In reality, this would imply a modification in the process strategy from being one-step to two-step leaching.

Considering that the aircraft in question would already be considerably sustainable because of the use of hydrogen and hydrogen-based fuels, further sustainability enhancement can be achieved with the implementation of the green hydrogen production method (AEMWE). If the suggested circular strategies for CRM retrieval from electrocatalysts are employed, sustainability can be ensured at all levels.

# 8. GUIDELINES FOR FUTURE WORK

Within the timeframe of this thesis, a rudimentary material demand for the future CRM demand and qualitative assessment of the applicable recovery strategies were carried out. But further steps can be taken to enhance CRM recovery at different levels. Considering EU imports 71% of platinum<sup>38</sup>, and 86% of cobalt<sup>39</sup>, and 75% of nickel [24], following the below suggestions can bring about a reduction in the dependency from other countries.

- Data availability and quality is key for getting higher quality predictions. Hence, the first suggestion is to wait for more AEMWE plants to come into existence, collect real-time data and then perform the analyses. For instance, in the present work, an ideal scenario of uninterrupted machine productivity was assumed for material demand. This can be recalculated using live data from a working plant.
- The same can be suggested regarding the catalyst loading used in material demand prediction. When run at a large scale, the actual loading required might be either above or below the lab-tested values.
- The material demand can be calculated at a regional/ continental scale. This can help in better strategizing the number of recycling plants, AEMWE systems, etc. needed in apt locations which can further lead to optimized material flow channels in the long run.
- Collaboration between different industries can lead to knowledge sharing and development of metal recovery routes that covers a wide range of materials.
- Material demand can also be calculated for other potential CRMs (Ir, Ru, Mn, etc.) that may be used in electrolyser technology.
- At a research level, looking for better catalyst designs that promotes facile dismantling during EoL is encouraged.
- Catalyst materials that either eliminates the use of CRMs or mitigates it to inconsequential levels can be developed.
- Research efforts regarding environment-friendly recovery methods are beneficial.
- Qualitative/quantitative analysis including the different pretreatment routes present can also be undertaken making use of CBA, MFA, and LCA studies incorporating elaborate sensitivity analyses. This is a reiteration of the statement presented in Chapter 6 - CAPEX and OPEX calculations depend strictly on the company's scale and must be evaluated. With advances in AI, the mentioned calculations can be made as complex as possible incorporating various Key Performance Indicators and capturing different scenarios.
- At a national/international level, establishing more effective frameworks for CRM sourcing and usage can be applied.
- Likewise, providing incentives that encourage both research efforts and practice of recycling can be adopted.

---

<sup>38</sup> [https://single-market-economy.ec.europa.eu/sectors/raw-materials/areas-specific-interest/critical-raw-materials\\_en](https://single-market-economy.ec.europa.eu/sectors/raw-materials/areas-specific-interest/critical-raw-materials_en)

<sup>39</sup> <https://investingnews.com/daily/resource-investing/battery-metals-investing/cobalt-investing/europes-cobalt-supply-chain/>

# REFERENCES

- [1] M. Mohsen *et al.*, “Comparing the generation of electricity from renewable and non-renewable energy sources in Iran and the world: Now and future,” *World J. Eng.*, vol. 12, no. 6, pp. 627–638, 2015, doi: 10.1260/1708-5284.12.6.627.
- [2] “World Energy Investment 2023,” *World Energy Invest. 2023*, 2023, doi: 10.1787/e0e92e98-en.
- [3] Y. Yang, S. Xia, and X. Qian, *Geopolitics of the energy transition*, vol. 33, no. 4, 2023. doi: 10.1007/s11442-023-2101-2.
- [4] International Renewable Energy Agency (IRENA), *World energy transitions outlook 2022*. 2022. [Online]. Available: <https://irena.org/Digital-Report/World-Energy-Transitions-Outlook-2022%0Ahttps://irena.org/publications/2021/March/World-Energy-Transitions-Outlook>
- [5] “Tracking SDG7: The energy progress report,” *World Bank*, 2023.
- [6] “Electricity Market Report,” *Electr. Mark. Rep.*, 2023, doi: 10.1787/f0aed4e6-en.
- [7] International Renewable Energy Agency (IRENA), *Renewable Energy Statistic 2023*. 2023.
- [8] I. Davydenko and H. Hilbers, “Decarbonization Paths for the Dutch Aviation Sector,” *Sustain.*, vol. 16, no. 3, 2024, doi: 10.3390/su16030950.
- [9] B. D. Catumba *et al.*, “Sustainability and challenges in hydrogen production: An advanced bibliometric analysis,” *Int. J. Hydrogen Energy*, vol. 48, no. 22, pp. 7975–7992, 2023, doi: 10.1016/j.ijhydene.2022.11.215.
- [10] M. A. Rosen and D. S. Scott, “Comparative efficiency assessments for a range of hydrogen production processes,” *Int. J. Hydrogen Energy*, vol. 23, no. 8, pp. 653–659, 1998, doi: 10.1016/s0360-3199(97)00080-3.
- [11] H. Ishaq, I. Dincer, and C. Crawford, “A review on hydrogen production and utilization: Challenges and opportunities,” *Int. J. Hydrogen Energy*, vol. 47, no. 62, pp. 26238–26264, 2022, doi: 10.1016/j.ijhydene.2021.11.149.
- [12] C. Ram, P. Rani, and A. Kumar, “Recent developments in biohydrogen production from wastewater: A review,” *Biocatal. Biotransformation*, vol. 0, no. 0, pp. 1–18, 2023, doi: 10.1080/10242422.2023.2181046.
- [13] S. A. Lee, J. Kim, K. C. Kwon, S. H. Park, and H. W. Jang, “Anion exchange membrane water electrolysis for sustainable large-scale hydrogen production,” *Carbon Neutralization*, vol. 1, no. 1, pp. 26–48, 2022, doi: 10.1002/cnl2.9.
- [14] S. Bruce, M. Temminghoff, J. Hayward, D. Palfreyman, C. Munnings, and N. Burke, “Opportunities for hydrogen in aviation,” *Csiro*, 2020.
- [15] P. Nikolaidis and A. Poullikkas, “A comparative overview of hydrogen production processes,” *Renew. Sustain. Energy Rev.*, vol. 67, pp. 597–611, 2017, doi: 10.1016/j.rser.2016.09.044.
- [16] J. M. M. Arcos and D. M. F. Santos, “The Hydrogen Color Spectrum: Techno-

- Economic Analysis of the Available Technologies for Hydrogen Production,” *Gases*, vol. 3, no. 1, pp. 25–46, 2023, doi: 10.3390/gases3010002.
- [17] A. Lim *et al.*, “A study on electrode fabrication and operation variables affecting the performance of anion exchange membrane water electrolysis,” *J. Ind. Eng. Chem.*, vol. 76, pp. 410–418, 2019, doi: 10.1016/j.jiec.2019.04.007.
- [18] M. Wang, Z. Wang, X. Gong, and Z. Guo, “The intensification technologies to water electrolysis for hydrogen production - A review,” *Renew. Sustain. Energy Rev.*, vol. 29, pp. 573–588, 2014, doi: 10.1016/j.rser.2013.08.090.
- [19] Q. Xu *et al.*, “Anion Exchange Membrane Water Electrolyser: Electrode Design, Lab-Scaled Testing System and Performance Evaluation,” *EnergyChem*, vol. 4, no. 5, p. 100087, 2022, doi: 10.1016/j.enchem.2022.100087.
- [20] P. Fortin, T. Khoza, X. Cao, S. Y. Martinsen, A. Oyarce Barnett, and S. Holdcroft, “High-performance alkaline water electrolysis using Aemion™ anion exchange membranes,” *J. Power Sources*, vol. 451, no. January, 2020, doi: 10.1016/j.jpowsour.2020.227814.
- [21] C. Li and J. B. Baek, “The promise of hydrogen production from alkaline anion exchange membrane electrolyzers,” *Nano Energy*, vol. 87, no. February, p. 106162, 2021, doi: 10.1016/j.nanoen.2021.106162.
- [22] E. K. Volk, M. E. Kreider, S. Kwon, and S. M. Alia, “Recent progress in understanding the catalyst layer in anion exchange membrane electrolyzers – durability, utilization, and integration,” *EES Catal.*, pp. 109–137, 2024, doi: 10.1039/d3ey00193h.
- [23] C. Grohol, M., Veeh, “Study on the critical raw materials for the EU 2023 : final report,” Publications Office of the European Union, 2023. [Online]. Available: <https://data.europa.eu/doi/10.2873/725585>
- [24] M. Grohol and C. Veeh, *Study on the Critical Raw Materials for the EU 2023 – Final Report*. 2023. doi: 10.2873/725585.
- [25] D. Reike, W. J. V. Vermeulen, and S. Witjes, “The circular economy: New or Refurbished as CE 3.0? — Exploring Controversies in the Conceptualization of the Circular Economy through a Focus on History and Resource Value Retention Options,” *Resour. Conserv. Recycl.*, vol. 135, no. November 2017, pp. 246–264, 2018, doi: 10.1016/j.resconrec.2017.08.027.
- [26] N. Aibada, M. Ramachandran, K. K. Gupta, and P. P. Raichurkar, “Review on Various Gaskets Based on the Materials, their Characteristics and Applications,” *Int. J. Text. Eng. Process.*, vol. 3, no. 1, pp. 12–18, 2017.
- [27] D. Jain, “PTFE Gasket: A Complete Guide,” *Asian sealing products*. <https://asiansealing.in/ptfe-gaskets-guide/> (accessed Mar. 19, 2024).
- [28] N. Du, C. Roy, R. Peach, M. Turnbull, S. Thiele, and C. Bock, “Anion-Exchange Membrane Water Electrolyzers,” *Chem. Rev.*, vol. 122, no. 13, pp. 11830–11895, 2022, doi: 10.1021/acs.chemrev.1c00854.
- [29] S. Wang, A. Lu, and C. J. Zhong, “Hydrogen production from water electrolysis: role of catalysts,” *Nano Converg.*, vol. 8, no. 1, 2021, doi: 10.1186/s40580-021-00254-x.

- [30] Z. Angeles-Olvera, A. Crespo-Yapur, O. Rodríguez, J. L. Cholula-Díaz, L. M. Martínez, and M. Videa, *Nickel-Based Electrocatalysts for Water Electrolysis*, vol. 15, no. 5, 2022. doi: 10.3390/en15051609.
- [31] S. Li, E. Li, X. An, X. Hao, Z. Jiang, and G. Guan, “Transition metal-based catalysts for electrochemical water splitting at high current density: Current status and perspectives,” *Nanoscale*, vol. 13, no. 30, pp. 12788–12817, 2021, doi: 10.1039/d1nr02592a.
- [32] W. Zhang, L. Cui, and J. Liu, “Recent advances in cobalt-based electrocatalysts for hydrogen and oxygen evolution reactions,” *J. Alloys Compd.*, vol. 821, p. 153542, 2020, doi: 10.1016/j.jallcom.2019.153542.
- [33] S. M. Stratton, S. Zhang, and M. M. Montemore, “Addressing complexity in catalyst design: From volcanos and scaling to more sophisticated design strategies,” *Surf. Sci. Rep.*, vol. 78, no. 3, p. 100597, 2023, doi: 10.1016/j.surfrep.2023.100597.
- [34] D. Schilter, “Electrocatalysis: Volcano spews out hot new catalyst,” *Nat. Rev. Chem.*, vol. 2, no. 2, p. 41570, 2018, doi: 10.1038/s41570-018-0116.
- [35] M. Liu, L. Y. S. Lee, and K.-Y. Wong, *Highly Efficient Electrocatalytic Water Splitting*. 2021. doi: 10.1007/978-3-030-36268-3\_131.
- [36] Y. Sugawara *et al.*, “Anion Exchange Membrane Water Electrolysers: An Overview,” *J. Chem. Eng. Japan*, vol. 56, no. 1, p., 2023, doi: 10.1080/00219592.2023.2210195.
- [37] D. Henkensmeier, M. Najibah, C. Harms, J. Žitka, J. Hnát, and K. Bouzek, “Overview: State-of-the Art Commercial Membranes for Anion Exchange Membrane Water Electrolysis,” *J. Electrochem. Energy Convers. Storage*, vol. 18, no. 2, 2021, doi: 10.1115/1.4047963.
- [38] B. Motealleh, Z. Liu, R. I. Masel, J. P. Sculley, Z. Richard Ni, and L. Meroueh, “Next-generation anion exchange membrane water electrolysers operating for commercially relevant lifetimes,” *Int. J. Hydrogen Energy*, vol. 46, no. 5, pp. 3379–3386, 2021, doi: 10.1016/j.ijhydene.2020.10.244.
- [39] J. J. Kaczur, H. Yang, Z. Liu, S. D. Sajjad, and R. I. Masel, “Carbon dioxide and water electrolysis using new alkaline stable anion membranes,” *Front. Chem.*, vol. 6, no. JUL, 2018, doi: 10.3389/fchem.2018.00263.
- [40] I. Vincent, E. C. Lee, and H. M. Kim, “Comprehensive impedance investigation of low-cost anion exchange membrane electrolysis for large-scale hydrogen production,” *Sci. Rep.*, vol. 11, no. 1, pp. 1–12, 2021, doi: 10.1038/s41598-020-80683-6.
- [41] M. Jin *et al.*, “Strategies for Designing High-Performance Hydrogen Evolution Reaction Electrocatalysts at Large Current Densities above 1000 mA cm<sup>-2</sup>,” *ACS Nano*, vol. 16, no. 8, pp. 11577–11597, 2022, doi: 10.1021/acsnano.2c02820.
- [42] L. Peng and Z. Wei, “Catalyst Engineering for Electrochemical Energy Conversion from Water to Water: Water Electrolysis and the Hydrogen Fuel Cell,” *Engineering*, vol. 6, no. 6, pp. 653–679, 2020, doi: 10.1016/j.eng.2019.07.028.
- [43] J. Linnemann, K. Kanokkanchana, and K. Tschulik, “Design Strategies for Electrocatalysts from an Electrochemist’s Perspective,” *ACS Catal.*, vol. 11, no. 9, pp. 5318–5346, 2021, doi: 10.1021/acscatal.0c04118.

- [44] Y. Peng *et al.*, “Organically Capped Iridium Nanoparticles as High-Performance Bifunctional Electrocatalysts for Full Water Splitting in Both Acidic and Alkaline Media: Impacts of Metal-Ligand Interfacial Interactions,” *ACS Catal.*, vol. 11, no. 3, pp. 1179–1188, 2021, doi: 10.1021/acscatal.0c03747.
- [45] J. Kim and J. Lee, “Recent Progress in Strategies for Ruthenium-Based Electrocatalysts for Alkaline Hydrogen Evolution and Oxidation Reactions,” *Energy and Fuels*, vol. 37, no. 23, pp. 17765–17781, 2023, doi: 10.1021/acs.energyfuels.3c02671.
- [46] H. Li and G. Li, “Novel palladium-based nanomaterials for multifunctional ORR/OER/HER electrocatalysis,” *J. Mater. Chem. A*, pp. 9383–9400, 2023, doi: 10.1039/d3ta01059g.
- [47] R. M. Bonifacio and M. G. Mena, “Activity of electrodeposited rhodium in acidic and basic water electrolysis,” *Int. J. Hydrogen Energy*, vol. 52, pp. 364–377, 2024, doi: 10.1016/j.ijhydene.2023.06.117.
- [48] D. Chen and S. Mu, “Revitalizing osmium-based catalysts for energy conversion,” *Energy Rev.*, vol. 2, no. 4, p. 100053, 2023, doi: 10.1016/j.enrev.2023.100053.
- [49] H. Osgood, S. V. Devaguptapu, H. Xu, J. Cho, and G. Wu, “Transition metal (Fe, Co, Ni, and Mn) oxides for oxygen reduction and evolution bifunctional catalysts in alkaline media,” *Nano Today*, vol. 11, no. 5, pp. 601–625, 2016, doi: 10.1016/j.nantod.2016.09.001.
- [50] Y. Chen, K. Rui, J. Zhu, S. X. Dou, and W. Sun, “Recent Progress on Nickel-Based Oxide/(Oxy)Hydroxide Electrocatalysts for the Oxygen Evolution Reaction,” *Chem. - A Eur. J.*, vol. 25, no. 3, pp. 703–713, 2019, doi: 10.1002/chem.201802068.
- [51] A. Abdelhafiz *et al.*, “Tri-Metallic Catalyst for Oxygen Evolution Reaction Enables Continuous Operation of Anion Exchange Membrane Electrolyser at 1A cm<sup>-2</sup> for Hundreds of Hours,” *Adv. Energy Mater.*, vol. 2303350, pp. 1–11, 2024, doi: 10.1002/aenm.202303350.
- [52] C. Huang *et al.*, “Recent progress and perspective of cobalt-based catalysts for water splitting: design and nanoarchitectonics,” *Mater. Today Energy*, vol. 23, p. 100911, 2022, doi: 10.1016/j.mtener.2021.100911.
- [53] V. S. Kumbhar, H. Lee, J. Lee, and K. Lee, “Recent advances in water-splitting electrocatalysts based on manganese oxide,” *Carbon Resour. Convers.*, vol. 2, no. 3, pp. 242–255, 2019, doi: 10.1016/j.crcon.2019.11.003.
- [54] P. Zhou *et al.*, “Recent progress on bulk Fe-based alloys for industrial alkaline water electrolysis,” *J. Mater. Chem. A*, vol. 11, no. 4, pp. 1551–1574, 2022, doi: 10.1039/d2ta09052j.
- [55] D. M. F. Santos, C. A. C. Sequeira, D. Macciò, A. Saccone, and J. L. Figueiredo, “Platinum-rare earth electrodes for hydrogen evolution in alkaline water electrolysis,” *Int. J. Hydrogen Energy*, vol. 38, no. 8, pp. 3137–3145, 2013, doi: 10.1016/j.ijhydene.2012.12.102.
- [56] X. Y. Zhang *et al.*, “Rare earth elements induced electronic engineering in Rh cluster toward efficient alkaline hydrogen evolution reaction,” *J. Colloid Interface Sci.*, vol. 666, no. January, pp. 346–354, 2024, doi: 10.1016/j.jcis.2024.04.015.

- [57] F. Rosalbino, D. Macciò, E. Angelini, A. Saccone, and S. Delfino, “Electrocatalytic properties of Fe-R (R = rare earth metal) crystalline alloys as hydrogen electrodes in alkaline water electrolysis,” *J. Alloys Compd.*, vol. 403, no. 1–2, pp. 275–282, 2005, doi: 10.1016/j.jallcom.2005.03.075.
- [58] W. Gao, D. Wen, J. C. Ho, and Y. Qu, “Incorporation of rare earth elements with transition metal–based materials for electrocatalysis: a review for recent progress,” *Mater. Today Chem.*, vol. 12, pp. 266–281, 2019, doi: 10.1016/j.mtchem.2019.02.002.
- [59] C. Li, P. Wang, M. He, X. Yuan, Z. Fang, and Z. Li, “Rare earth-based nanomaterials in electrocatalysis,” *Coord. Chem. Rev.*, vol. 489, p. 215204, 2023, doi: 10.1016/j.ccr.2023.215204.
- [60] M. L. Grilli, A. E. Slobozeanu, C. Larosa, D. Paneva, I. Yakoumis, and Z. Cherkezova-Zheleva, “Platinum Group Metals: Green Recovery from Spent Auto-Catalysts and Reuse in New Catalysts—A Review,” *Crystals*, vol. 13, no. 4, pp. 1–30, 2023, doi: 10.3390/cryst13040550.
- [61] X. Kuangdi and Q. Tao, “Hydrometallurgy,” pp. 1–23, 2024.
- [62] C. Tunsu and T. Retegan, *Hydrometallurgical Processes for the Recovery of Metals from WEEE*, no. Lcd. Elsevier Inc., 2016. doi: 10.1016/B978-0-12-803363-0.00006-7.
- [63] Z. Peng *et al.*, “Pyrometallurgical Recovery of Platinum Group Metals from Spent Catalysts,” *Jom*, vol. 69, no. 9, pp. 1553–1562, 2017, doi: 10.1007/s11837-017-2450-3.
- [64] X. Wen, J. Wang, and H. Wang, “The distribution behavior of elements during the top-blowing smelting process of electronic waste,” *Metals (Basel)*, vol. 11, no. 10, pp. 1–15, 2021, doi: 10.3390/met11101615.
- [65] H. Srichandan, R. K. Mohapatra, P. K. Parhi, and S. Mishra, “Bioleaching approach for extraction of metal values from secondary solid wastes: A critical review,” *Hydrometallurgy*, vol. 189, no. July, p. 105122, 2019, doi: 10.1016/j.hydromet.2019.105122.
- [66] M. N. Le and M. S. Lee, “A Review on Hydrometallurgical Processes for the Recovery of Valuable Metals from Spent Catalysts and Life Cycle Analysis Perspective,” *Miner. Process. Extr. Metall. Rev.*, vol. 42, no. 5, pp. 335–354, 2021, doi: 10.1080/08827508.2020.1726914.
- [67] E. Hsu, K. Barmak, A. C. West, and A. H. A. Park, “Advancements in the treatment and processing of electronic waste with sustainability: A review of metal extraction and recovery technologies,” *Green Chem.*, vol. 21, no. 5, pp. 919–936, 2019, doi: 10.1039/c8gc03688h.
- [68] P. Kinnunen and S. Hedrich, “Biotechnological strategies to recover value from waste,” *Hydrometallurgy*, vol. 222, no. March, 2023, doi: 10.1016/j.hydromet.2023.106182.
- [69] M. Gavrilescu, “Microbial recovery of critical metals from secondary sources,” *Bioresour. Technol.*, vol. 344, no. PA, p. 126208, 2022, doi: 10.1016/j.biortech.2021.126208.
- [70] P. Diep, R. Mahadevan, and A. F. Yakunin, “Heavy metal removal by bioaccumulation using genetically engineered microorganisms,” *Front. Bioeng.*

- Biotechnol.*, vol. 6, no. OCT, 2018, doi: 10.3389/fbioe.2018.00157.
- [71] K. S. Barros, M. C. Martí-Calatayud, T. Scarazzato, A. M. Bernardes, D. C. R. Espinosa, and V. Pérez-Herranz, “Investigation of ion-exchange membranes by means of chronopotentiometry: A comprehensive review on this highly informative and multipurpose technique,” *Adv. Colloid Interface Sci.*, vol. 293, 2021, doi: 10.1016/j.cis.2021.102439.
- [72] É. Kiss, *Characterization of Polymer Blends: Ellipsometry*, vol. 9783527331. 2015. doi: 10.1002/9783527645602.ch09.
- [73] X. Luo, D. I. Kushner, and A. Kusoglu, “Anion exchange membranes: The effect of reinforcement in water and electrolyte,” *J. Memb. Sci.*, vol. 685, no. July, p. 121945, 2023, doi: 10.1016/j.memsci.2023.121945.
- [74] V. K. Undavalli, C. Ling, and B. Khandelwal, *Impact of alternative fuels and properties on elastomer compatibility*. Elsevier Inc., 2021. doi: 10.1016/B978-0-12-818314-4.00001-7.
- [75] M. A. Mohamed, J. Jaafar, A. F. Ismail, M. H. D. Othman, and M. A. Rahman, *Fourier Transform Infrared (FTIR) Spectroscopy*. Elsevier B.V., 2017. doi: 10.1016/B978-0-444-63776-5.00001-2.
- [76] A. H. Faqeeh and M. D. Symes, “A standard electrolyser test cell design for evaluating catalysts and cell components for anion exchange membrane water electrolysis,” *Electrochim. Acta*, vol. 444, no. October 2022, p. 142030, 2023, doi: 10.1016/j.electacta.2023.142030.
- [77] A. B. Laursen *et al.*, “Nanocrystalline Ni<sub>5</sub>P<sub>4</sub>: A hydrogen evolution electrocatalyst of exceptional efficiency in both alkaline and acidic media,” *Energy Environ. Sci.*, vol. 8, no. 3, pp. 1027–1034, 2015, doi: 10.1039/c4ee02940b.
- [78] R. A. Krivina *et al.*, “Three-Electrode Study of Electrochemical Ionomer Degradation Relevant to Anion-Exchange-Membrane Water Electrolysers,” *ACS Appl. Mater. Interfaces*, vol. 14, no. 16, pp. 18261–18274, 2022, doi: 10.1021/acsami.1c22472.
- [79] J. Fang, Y. Xuan, and Q. Li, “Preparation of polystyrene spheres in different particle sizes and assembly of the PS colloidal crystals,” *Sci. China Technol. Sci.*, vol. 53, no. 11, pp. 3088–3093, 2010, doi: 10.1007/s11431-010-4110-5.
- [80] K. Oesingmann, W. Grimme, and J. Scheelhaase, “Hydrogen in aviation: A simulation of demand, price dynamics, and CO<sub>2</sub> emission reduction potentials,” *Int. J. Hydrogen Energy*, vol. 64, no. October 2023, pp. 633–642, 2024, doi: 10.1016/j.ijhydene.2024.03.241.
- [81] W. Grimme and M. Braun, “Estimation of potential hydrogen demand and CO<sub>2</sub> mitigation in global passenger air transport by the year 2050,” *Transp. Res. Procedia*, vol. 65, no. C, pp. 24–33, 2022, doi: 10.1016/j.trpro.2022.11.004.
- [82] F. C. & H. J. Undertaking, *Hydrogen-powered aviation* / [www.fch.europa.eu](http://www.fch.europa.eu), no. May. 2020. doi: 10.2843/766989.
- [83] F. Report, *Market Uptake and Impact of Key Green Aviation Technologies*. doi: 10.2777/72358.
- [84] H. P. Cost and A. E. M. W. E. Fm-, “Ionomr Innovations, Inc. Pemion..pdf,” no. June,

- pp. 1–14, 2020.
- [85] G. M. Pi, “AEM Water Electrolyser for Hydrogen Production from Offshore Wind,” 2022.
- [86] S. M. Alia, M. A. Ha, C. Ngo, G. C. Anderson, S. Ghoshal, and S. Pylypenko, “Platinum-Nickel Nanowires with Improved Hydrogen Evolution Performance in Anion Exchange Membrane-Based Electrolysis,” *ACS Catal.*, vol. 10, no. 17, pp. 9953–9966, 2020, doi: 10.1021/acscatal.0c01568.
- [87] L. Wang *et al.*, “High performance anion exchange membrane electrolysis using plasma-sprayed, non-precious-metal electrodes,” *ACS Appl. Energy Mater.*, vol. 2, no. 11, pp. 7903–7912, 2019, doi: 10.1021/acsaem.9b01392.
- [88] I. Gatto, A. Capri, C. Lo Vecchio, S. Zignani, A. Patti, and V. Baglio, “Optimal operating conditions evaluation of an anion-exchange-membrane electrolyser based on FUMASEP® FAA3-50 membrane,” *Int. J. Hydrogen Energy*, vol. 48, no. 32, pp. 11914–11921, 2023, doi: 10.1016/j.ijhydene.2022.04.176.
- [89] N. Chen, S. Y. Paek, J. Y. Lee, J. H. Park, S. Y. Lee, and Y. M. Lee, “High-performance anion exchange membrane water electrolyzers with a current density of 7.68 A cm<sup>-2</sup> and a durability of 1000 hours,” *Energy Environ. Sci.*, vol. 14, no. 12, pp. 6338–6348, 2021, doi: 10.1039/d1ee02642a.
- [90] A. R. Motz *et al.*, “Performance and durability of anion exchange membrane water electrolyzers using down-selected polymer electrolytes,” *J. Mater. Chem. A*, vol. 9, no. 39, pp. 22670–22683, 2021, doi: 10.1039/d1ta06869e.
- [91] C. Hu *et al.*, “Reinforced poly(dibenzyl-co-terphenyl piperidinium) membranes for highly durable anion-exchange membrane water electrolysis at 2 A cm<sup>-2</sup> for 1000 h,” *Next Energy*, vol. 1, no. 3, p. 100044, 2023, doi: 10.1016/j.nxener.2023.100044.
- [92] A. Y. Faid, A. O. Barnett, F. Seland, and S. Sunde, “Highly active nickel-based catalyst for hydrogen evolution in anion exchange membrane electrolysis,” *Catalysts*, vol. 8, no. 12, 2018, doi: 10.3390/catal8120614.
- [93] X. Wu and K. Scott, “A Li-doped Co<sub>3</sub>O<sub>4</sub> oxygen evolution catalyst for non-precious metal alkaline anion exchange membrane water electrolyzers,” *Int. J. Hydrogen Energy*, vol. 38, no. 8, pp. 3123–3129, 2013, doi: 10.1016/j.ijhydene.2012.12.087.
- [94] K. Y. Yoon *et al.*, “Improved Oxygen Evolution Reaction Kinetics with Titanium Incorporated Nickel Ferrite for Efficient Anion Exchange Membrane Electrolysis,” *ACS Catal.*, vol. 14, no. 7, pp. 4453–4462, 2024, doi: 10.1021/acscatal.3c05761.
- [95] X. Yu *et al.*, “Hydrogen Evolution Reaction in Alkaline Media: Alpha- or Beta-Nickel Hydroxide on the Surface of Platinum?,” *ACS Energy Lett.*, vol. 3, no. 1, pp. 237–244, 2018, doi: 10.1021/acsenerylett.7b01103.
- [96] I. Vincent, E. C. Lee, and H. M. Kim, “Highly Active Ni–Fe Based Oxide Oxygen Evolution Reaction Electrocatalysts for Alkaline Anion Exchange Membrane Electrolyser,” *Catalysts*, vol. 12, no. 5, 2022, doi: 10.3390/catal12050476.
- [97] J. Chang *et al.*, “Ultrathin cobalt phosphide nanosheets as efficient bifunctional catalysts for a water electrolysis cell and the origin for cell performance degradation,” *Green Chem.*, vol. 18, no. 8, pp. 2287–2295, 2016, doi: 10.1039/c5gc02899j.

- [98] M. J. Jang *et al.*, “Superior performance and stability of anion exchange membrane water electrolysis: PH-controlled copper cobalt oxide nanoparticles for the oxygen evolution reaction,” *J. Mater. Chem. A*, vol. 8, no. 8, pp. 4290–4299, 2020, doi: 10.1039/c9ta13137j.
- [99] C. Zhang *et al.*, “Highly Efficient and Durable Electrocatalyst Based on Nanowires of Cobalt Sulfide for Overall Water Splitting,” *ChemNanoMat*, vol. 4, no. 12, pp. 1240–1246, 2018, doi: 10.1002/cnma.201800301.
- [100] T. Liu, X. Sun, A. M. Asiri, and Y. He, “One-step electrodeposition of Ni-Co-S nanosheets film as a bifunctional electrocatalyst for efficient water splitting,” *Int. J. Hydrogen Energy*, vol. 41, no. 18, pp. 7264–7269, 2016, doi: 10.1016/j.ijhydene.2016.03.111.
- [101] Y. Sun, C. Wang, T. Ding, J. Zuo, and Q. Yang, “Fabrication of amorphous CoMoS<sub>4</sub> as a bifunctional electrocatalyst for water splitting under strong alkaline conditions,” *Nanoscale*, vol. 8, no. 45, pp. 18887–18892, 2016, doi: 10.1039/c6nr07676a.
- [102] Enapter, “AEM Flex 120,” pp. 2–3.
- [103] Enapter, “AEM Nexus 1000,” pp. 2–3, 2024, [Online]. Available: [www.enapter.com/aem-nexus](http://www.enapter.com/aem-nexus)
- [104] ENAPTER, “LCOH Assumptions (Enapter AEM Electrolysers),” p. 2, 2023.
- [105] K. Westphal, M. Pastukhova, and J. M. Pepe, “SWP Research Paper Stiftung Wissenschaft und Politik German Institute for International and Security Affairs Geopolitics of Electricity: Grids, Space and (political) Power,” no. March, 2022.
- [106] R. Connolly, “Western economic sanctions and Russia’s place in the global economy,” *Ukr. Russ.*, no. March 2014, p. 212, 2015.
- [107] P. Sinisalo and M. Lundström, “Refining approaches in the platinum group metal processing value chain - A review,” *Metals (Basel)*, vol. 8, no. 4, pp. 1–12, 2018, doi: 10.3390/met8040203.
- [108] Umicore, “Hoboken site visit,” no. September, p. 73, 2012.
- [109] P. R. Taylor, E. H. Partelpeog, and G. E. Hoffman, “Pyrometallurgy,” in *Mineral Processing and Extractive Metallurgy: 100 Years of Innovation*, Society for Mining, Metallurgy & Exploration, Inc, 2014, pp. 503–566.
- [110] C. Liu, S. C. Sun, X. P. Zhu, G. F. Tu, and J. Y. Zhang, “Recovery of platinum from the spent auto-catalysts by pyrometallurgy,” *IOP Conf. Ser. Mater. Sci. Eng.*, vol. 479, no. 1, 2019, doi: 10.1088/1757-899X/479/1/012058.
- [111] Z. Wang *et al.*, “Reduction-Sulfurization Smelting Process of Waste Hydrogenation Catalysts, Automotive Exhaust Purifier Waste Catalysts, and Laterite Nickel Ore,” *ACS Omega*, vol. 8, no. 43, pp. 40713–40728, 2023, doi: 10.1021/acsomega.3c05772.
- [112] S. Hughes, “Applying Ausmelt technology to recover Cu, Ni, and Co from slags,” *Jom*, vol. 52, no. 8, pp. 30–33, 2000, doi: 10.1007/s11837-000-0170-5.
- [113] R. Guoxing, “RECOVERY OF VALUABLE METALS FROM SPENT LITHIUM-ION BATTERIES BY SMELTING REDUCTION PROCESS BASED ON MnO-SiO<sub>2</sub>-Al<sub>2</sub>O<sub>3</sub> SLAG SYSTEM,” *Appl. Mech. Mater.*, 2016, doi:

10.4028/www.scientific.net/AMM.440.97.

- [114] O. Velázquez-Martínez, J. Valio, A. Santasalo-Aarnio, M. Reuter, and R. Serna-Guerrero, “A critical review of lithium-ion battery recycling processes from a circular economy perspective,” *Batteries*, vol. 5, no. 4, pp. 5–7, 2019, doi: 10.3390/batteries5040068.
- [115] V. H. de Mello Santos, T. L. R. Campos, M. Espuny, and O. J. de Oliveira, “Towards a green industry through cleaner production development,” *Environ. Sci. Pollut. Res.*, vol. 29, no. 1, pp. 349–370, 2022, doi: 10.1007/s11356-021-16615-2.
- [116] C. Hagelüken, “Recycling of electronic scrap at Umicore’s integrated metals smelter and refinery,” *Proc. - Eur. Metall. Conf. EMC 2005*, vol. 1, no. May 2006, pp. 307–323, 2005.
- [117] H. Ch, “Recycling of electronic scrap at Umicore precious metals refining,” *Acta Metall. Slovaca*, vol. 12, no. 2006, pp. 111–120, 2006.
- [118] J. P. Harvey *et al.*, “Greener reactants, renewable energies and environmental impact mitigation strategies in pyrometallurgical processes: A review,” *MRS Energy Sustain.*, vol. 9, no. 2, pp. 212–247, 2022, doi: 10.1557/s43581-022-00042-y.
- [119] A. Fleuriault *et al.*, *Advances in pyrometallurgy: developing low carbon pathways*. 2023.
- [120] C. W. Scheeren, J. B. Domingos, G. Machado, and J. Dupont, “Hydrogen reduction of Adams’ catalyst in ionic liquids: Formation and stabilization of Pt(0) nanoparticles,” *J. Phys. Chem. C*, vol. 112, no. 42, pp. 16463–16469, 2008, doi: 10.1021/jp804870j.
- [121] K. C. Sabat, R. K. Paramguru, S. Pradhan, and B. K. Mishra, “Reduction of Cobalt Oxide (Co<sub>3</sub>O<sub>4</sub>) by Low Temperature Hydrogen Plasma,” *Plasma Chem. Plasma Process.*, vol. 35, no. 2, pp. 387–399, 2015, doi: 10.1007/s11090-014-9602-9.
- [122] K. V. Manukyan *et al.*, “Nickel Oxide Reduction by Hydrogen: Kinetics and Structural Transformations,” *J. Phys. Chem. C*, vol. 119, no. 28, pp. 16131–16138, 2015, doi: 10.1021/acs.jpcc.5b04313.
- [123] A. Liu, G. Hu, Y. Wu, and F. Guo, “Life cycle environmental impacts of pyrometallurgical and hydrometallurgical recovery processes for spent lithium-ion batteries: present and future perspectives,” *Clean Technol. Environ. Policy*, vol. 26, no. 2, pp. 381–400, 2024, doi: 10.1007/s10098-023-02640-x.
- [124] H. Tang *et al.*, “Recovery of platinum-group metals from spent catalysts by microwave smelting,” *J. Clean. Prod.*, vol. 318, no. July, p. 128266, 2021, doi: 10.1016/j.jclepro.2021.128266.
- [125] Y. Fu, Y. He, Y. Yang, L. Qu, J. Li, and R. Zhou, “Microwave reduction enhanced leaching of valuable metals from spent lithium-ion batteries,” *J. Alloys Compd.*, vol. 832, p. 154920, 2020, doi: 10.1016/j.jallcom.2020.154920.
- [126] S. V. Komarov, M. Kuwabara, and O. V. Abramov, “High power ultrasonics in pyrometallurgy: Current status and recent development,” *ISIJ Int.*, vol. 45, no. 12, pp. 1765–1782, 2005, doi: 10.2355/isijinternational.45.1765.
- [127] K. S. Liddell and M. D. Adams, “Kell hydrometallurgical process for extraction of platinum group metals and base metals from flotation concentrates,” *J. South. African*

*Inst. Min. Metall.*, vol. 112, no. 1, pp. 31–36, 2012.

- [128] D. Patil, S. Chikkamath, S. Keny, V. Tripathi, and J. Manjanna, “Rapid dissolution and recovery of Li and Co from spent LiCoO<sub>2</sub> using mild organic acids under microwave irradiation,” *J. Environ. Manage.*, vol. 256, no. December 2019, p. 109935, 2020, doi: 10.1016/j.jenvman.2019.109935.
- [129] P. K. Parhi and P. K. Misra, “Hydrometallurgical investigation routed through microwave (MW) assisted leaching and solvent extraction using ionic liquids for extraction and recovery of molybdenum from spent desulphurization catalyst,” *Inorg. Chem. Commun.*, vol. 149, no. December 2022, p. 110394, 2023, doi: 10.1016/j.inoche.2023.110394.
- [130] D. Jafarifar, M. R. Daryanavard, and S. Sheibani, “Ultra fast microwave-assisted leaching for recovery of platinum from spent catalyst,” *Hydrometallurgy*, vol. 78, no. 3–4, pp. 166–171, 2005, doi: 10.1016/j.hydromet.2005.02.006.
- [131] L. P. D. I. Prawira, Yuliusman, K. Shauma, A. R. Nafisah, and M. P. Ayu, “Platinum metal recovery from spent CCR platforming catalyst with microwave-assisted digestion method,” *AIP Conf. Proc.*, vol. 2255, 2020, doi: 10.1063/5.0014345.
- [132] S. Bao *et al.*, “A comprehensive review on the ultrasound-enhanced leaching recovery of valuable metals: Applications, mechanisms and prospects,” *Ultrason. Sonochem.*, vol. 98, no. April, p. 106525, 2023, doi: 10.1016/j.ultsonch.2023.106525.
- [133] G. Rahimi, S. O. Rastegar, F. Rahmani Chianeh, and T. Gu, “Ultrasound-assisted leaching of vanadium from fly ash using lemon juice organic acids,” *RSC Adv.*, vol. 10, no. 3, pp. 1685–1696, 2020, doi: 10.1039/c9ra09325g.
- [134] R. Kurniawan *et al.*, “Time-Dependent Ultrasonic Assisted Recovery of Platinum from Spent Removing Catalyst of Pt/Al<sub>2</sub>O<sub>3</sub> by Acid Leaching,” *IOP Conf. Ser. Mater. Sci. Eng.*, vol. 515, no. 1, 2019, doi: 10.1088/1757-899X/515/1/012068.
- [135] W. Liu *et al.*, “Optimization of ultrasonic enhanced chloride-hydrogen peroxide system for leaching platinum from propane dehydrogenation spent catalyst by response surface methodology,” *Sep. Purif. Technol.*, vol. 353, no. PA, p. 128384, 2025, doi: 10.1016/j.seppur.2024.128384.
- [136] C. N. Mpinga, J. J. Eksteen, C. Aldrich, and L. Dyer, “Direct leach approaches to Platinum Group Metal (PGM) ores and concentrates: A review,” *Miner. Eng.*, vol. 78, pp. 93–113, 2015, doi: 10.1016/j.mineng.2015.04.015.
- [137] T. Sakamoto, T. Hanada, H. Sato, M. Kamisono, and M. Goto, “Hydrophobic deep eutectic solvents for the direct leaching of nickel laterite ores: Selectivity and reusability investigations,” *Sep. Purif. Technol.*, vol. 331, no. October 2023, p. 125619, 2024, doi: 10.1016/j.seppur.2023.125619.
- [138] M. I. H. Khan, M. Rana, T. Nshizirungu, Y. T. Jo, and J. H. Park, “Recovery of Valuable and Hazardous Metals (Ni, Co, and Cd) from Spent Ni-Cd Batteries Using Polyvinyl Chloride (PVC) in Subcritical Water,” *ACS Sustain. Chem. Eng.*, vol. 10, no. 7, pp. 2368–2379, 2022, doi: 10.1021/acssuschemeng.1c06652.
- [139] O. Lanaridi *et al.*, “Toward the Recovery of Platinum Group Metals from a Spent Automotive Catalyst with Supported Ionic Liquid Phases,” *ACS Sustain. Chem. Eng.*, vol. 9, no. 1, pp. 375–386, 2021, doi: 10.1021/acssuschemeng.0c07384.

- [140] P. P. Sun, T. Y. Kim, B. J. Min, and S. Y. Cho, "Separation of platinum (IV) and rhodium (III) from hydrochloric acid solutions using diaion resins," *Mater. Trans.*, vol. 56, no. 11, pp. 1863–1867, 2015, doi: 10.2320/matertrans.M2015254.
- [141] R. Liu *et al.*, "Extraction of platinum(IV) by hydrophobic deep eutectic solvents based on trioctylphosphine oxide," *Hydrometallurgy*, vol. 199, no. October 2020, p. 105521, 2021, doi: 10.1016/j.hydromet.2020.105521.
- [142] O. Mokhodoeva, V. Maksimova, A. Shishov, and V. Shkinev, "Separation of platinum group metals using deep eutectic solvents based on quaternary ammonium salts," *Sep. Purif. Technol.*, vol. 305, no. October 2022, p. 122427, 2023, doi: 10.1016/j.seppur.2022.122427.
- [143] X. Liang, J. Tang, L. Li, Y. Wu, and Y. Sun, "A review of metallurgical processes and purification techniques for recovering Mo, V, Ni, Co, Al from spent catalysts," *J. Clean. Prod.*, vol. 376, no. August, p. 134108, 2022, doi: 10.1016/j.jclepro.2022.134108.
- [144] K. C. Wanta, W. T. Gunawan, R. F. Susanti, G. P. Gemilar, H. T. B. M. Petrus, and W. Astuti, "Subcritical Water as a Solvent for Extraction of Nickel and Aluminum Ions from Reforming Spent Catalysts," *IOP Conf. Ser. Mater. Sci. Eng.*, vol. 742, no. 1, 2020, doi: 10.1088/1757-899X/742/1/012025.
- [145] B. Onghena, T. Opsomer, and K. Binnemans, "Separation of cobalt and nickel using a thermomorphic ionic-liquid-based aqueous biphasic system," *Chem. Commun.*, vol. 51, no. 88, pp. 15932–15935, 2015, doi: 10.1039/c5cc06595j.
- [146] E. A. Othman, A. G. J. van der Ham, H. Miedema, and S. R. A. Kersten, "Recovery of metals from spent lithium-ion batteries using ionic liquid [P8888][Oleate]," *Sep. Purif. Technol.*, vol. 252, no. July, p. 117435, 2020, doi: 10.1016/j.seppur.2020.117435.
- [147] M. Liu, W. Ma, X. Zhang, Z. Liang, and Q. Zhao, "Recycling lithium and cobalt from LIBs using microwave-assisted deep eutectic solvent leaching technology at low-temperature," *Mater. Chem. Phys.*, vol. 289, no. June, p. 126466, 2022, doi: 10.1016/j.matchemphys.2022.126466.
- [148] E. Ebrahimi, H. Safari, M. Rezaee, A. Rezaei, and H. Abdollahi, "An environmentally friendly method for extraction of cobalt and molybdenum from spent catalysts using deep eutectic solvents (DESs)," *Environ. Sci. Pollut. Res.*, vol. 30, no. 39, pp. 90243–90255, 2023, doi: 10.1007/s11356-023-26806-8.
- [149] D. Shin, J. Park, J. Jeong, and B. S. Kim, "A biological cyanide production and accumulation system and the recovery of platinum-group metals from spent automotive catalysts by biogenic cyanide," *Hydrometallurgy*, vol. 158, pp. 10–18, 2015, doi: 10.1016/j.hydromet.2015.09.021.
- [150] S. Karim and Y. P. Ting, "Bioleaching of platinum, palladium, and rhodium from spent automotive catalyst using bacterial cyanogenesis," *Bioresour. Technol. Reports*, vol. 18, no. February, p. 101069, 2022, doi: 10.1016/j.biteb.2022.101069.
- [151] M. Motaghed, S. M. Mousavi, S. O. Rastegar, and S. A. Shojaosadati, "Platinum and rhenium extraction from a spent refinery catalyst using *Bacillus megaterium* as a cyanogenic bacterium: Statistical modeling and process optimization," *Bioresour. Technol.*, vol. 171, pp. 401–409, 2014, doi: 10.1016/j.biortech.2014.08.032.

- [152] H. Brandl, S. Lehmann, M. A. Faramarzi, and D. Martinelli, “Biomobilization of silver, gold, and platinum from solid waste materials by HCN-forming microorganisms,” *Hydrometallurgy*, vol. 94, no. 1–4, pp. 14–17, 2008, doi: 10.1016/j.hydromet.2008.05.016.
- [153] H. Brandl, R. Bosshard, and M. Wegmann, “Computer-munching microbes: Metal leaching from electronic scrap by bacteria and fungi,” *Process Metall.*, vol. 9, no. C, pp. 569–576, 1999, doi: 10.1016/S1572-4409(99)80146-1.
- [154] T. Abashina, A. Yachkula, E. Kaparullina, and M. Vainshtein, “Intensification of nickel bioleaching with neutrophilic bacteria guyparkeria halophila as an approach to limitation of sulfuric acid pollution,” *Microorganisms*, vol. 9, no. 12, pp. 4–11, 2021, doi: 10.3390/microorganisms9122461.
- [155] A. K. Saim and F. K. Darteh, “A Comprehensive Review on Cobalt Bioleaching from Primary and Tailings Sources,” *Miner. Process. Extr. Metall. Rev.*, vol. 00, no. 00, pp. 1–27, 2023, doi: 10.1080/08827508.2023.2181346.
- [156] C. García-Balboa, P. Martínez-Alesón García, V. López-Rodas, E. Costas, and B. Baselga-Cervera, “Microbial biominers: Sequential bioleaching and biouptake of metals from electronic scraps,” *Microbiologyopen*, vol. 11, no. 1, 2022, doi: 10.1002/mbo3.1265.
- [157] D. Kraemer, M. Junge, T. Oberthür, and M. Bau, “Improving recoveries of platinum and palladium from oxidized Platinum-Group Element ores of the Great Dyke, Zimbabwe, using the biogenic siderophore Desferrioxamine B,” *Hydrometallurgy*, vol. 152, pp. 169–177, 2015, doi: 10.1016/j.hydromet.2015.01.002.
- [158] R. N. Kar, L. B. Sukla, K. M. Swamy, V. V. Panchanadikar, and K. L. Narayana, “Bioleaching of lateritic nickel ore by ultrasound,” *Metall. Mater. Trans. B Process Metall. Mater. Process. Sci.*, vol. 27, no. 3, pp. 351–354, 1996, doi: 10.1007/BF02914897.
- [159] K. M. Swamy, K. L. Narayana, and V. N. Misra, “Bioleaching with ultrasound,” *Ultrason. Sonochem.*, vol. 12, no. 4, pp. 301–306, 2005, doi: 10.1016/j.ultsonch.2004.01.035.
- [160] F. Anjum, H. N. Bhatti, and M. A. Ghauri, “Enhanced bioleaching of metals from black shale using ultrasonics,” *Hydrometallurgy*, vol. 100, no. 3–4, pp. 122–128, 2010, doi: 10.1016/j.hydromet.2009.10.016.
- [161] Y. C. Lo, C. L. Cheng, Y. L. Han, B. Y. Chen, and J. S. Chang, “Recovery of high-value metals from geothermal sites by biosorption and bioaccumulation,” *Bioresour. Technol.*, vol. 160, pp. 182–190, 2014, doi: 10.1016/j.biortech.2014.02.008.
- [162] G. Dönmez and Z. Aksu, “Bioaccumulation of copper(ii) and nickel(ii) by the non-adapted and adapted growing CANDIDA SP,” *Water Res.*, vol. 35, no. 6, pp. 1425–1434, 2001, doi: 10.1016/S0043-1354(00)00394-8.
- [163] F. Aslam, A. Yasmin, and S. Sohail, “Bioaccumulation of lead, chromium, and nickel by bacteria from three different genera isolated from industrial effluent,” *Int. Microbiol.*, vol. 23, no. 2, pp. 253–261, 2020, doi: 10.1007/s10123-019-00098-w.
- [164] L. Dusengemungu, G. Kasali, C. Gwanama, and K. O. Ouma, “Recent Advances in Biosorption of Copper and Cobalt by Filamentous Fungi,” *Front. Microbiol.*, vol. 11,

- no. December, pp. 1–16, 2020, doi: 10.3389/fmicb.2020.582016.
- [165] A. Bajpai, N. Atoliya, and A. Prakash, *Genetically engineered microbes in micro-remediation of metals from contaminated sites*. INC, 2022. doi: 10.1016/B978-0-323-88504-1.00016-9.
- [166] S. Sun *et al.*, “Efficient HCl leaching of platinum group metals from waste three-way catalysts: A study on kinetics and mechanisms,” *Environ. Res.*, vol. 238, no. P1, p. 117148, 2023, doi: 10.1016/j.envres.2023.117148.
- [167] M. Joulié, R. Laucournet, and E. Billy, “Hydrometallurgical process for the recovery of high value metals from spent lithium nickel cobalt aluminum oxide based lithium-ion batteries,” *J. Power Sources*, vol. 247, pp. 551–555, 2014, doi: 10.1016/j.jpowsour.2013.08.128.
- [168] B. Qin *et al.*, “Nickel ion removal from wastewater using the microbial electrolysis cell,” *Bioresour. Technol.*, vol. 121, pp. 458–461, 2012, doi: 10.1016/j.biortech.2012.06.068.
- [169] J. Ndlovu, “Overview of Pgm Processing,” *SBG Secur. Min. Conf. Overv. PGM Process.*, 2014, [Online]. Available: <http://www.angloamericanplatinum.com/~media/Files/A/Anglo-American-Platinum/presentations-and-speeches/standardbankconference-anglo-american-platinum-processing-111114.pdf>
- [170] K. C. Sole, A. M. Feather, and P. M. Cole, “Solvent extraction in southern Africa: An update of some recent hydrometallurgical developments,” *Hydrometallurgy*, vol. 78, no. 1-2 SPEC. ISS., pp. 52–78, 2005, doi: 10.1016/j.hydromet.2004.11.012.
- [171] F. Tesfaye, D. Lindberg, and J. Hamuyuni, “Valuable metals and energy recovery from electronic waste streams,” *Miner. Met. Mater. Ser.*, no. 9783319521916, pp. 103–116, 2017, doi: 10.1007/978-3-319-52192-3\_11.
- [172] G. Nicol *et al.*, “Platinum group metals recovery using secondary raw materials (platinum): Project overview with a focus on processing spent autocatalyst,” *Johnson Matthey Technol. Rev.*, vol. 65, no. 1, pp. 127–147, 2021, doi: 10.1595/205651321x16057842276133.

# APPENDICES

# APPENDIX A

## DIFFERENT INDUSTRIAL RECOVERY ROUTES

### Anglo Platinum process

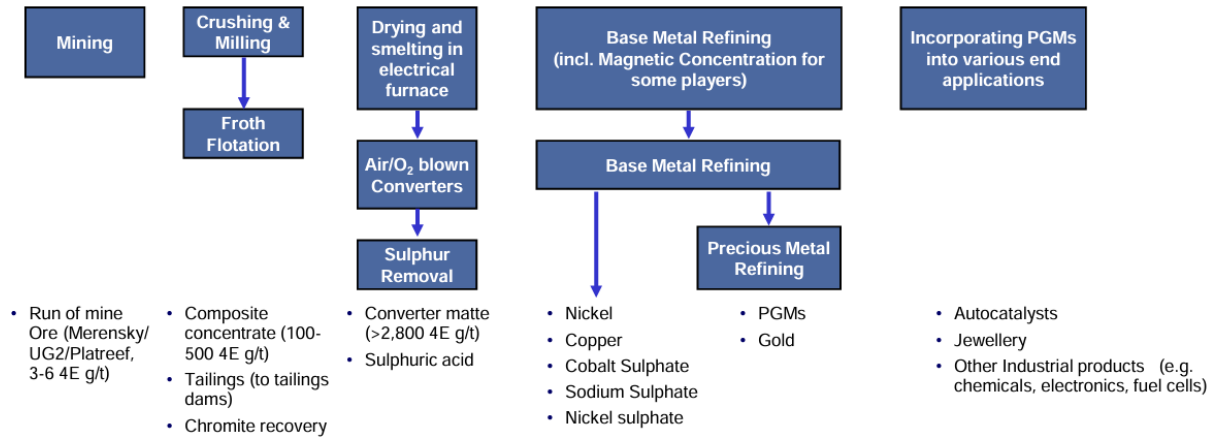


Figure 51: Anglo Platinum metal recovery process (Adapted from [169])

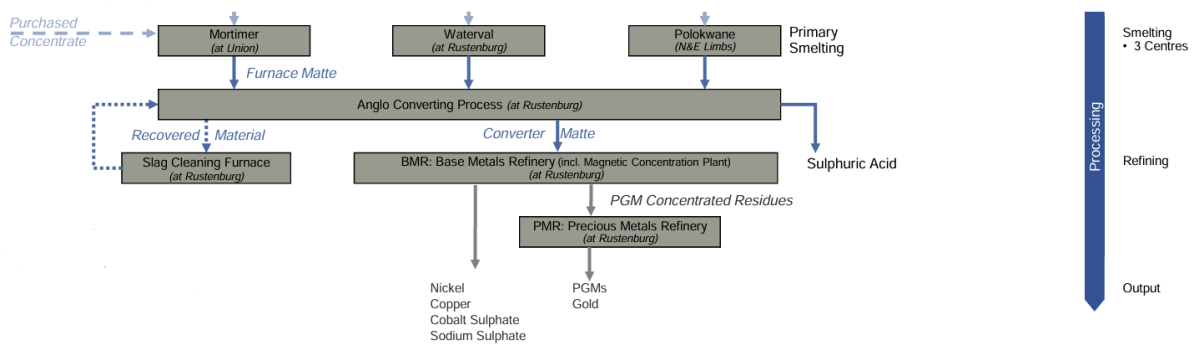


Figure 52: Rustenburg smelter (source: Adapted from [169])



## Impala Platinum process

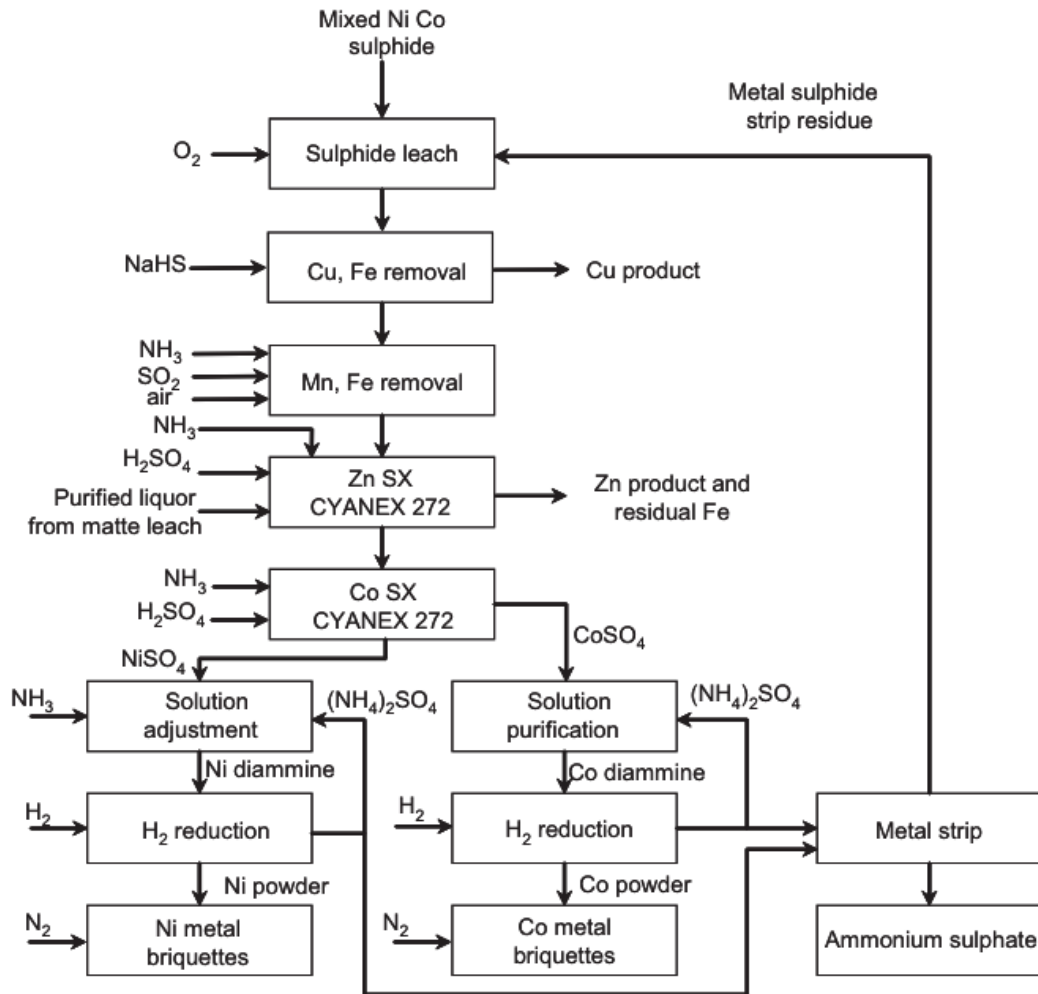


Figure 54: Impala Platinum nickel and cobalt recovery circuit (source: [170])

## Boliden Rönnskär route

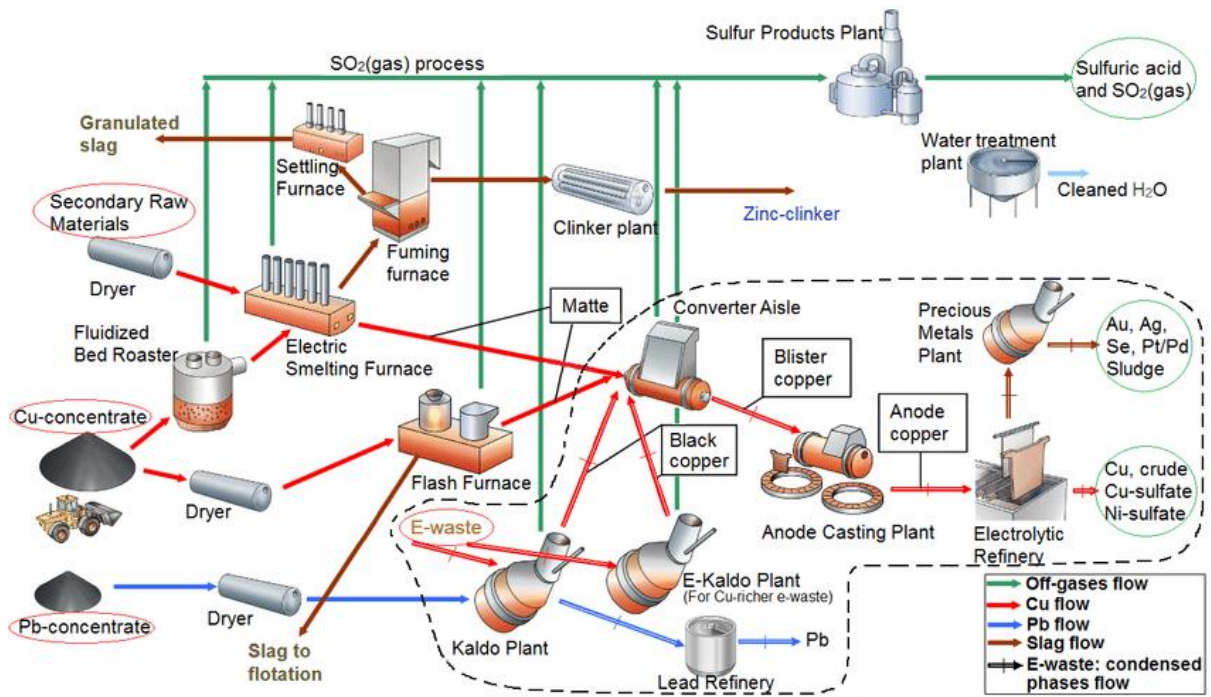


Figure 55: Boliden Rönnskär precious and base metal recovery route (source: [171])

## PLATIRUS project

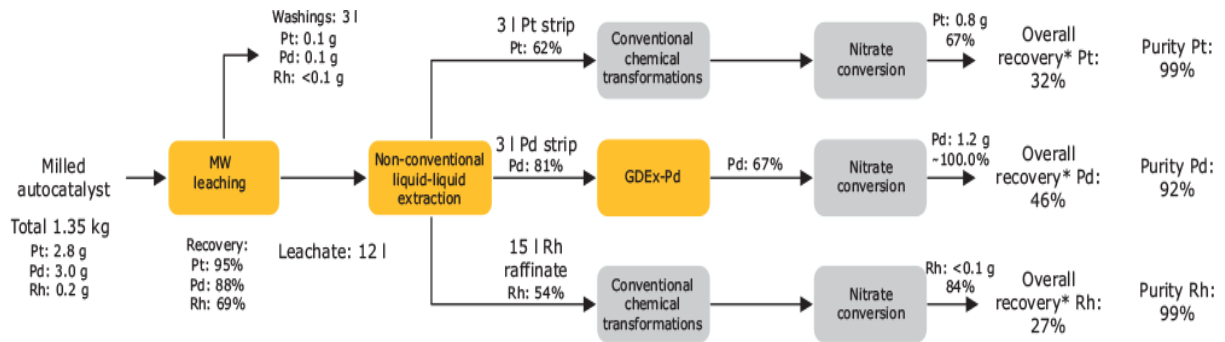


Figure 56: PLATIRUS circuit for PGM recovery (Source: [172])

## Panton process

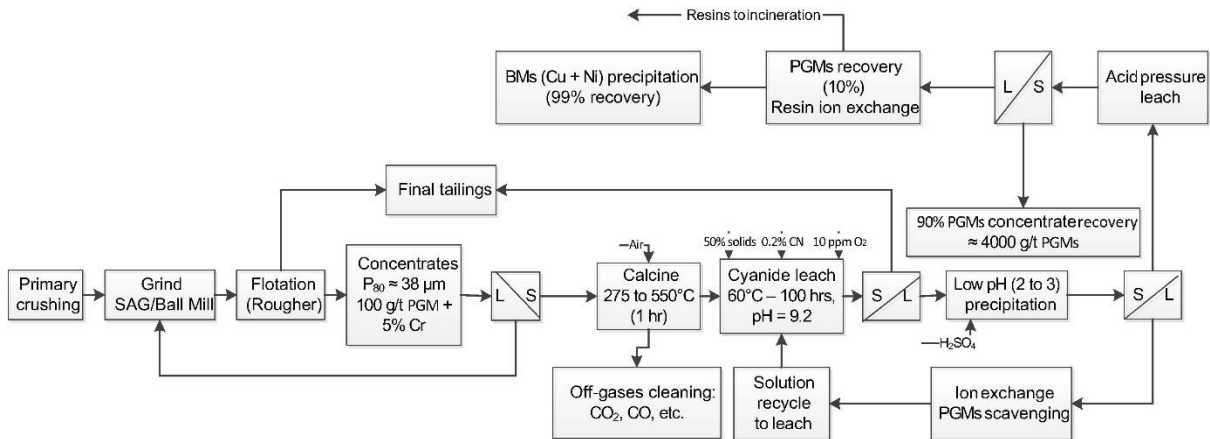


Figure 57: Panton process (Source: [83])